FREE FALL GAS ATOMIZATION OF LIQUID METALS

by

DEVENDRA SINGH

DEPARTMENT OF MATERIALS AND METALLURGICAL ENGINEERING

INDIAN INSTITUTE OF TECHNOLOGY, KANPUR

AUGUST, 1998

FREE FALL GAS ATOMIZATION OF LIQUID METALS

A Thesis Submitted

in Partial Fulfilment of the Requirements

for the Degree of

DOCTOR OF PHILOSOPHY

by

DEVENDRA SINGH

to the

DEPARTMENT OF MATERIALS AND METALLURGICAL ENGINEERING

INDIAN INSTITUTE OF TECHNOLOGY KANPUR, KANPUR 208016

AUGUST, 1998

CERTIFICATE

It is certified that the work contained in the thesis entitled "Free fall gas atomization of liquid metals", by "Devendra Singh", has been carried out under our supervisions and that this work has not been submitted elsewhere for a degree.

Dr. S. C. Koria
Professor
Department of Materials
& Metallurgical Engineering
Indian Institute of Technology, Kanpur

Dr. R. K. Dube
Professor
Department of Materials
& Metallurgical Engineering
Indian Institute of Technology, Kanpur

ABSTRACT

In the free fall gas atomization technique, a vertically falling molten stream is disintegrated by the energetic gas field created by an atomizer. The resulting droplets can either be deposited on the substrate to produce pre-forms or be solidified during their flight in the cooling chamber to produce metal powder. The present work concerns with the gas atomization of freely falling liquid metal stream to produce powder. For the successful application of gas atomization technique to produce metal powder, a detailed quantitative knowledge of the dynamics of gas field and solidification of droplets during their flight is necessary to select optimum distances of location of atomizer and the powder collection arrangement with reference to the geometric point of the atomizer.

In the experiments, dynamics of gas field is studied by measuring pitot pressure and its variation as a function of plenum pressure for several different types of atomizers. The atomization of aluminium, lead, zinc and tin is performed in a cooling chamber of 2.4 m height, at the bottom of which powder is collected. The gas field created by an atomizer is found to show large variation in velocities around its geometric point. The atomizing gas is found to posses maximum velocity at geometric point of all atomizer. The velocity at downstream the geometric point is correlated for the first time with pressure and other design parameters of the atomizer such as focal length, nozzle diameter.

Aluminium, lead, zinc and tin streams at various superheats are atomized in a chamber of constant height at various pressures by atomizers of different focal lengths,

apex angles and number and diameter of nozzles. The free fall distance of the liquid stream is equal to focal length of atomizers. In some experiments atomized droplets are found to be deposited either on the atomizer surface or not completely solidified even after covering the full height of the chamber. This is observed at high velocity of gas field for all metals. Critical velocity at which droplets do not deposit on the atomizer surface is found to vary with apex angle, free fall distance of the liquid stream and the type of metal. At and below the critical velocities of the gas field droplets of Al, Sn and Zn are solidified into powder for a very narrow range of velocities, whereas droplets of lead are solidified into powder for a wide range of velocities. All the powder collectives are found to follow log normal distribution function and the mass median size is correlated successfully with atomizer/liquid related parameters. The geometric standard deviation is found to be independent of all parameters. The atomization efficiency is found to be less than 1%. The shape of the particles of the powder is found to be spherical, rounded and irregular.

ACKNOWLEDGMENTS

I would like to extend my sincere gratitude to Drs. S. C. Koria and R. K. Dube for suggesting an interesting study, for their able guidance, for the informative discussions and for their assistance which made this work possible and successful.

I also thank Mr. S. C. Soni for his assistance at various stages of work.

I am deeply indebted to the technicians of the Department of Materials and Metallurgical Engineering and Department of Material Science whose assistance with experimental work proved invaluable.

I am also grateful to Mr. V. P. Gupta who made drawings and figures.

Finally, I thank Mr. Yash Pal for his patient and neat typing.

- Devendra Singh

TABLE OF CONTENTS

LIST OF FIGURES

LIST OF TABLES

LIST OF SYMBOLS

A	cross sectional area for gas passage, m^2
C_D	discharge coefficient of atomizer
C_d	gas drag coefficient
d	diameter of liquid metal delivery tube, m
d_p	diameter of spherical shape particle, m
D	diameter of nozzle, m
D_t	diameter of crucible, m
E	atomization efficiency
E_c	atomization efficiency at $V_g = V_c$
f	friction factor
F	focal length, m.
g	acceleration due to gravity, m/s^2
h_o	initial height of liquid metal in crucible, m
l	length of liquid metal delivery tube, m
L	free fall distance, m
M_a	mach number
m	mass flow rate of gas, kg/s
m_c	critical mass of gas, kg/s
m_i	mass flow rate of gas under isentropic condition, kg/s
M	mass flow rate of metal, kg/s
M_c	mass collected of metal, gm
M_r	mass left in crucible, gm
M_s	mass (-600 μm) used for sieve analysis
$M+$	mass (+600 μm), gm
M_l	mass lost, gm
N	number of nozzles
P	plenum pressure, Pa
P_c	critical pressure, Pa
P_s	static pressure, kPa

P_t	pitot pressure, kPa
R	universal gas constant, kj/kg mole K
R_p	particle radius after transformation to spherical shape, m
r_p	partial radius before transformation to spherical shape, m
S	specific surface of produced powder particles, cm^2/gm
t	time
T	static temperature, K
ΔT_s	superheat of liquid metal, K
T_o	stagnation temperature, K
v_g	gas velocity, m/s
v_p	particle velocity, m/s
V	volume of particle, m^3
V_m	velocity of liquid metal at exit of liquid metal delivery tube, m/s
V_g	gas velocity at geometric point, m/s
V_z	downstream velocity of gas, m/s
w	molecular mass of gas, kg/kg mole
X_g	mass median size of powder particles, μm
X_c	critical median size of powder particles, μm
Z	vertical distance from geometric point, m
z_p	axial position of the particle from geometric point, m
γ	specific heat ratio
ρ_a	density of air, kg/m^3
ρ_g	density of gas, kg/m^3
ρ_m	density of metal, kg/m^3
α	apex angle of atomizer
σ_g	geometric standard deviation of particle size distribution
σ_m	surface tension of metal, N/m
μ_g	viscosity of gas, Pa-S
μ_m	Viscosity of metal, Pa-S

CHAPTER - 1

INTRODUCTION

Atomization is defined as the break-up of a liquid into fine droplets. Thus a metal in the molten state can be atomized. The atomization of liquid metals can be used either for powder production[1], or spray deposition of preforms[2]. In the former case, the atomized droplets are allowed to solidify into discrete powder particles. In the later case, the atomized liquid metal droplets are directed to a suitable substrate i.e., a mould or collecting surface on which an agglomerated mass of metal, known as "preforms", results after solidification. The present work is related to the atomization of liquid metals for making powder.

The energy needed for atomization of liquid metals can be supplied in a variety of ways. Depending on the mode in which the energy is supplied, atomization process can be classified into the following major categories[1-3]:

1, Two fluid atomization

2. Vacuum atomization

3. Centrifugal atomization, and

4. Mono-sized droplet atomization

In two fluid atomization, a fluid is used as the atomization media to breakup the liquid metal stream into droplets. The fluid may be either gas, water or oil, and the respective processes are known as gas, water or oil atomization.

In vacuum atomization liquid metals containing dissolved gasses under pressure are injected into a low pressure/vacuum environment[1,3]. On exposure to the vacuum, the dissolved gases are released into the low pressure atmosphere causing the deformation and disintegration of the liquid metal into droplets.

In centrifugal atomization, centrifugal force is used to breakup the liquid metal stream [1]. The energy imparted to the molten metal in the centrifugal atomization process is in the form of kinetic energy generated by means of a rotating surface. This type of atomization method is best represented by rotating electrode atomization and rotating disc atomization.

The monosized droplet atomization is based on the Rayleigh mechanism of liquid column breakup[2]. When the length to diameter ratio of a liquid metal stream exceeds a certain limiting value, the liquid column becomes unstable under the action of surface tension forces. Consequently, it will breakup into droplets by the growth of swollen and contracting waves which exhibit wavelength greater than the circumference of the column.

Out of all the above methods, gas and water atomizations are the most widely used methods for powder production. The present work is related to the gas atomization, and hence it would be discussed in detail as follows.

The early technology of gas atomization was based primarily on the use of a single gas jet for the disintegration of the liquid metal. Typically, a horizontally moving gas jet impinges a vertically falling liquid metal stream. This method was known as horizontal gas atomization. This technique has not found much application in gas atomization technology.

Subsequently gas atomization process based on more than one gas jet was developed, which has found greater acceptability. The gas atomizers can be classified into two basic types according to the relative positions between the atomization gas jets and the liquid metal stream. These are closed or confined type atomizers and open or free fall type atomizers. The respective atomization process is known as confined gas atomization and free fall gas atomization.

In confined gas atomization, the gas jet hits the liquid metal stream as it leaves the liquid metal delivery tube. The gas jet is generally tangential to the edge of the liquid metal delivery tube. One of the advantages of confined atomizers is their higher atomization efficiency relative to that associated with free fall atomizers. However, confined atomizers are extremely sensitive to metal freeze up at the orifice of the metal delivery tube.

In free fall gas atomization liquid metal is allowed to fall under the action of gravitational forces for a certain distance prior to interacting with the gas field formed by the impingement of various gas jets at its apex point. The interaction of liquid metal stream with the gas field brings about the disintegration of the stream into droplets.

The present work is concerned with the free fall gas atomization of liquid metals. Chapter 2 describes the literature review on this subject and the objectives of the present study. In chapter 3 experimental set-up and procedure are described to achieve the objectives. Chapter 4 contains the results of present work. The discussion of the results constitutes Chapter 5. The conclusions of the work and the suggestions for further work are included in Chapter 6 and 7 respectively.

CHAPTER 2

LITERATURE REVIEW

In free fall gas atomization, molten metal stream is disintegrated either by horizontal gas jet produced by a nozzle or by the energetic gas field created by an atomizer. Out of both methods of supply of gas, atomizer is most commonly used. The resulting droplets are either solidified during their flight in the cooling chamber to produce metal powder or deposited on the substrate to produce a three dimensional preform. The present work concerns with the study of free fall gas atomization to produce metal powder. In the following the available literature on free fall atomization is presented. The literature is organised in terms of atomizer, atomizing gas field, droplet behavior during their flight and the resulting powder characteristics.

2.1 ATOMIZER

Figure 2.1 shows the schematic sketch of an atomizer used in free fall atomization. The point of intersection of the axes of nozzles is termed geometric point[4] or focal point[5]. The angle of the intersection of the axes of nozzles is defined as the apex angle[6] or impingement angle[4,5].

In the atomizer concentric arrangement of gas nozzles with respect to metal stream is commonly used. However, Tornberg[7] reported also an eccentric arrangement. The gas nozzles are of the flat V-jet, a combination of discrete nozzles or 360° annular ring

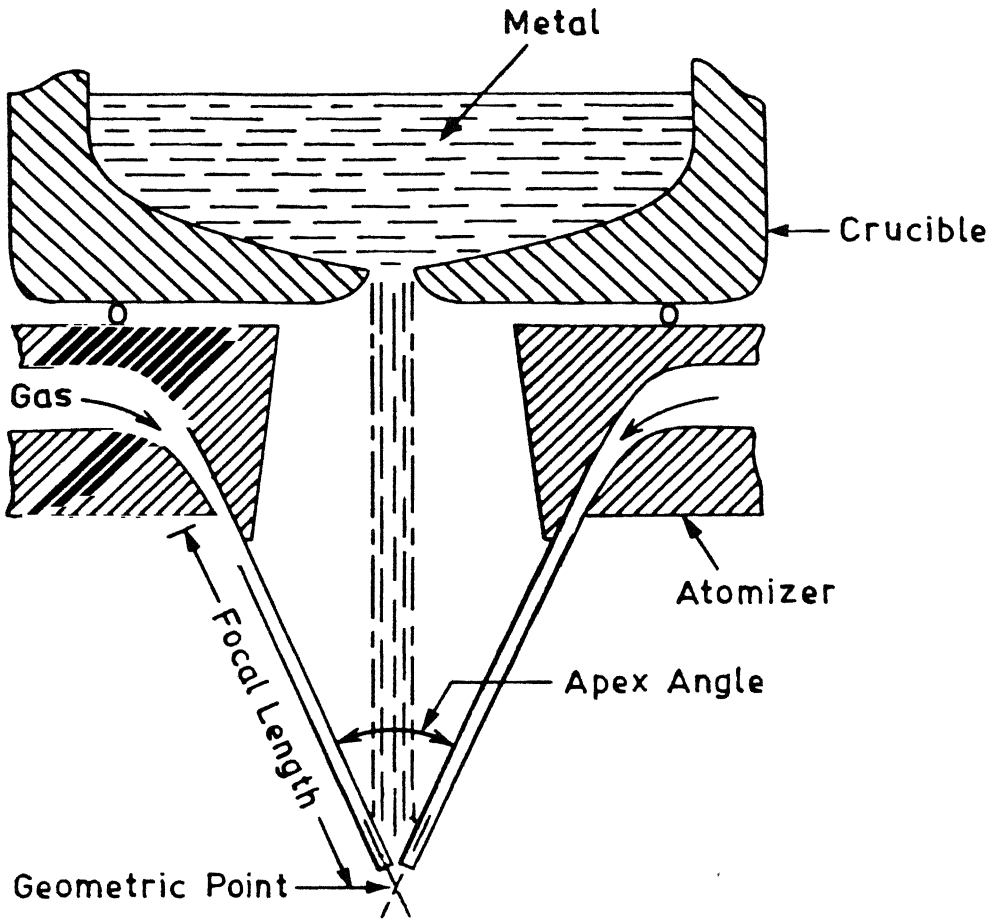

Figure 2.1 : Schematic sketch of a free fall gas atomiz

opening[7]. At the centre of the atomizer a hole is provided to direct the liquid metal stream towards geometric point.

2.2 ATOMIZING GAS FIELD

The atomizing gas field is created by the impingement of gas jets produced by the nozzles of an atomizer. The atomization of liquid metal stream takes place in the gas field and the atomized droplets fly in the gas field during their solidification. Therefore, the knowledge of the variation of gas velocity and its correlation with operating parameters of atomizer in the gas field are very important. The commercially used gases are air, steam, nitrogen, argon and helium[8]. However, air and nitrogen are the commonly used gases.

Some investigators studied the velocity variation in the gas field created by an atomizer of free fall types[4,9,10]. A summary of their experimental parameters is given in Table 2.1. See and Johnston[4] reported the variation of gas velocity in the gas field. They observed that the point of maximum velocity does not correspond with the geometric point. It was revealed by Schlieren photography that the velocity distribution in the gas field was not altered by the presence of a liquid stream. The maximum velocity in the gas field was found to be unique for each mass flow rate of gas, and was independent of impingement angle.

Moir and Jones[9], and Moir et al.[10] investigated the velocity variation by changing simultaneously both the focal length and apex angle of the atomizer. The velocity variation is reported at different plenum pressure and for different number of nozzles. Gas velocities were measured by both Pitot tube and hot wire anemometer and the results obtained were found in good agreement. It was reported that the velocity increases by

increasing the plenum pressure or decreasing the number of nozzles. They have not correlated the variation of velocity with parameters related to atomizer.

2.3 DROPLET BEHAVIOR DURING THEIR FLIGHT

The atomized droplets fly in both upstream and downstream of the geometric point[5]. However, major proportion of produced droplets fly in downstream of the geometric point and release heat to solidify during their flight. See and Johnston[4] atomized lead and tin by atomizers of apex angles 30°, 60° and 90°. The droplets moving upstream the geometric point were found to be deposited over the gas ring of atomizer of apex angle 90°. There was no deposition of droplets on the atomizers of 30° and 60° apex angles.

The atomized droplets moving downstream the geometric point solidify during their flight. If sufficient flight distance is provided to release superheat and latent heat these droplets solidify into powder. Some workers have studied the height of cooling chamber required to completely solidify the droplets into powder. Naida et al.[17] calculated that for the manufacture of tin powder by air atomization of upto 300 μm particle size, the height of the chamber should not be less than 5 m[17]. Based on mathematical analysis Schmitt[18] reported that for complete solidification, distance from 1 m to 20 m is required for particle size from 100 μm to 450 μm during argon gas atomization of Ni-base alloys[18]. Howells[8] et al. claimed that a height of 4.5 m of cooling chamber is sufficient to produce powder of high melting point alloys.

2.4 POWDER CHARACTERISTICS

Size and size distribution, particle shape and yield of powder in different size ranges are the important powder characteristics.

2.4.1 SIZE AND SIZE DISTRIBUTION

See and Johnston[4] and Dube et al. [11] reported log-normal distribution of the weighed sieve fractions of atomized metal powder of lead, tin and aluminum, respectively, while Helmersson et al.[12] reported log-normal and bimodal distribution of atomized nickel-based alloys. Their experimental parameters are given in Table 2.1.

Lubanska[13] presented an empirical correlation, using spray ring data for gas atomization of liquid metal, for calculating the mass median size of atomized liquid metal droplet. Tornberg[7] presented a mathematical model to calculate the particle size. The mean particle size of the powder is related to the surface tension, viscosity of the metal and the forces acting on the liquid metal in the atomization system. This model is based on a number of assumptions.

2.4.1.1 Effect of Atomization Parameters on Particle Size

The parameters affecting the particle size are related to atomizer, atomizing gas and liquid metal to be atomized.

A. ***Related to Atomizer***

The parameters related to atomizer are diameter of nozzle, number of nozzles, apex angle, and focal length. See and Johnston[4], See et al. [5] and Helmersson[12] studied the effect of some of them on the powder characteristics. They mainly varied apex angle

Table 2.1 : Experimental parameters of various investigators

Ref	Atomizer				Metal Parameter					Gas Parameter		
	D mm	N	α deg	F mm	L mm	Metal	ΔT_s K	d mm	$\dot{M}$ gm/s	Gas	P kPa	$\dot{m}$ gm/s
4	4.7	4	30, 60, 90	7.8	20	Pb, Sn	- 43, 118, 218	3.17, 4.76	50, 199, 90, 262	N_2	-	13-46
5	4.5	4	55, 69	6.5 8.0	-	Pb	86	4.37	130	N_2	-	13-30 5
8	-	-	-	-	-	Co alloy Cu alloy steel, etc.	-	-	-	N_2 Ar etc	-	-
9	-	6, 12	40, 44, 60	-	170	Al alloy	-	1	-	N_2	690-1390	-
10	1	6	60	-	-	-	-	-	-	N_2	552-1380	3.96-9 96
11	2	12	35	-	-	Al	100, 150, 200	6.0	-	N_2	608 1216	-
12	-	2	-	-	-	Ni alloy	50, 100	-	-	N_2	-	-
13	-	3-8	50, 34	-	-	Sn and Sn alloy Iron	-	6.35-22.2	-	Air	-	-
14	-	-	-	-	25	Al & Al alloy	-	-	-	N_2	-	-
15	-	-	-	-	-	High speed steel, tool steel	-	-	-		-	-
16	-	2	-	-	-	Ni alloy	-	-	-	N_2	-	-

and focal length. See et al. and Helmersson changed both apex angle and focal length, simultaneously. See and Johnston has shown that an increase in apex angle increases the mass median diameter of powder particles. See et al. and Helmersson et al. have reported that the increase in apex angle has decreased the particle size. It was due to the decrease in focal length with that of apex angle. A summary of the values of experimental parameters related to atomizer is given in Table 2.1.

B. ***Related to Atomizing Gas***

The parameters related to atomizing gas in general are pressure, mass flow rate and its type, i.e. nitrogen, argon or air, etc. Almost all workers [4,11] varied simultaneously the pressure and flow rate of the gas. All of them have reported a decrease in particle size with an increase in the pressure or gas flow rate. Values of experimental parameters related to atomizing gas are summarized in Table 2.1. Howells et al.[8] reported geometric standard deviation to be a function of mass flow rate of gas.

C. ***Related to Metal***

Parameters related to metal are superheat of the liquid metal, diameter of the liquid metal delivery tube, free fall distance of the liquid metal stream, mass flow rate of the metal, and the type of metal. See and Johnston[4] reported the particle size to be independent, and Dube et al.[11] dependent on the superheat of liquid metals. Lubanska reported that size of metal powder is a function of mass flow rate of liquid metal. As metal flow rate increases size of powder particles increases. Particle size decreases by increasing the superheat of liquid metal[11] . Howells et al [8] observed geometric standard

deviation to be a function of mass flow rate of metal. The experimental values of parameters related to metal of various workers are given in Table 2.1.

2.4.2 PARTICLE SHAPE

Particle shape depends on the spherodization and solidification time. If solidification time is greater than that of spherodization time, particle will be spherical[4]. See and Johnston[4] atomized lead and tin by nitrogen gas, and calculated the spherodization and solidification time of the atomized droplets. They found that the solidification time was greater than the spherodization time. Therefore, they argued that powder particles should have been spherical, but practically it was not the case. The reported reason of it was the oxidation of powder particles.

2.5 OBJECTIVES OF THE PRESENT WORK

The objectives of the present work are as follows:

1. To characterize qualitatively and quantitatively the atomizing gas field produced by atomizers of the free fall type.
2. To study droplet behavior during their flight in the cooling chamber.
3. To study the size, size distribution, shape, and yield of powder.
4. To relate atomization efficiency with parameters related to atomizer, liquid metal and atomizing gas.
5. And finally, to develop various empirical correlations which are useful for free fall gas atomization.

CHAPTER 3

EXPERIMENTAL

This chapter describes the experimental set up and the procedure to investigate the dynamics of gas flow rate through free fall type atomizers and atomization of liquid metals.

3.1 SET-UP

3.1.1 Dynamics of Gas Flow Rate

Dynamics of gas flow rate through atomizers is studied as a function of plenum pressure by measuring the Pitot pressure and its spatial variation in the gas field created by impingement of gas jets. Figure 3.1 shows the experimental set-up. The set-up mainly consists of an atomizer and pressure measuring devices.

3.1.1.1 Atomizer

In atomizers of the present study nozzles were arranged concentric to the central axis of the atomizer. The atomizer consists of a manifold having a number of holes for fitting nozzles and gas supply arrangement as shown in Figure 3.2. The holes were designed to be positioned at equal circumferential distances and inclined conically making an apex angle α such that the geometric point (it is the point of intersection of the axes of

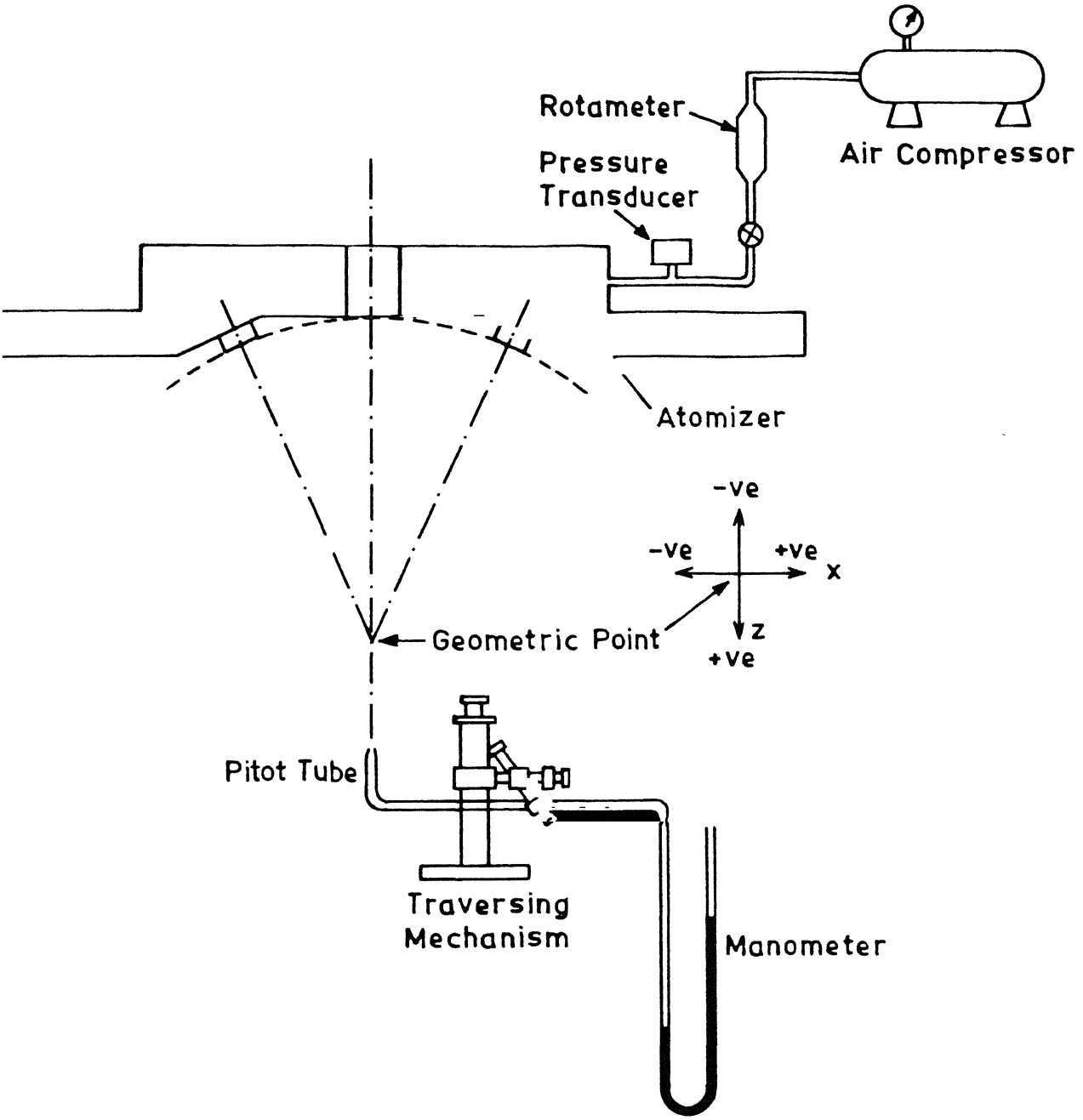

Figure 3.1 : Experimental set-up to investigate the gas field created by an atomizer

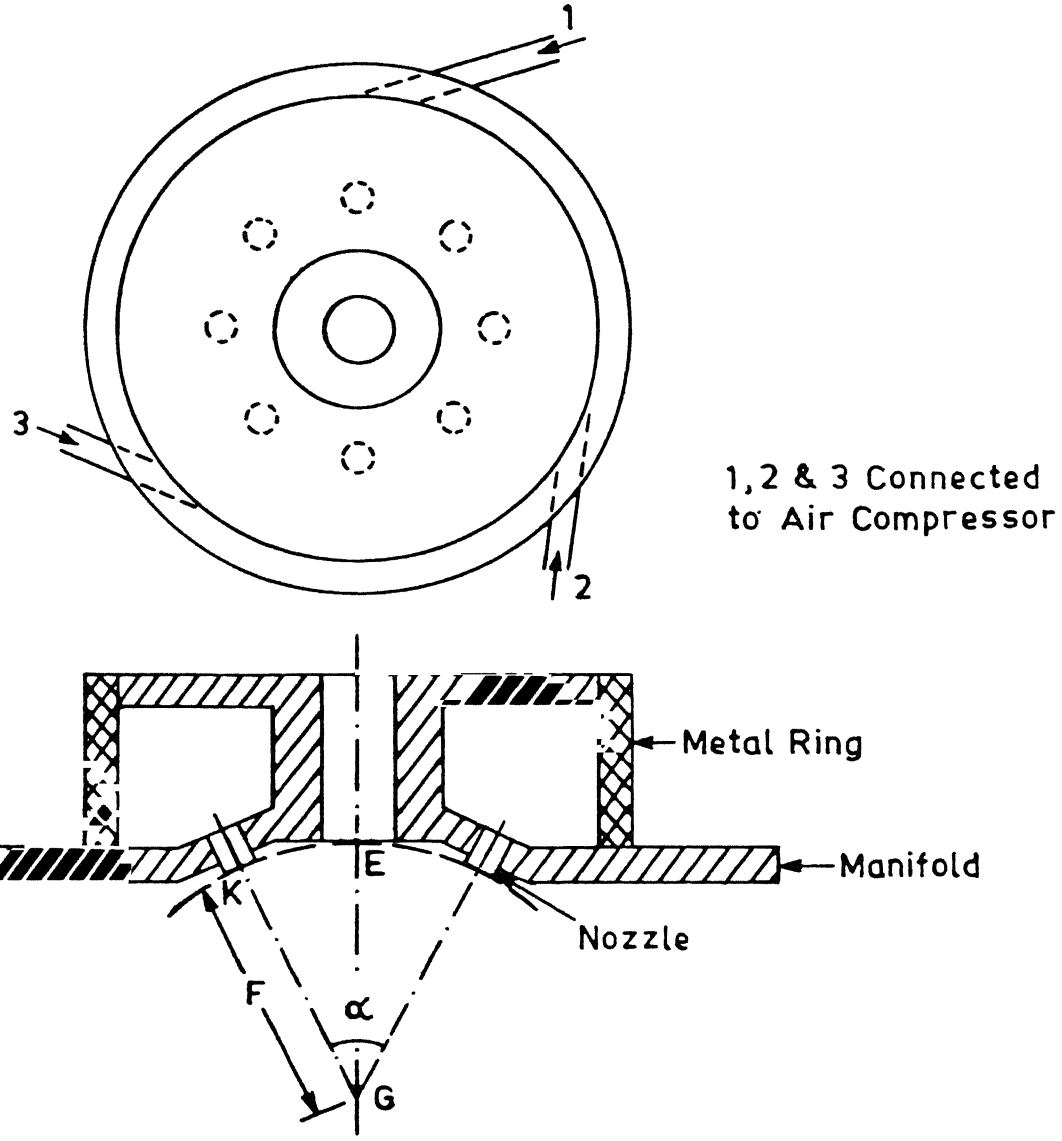

Figure 3.2 : Schematic diagram of the design of a free fall type atomizer

holes) lies on the central axis of the manifold. The holes were plugged according to the desired number of nozzles. Manifolds of apex angle 20°, 40° and 60° were fabricated to obtain atomizers with different focal lengths and number of nozzles. Convergent type nozzles were fitted into the holes such that the arc of a circle (drawn from the geometric point as a center with radius equal to GK) passes through the exit of all the nozzles and the central point E of the manifold (E is the centre of the bottom of the manifold) as shown in the above Figure. The radial distance GK is termed 'focal length' of the atomizer. The throat diameter of each nozzle was either 2 mm or 3 mm. The focal length of the atomizer was varied by using nozzles of different lengths.

A circular groove was machined in the manifold to make a channel for supplying the gas to the nozzles. A metal ring with three separate and equally spaced inlet tubes was fitted tightly over the groove to complete the gas channel as shown in the Figure 3.2. All the three inlets were commonly connected to the air compressor.

The characteristics of all atomizers are described in Table 3.1 by letters A, B, C, a, b and c followed by digits. 'A' and 'a' types of atomizers contain four, 'B' and 'b' six and 'C' and 'c' eight nozzles. The capital letters denote 3 mm nozzle diameter, whereas small ones 2 mm. The first digit X 10 after capital or small letters denote apex angle of the atomizer, whereas later digit (S) X 10 denote focal length of the atomizers. As an example, a27 in Table 3.1 is an atomizer which contains 4 nozzles, each of 2 mm diameter, and it has an apex angle of 20° and focal length of 70 mm. As seen in the above Table, each atomizer is different from another either in its focal length, or apex angle, or number of nozzles, or diameter of nozzle.

Table 3.1: Chracteristics of atomizers

Atomizer	N	D mm	α deg.	F mm
a27	4	2	20	70
a45	4	2	40	50
a47	4	2	40	70
a49	4	2	40	90
a412	4	2	40	120
a65	4	2	60	50
a67	4	2	60	70
a612	4	2	60	120
A27	4	3	20	70
A29	4	3	20	90
A212	4	3	20	120
A45	4	3	40	50
A47	4	3	40	70
A49	4	3	40	90
A412	4	3	40	120
A62	4	3	60	20
A65	4	3	60	50
A67	4	3	60	70
A69	4	3	60	90
A612	4	3	60	120
b412	6	2	40	120
B45	6	3	40	50
B47	6	3	40	70
B49	6	3	40	90
B412	6	3	40	120
B67	6	3	60	70
c412	8	2	40	120
C49	8	3	40	90
C412	8	3	40	120

A, B, C : *Atomizers with* N = *4, 6 and 8, respectively and* D = *3 mm.*
a, b, c : *Same as above but* D = *2 mm.*
Ist *digit after capital or small letter * 10 = apex angle (degree) and following later digit(s) * 10 = focal length (mm).*
Example- A62 : *Atomizer having* N = 4, D = 3 mm, α = 6 * 10 = 60^{o}
F = 2 * 10 = 20 mm.

Table 3.2: Maximum plenum pressures and air flow rates achievable by the air compressor for different types of atomizers

Atomizer	Maximum P kPa	Maximum m gm/s
a type	2100	51.7
b "	1750	54.2
c "	1400	69.7
A "	1950	74.3
B "	1600	88.1
C "	1200	92.6

3.1.1.2 Pressure Measurements

The pressure of air upstream of the atomizer was measured by means of a calibrated pressure transducer (see Figure 3.1 for its location), and it is termed as 'plenum pressure', while the pressures in the air field around the geometric point were measured by a Pitot tube connected to a water/mercury manometer. The Pitot tube was made of stainless steel of 0.7 mm inner diameter x 1.3 mm outer diameter. The Pitot tube was fixed on a traversing mechanism as shown in the Figure 3.1. By means of knobs on the traversing mechanism, it was possible to move the tube spatially within the air field. The accuracy of the movement of the tube was $\pm$ 0.1 mm.

The flow rate was measured by a calibrated rotameter (location of the rotameter is shown in the above Figure). Depending on the number and diameter of nozzles an air compressor gave a sustained air supply at the maximum plenum pressure reported in Table 3.2 for about 10 seconds which was sufficient to atomize 500 gm metal used in the present study.

3.1.2 Atomization Unit

In Figure 3.3 a schematic sketch of the atomization unit is shown which was employed to produce metal powder. In the same set-up solidification distances of droplets in flight are also studied by fixing an additional arrangement of trays which is shown in Figure 3.4.

As shown in Figure 3.3, a resistance type of furnace was used to heat the graphite crucible. At the center of bottom of the crucible an exchangeable graphite tube (hereafter

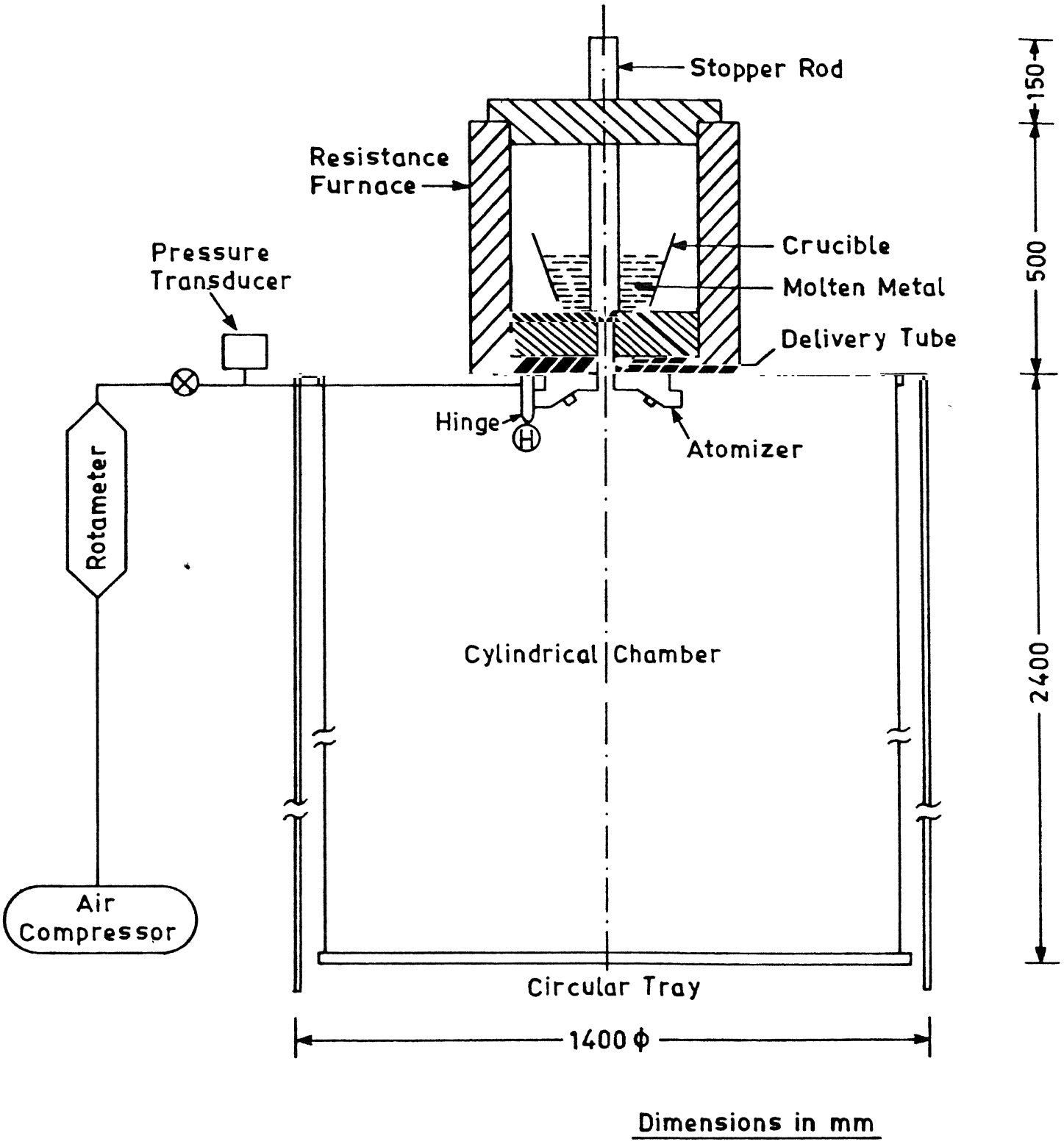

Figure 3.3 : Set-up to study atomization and solidification of droplets during their flight. H is the location for fitting solidification tray arrangement of figure 3.4

termed liquid delivery tube) was fitted to produce the liquid stream. A stopper rod either opens or closes the liquid delivery tube. Different liquid stream rates were obtained by fitting graphite tubes of different internal diameters varying from 3.5 mm to 12.00 mm. The liquid flow rates were calculated by the equation A-1 as shown in Appendix-A, and the values are given in Table 3.3.

The design of the atomizer is described in Section 3.1.1. For the atomization purpose, a hole of 16 mm diameter was drilled at the center of all atomizers of Table 3.1 in order to fit the liquid delivery tube.

The atomizer was mounted on the inner side of a circular plate, while the furnace with the graphite crucible was placed on the outer side such that the axis of the liquid delivery tube passes through the geometric point of atomizer.

The vertically falling liquid stream was atomized in the cylindrical chamber of 1.4 m diameter. The maximum height of the chamber (limited by the space of the room) was 2.4 m. All experiments were carried out by allowing liquid stream to fall at a distance (termed as free fall distance) equal to focal length of the atomizers. Different free fall distances were achieved by rising or lowering the graphite crucible in the furnace and by inserting each time an extra circular metal sheet around the liquid delivery tube so that OD always remains equal to OB (Figure 3.2) for all atomizers of Table 3.1.

In order to know the maximum size of the spherical shape powder particle solidified during their downward movement in the gas stream, six conical trays numbered from 1 to 6 were arranged on a rotating rod at different vertical distances measured from the point G (G = geometric point) such that each successive tray does not interfere with

the other (see Figure 3.4 for values of different distances of trays numbered from 1 to 6). This is achieved by positioning the trays at equal circumferential distances around the rod (see Figure 3.4). The radial dimension of each tray was 300 mm. This arrangement was hinged vertically on the circular plate (see Figure 3.3) at a distance equal to half the radial dimension of the tray. This distance was selected to ensure the passing of the center of each tray through the axis of the atomizer during the rotation of the rod. The rod was rotated manually.

3.2 PROCEDURE

3.2.1 Pressure Measurements

The geometric point was taken as the reference point for the measurement of pressure in the gas field. The Pitot pressures were measured as a function of plenum pressure for all atomizers of Table 3.1, at and upstream (up to the lower surface of the atomizer), and downstream of the geometric point by directing the stagnation point of the Pitot tube opposite to the direction of flow. Pressures were also measured normal to atomizer axis passing through the geometric point. The flow rate of air was also measured simultaneously. Plenum pressure was varied within the range 200 kPa to 1900 kPa. In this way large number of data were collected to investigate the interrelationship between Pitot pressure and parameters characterising the types of atomizer such as focal length, apex angle and number and diameter of nozzles. The range of variation of each parameter is given in Table 3.1.

All measurements were taken for one to three time(s) under identical conditions and the mean was taken. The observed value is therefore equal to mean $\pm \delta$. The value of

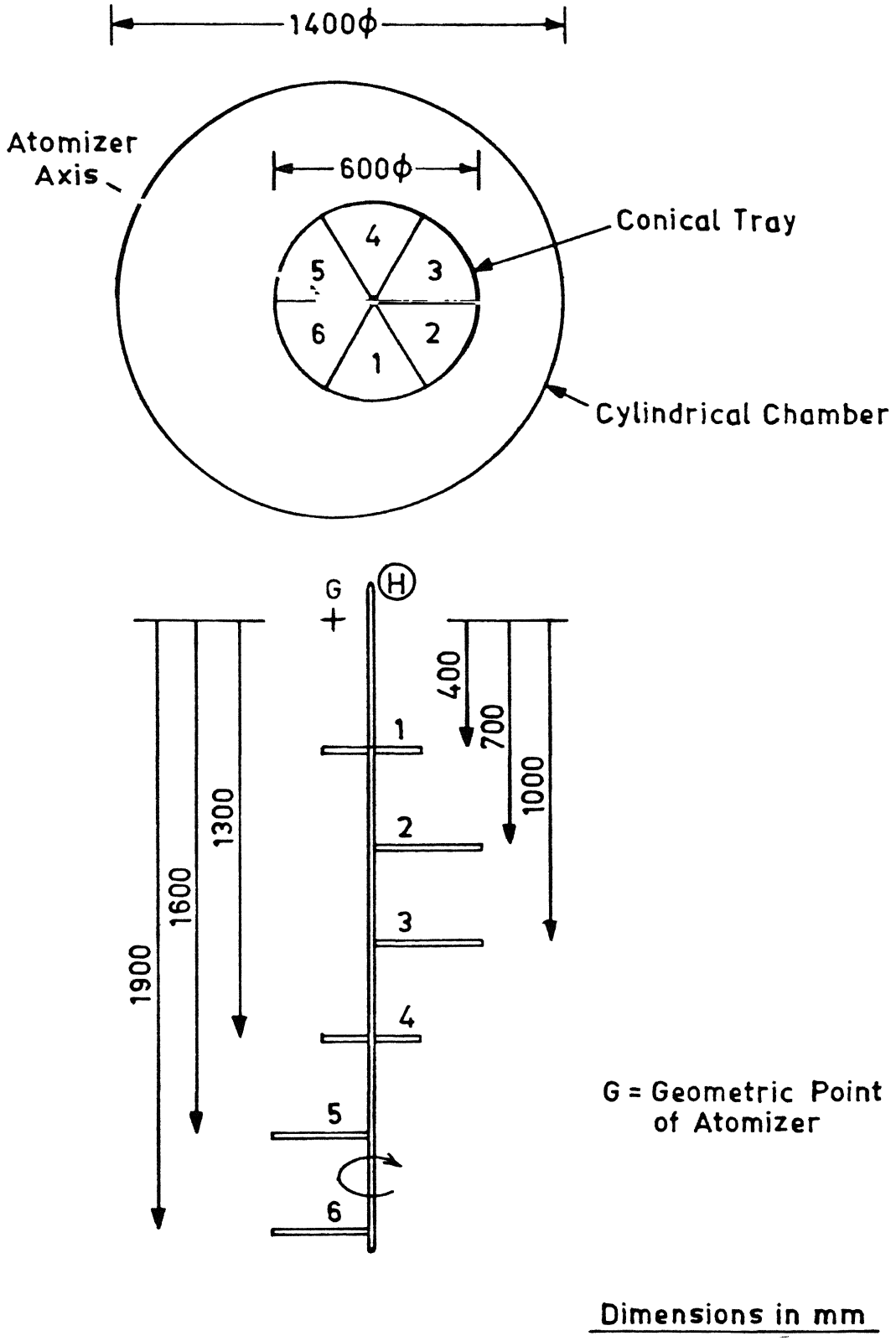

Figure 3.4 : Arrangement of trays to study solidification distances of droplets moving in the gas stream

TABLE 3.3: Characteristics of runs for atomization of liquid metals

Run No	Atomizer	Metal			Gas		Observation		
		ΔT K	d mm	M gm/s	P kPa	m gm/s	O1	O2	O3
1	a27	150	5.5	250	1800	45.0			+ $
2					1900	46.0		+	
3	a45	150	5.5	250	500	12.5			+ $
4					550	13.8		+	
5					500	12.5			+
6	a47	150	5.5	250	800	20.0			+ $
7					900	22.5		+	
8					500	12.5			+
9					700	17.5			+
10	a49	150	5.5	250	1000	25.0			+
11					1500	37.5			+ $
12					1600	38.7		+	
13	a67	150	5.5	250	600	15.0			+ $
14					650	16.2		+	
15	A27	150	5.5	250	1500	56.2			+ $
16					1600	58.0		+	
17					700	27.9			+
18	A212	150	5.5	250	1000	38.9			+
19					1500	56.2			+
20					1900	68.9			+
21	A212	70	5.5	250	1500	56.2			+
22					400	15.6			+
23	A45	150	5.5	250	500	19.5			+ $
24					550	21.9		+	
25					400	15.6			+
26	A47	150	5.5	250	500	19.5			+
27					700	27.9			+ $
28					750	29.2		+	
28M	A47	150	5.5	250	750	29.2		+	
29	A47	150	3.5	76	700	27.9			+ $

O1, O2. O3 : *Type of observation, namely incomplete solidification, deposition and complete solidification of droplets, respectively.*

\+ *against each run : Select the type of observation.*

$ against a run : critical pressure condition

Run No	Atmosphere	Metal			Gas		Observation		
		ΔT K	d mm	M gm/s	P kPa	m gm/s	O1	O2	O3
30					500	19.5			+
31	A49	150	5.5	250	700	27.9			+
32					1000	38.9			+ $
33					1100	41.2		+	
34	A49	150	3.5	76	1000	38.9			+ $
35					700	27.9			+
36	A412	150	5.5	250	1000	38.9			+
37					1500	56.2			+
38					1900	68.9			+
39		150	3.5	76					+
40	A412	150	7.0	357	1000	38.9			+
41		150	9.0	610					+
42		150	12.0	1000					+
43		150	3.5	76					+
44		150	4.5	135					+
45		150	6.0	250					+
46	A412	150	6.3	281	1500	56.2			+
47		150	7.0	357					+
48		150	9.0	610					+
49		150	12.0	1000					+
50		150	3.5	76					+
51	A412	150	7.0	357	1900	68.9			+
52		150	9.0	610					+
53		150	12.0	1000					+
54	A412	70	5.5	250	1500	56.2			+
55	A62	150	5.5	250	200	7.8	+		$
56					250	9.7		+	
57	A65	150	5.5	250	350	13.6	+		$
58					400	15.6		+	
59	A65	110	5.5	250	350	13.6	+		$
60					400	15.6		+	
61	A65	70	5.5	250	350	13.6	+		$
62					400	15.6		+	

O1, O2. O3 : *Type of observation, namely incomplete solidification, deposition and complete solidification of droplets, respectively.*

\+ *against each run : Select the type of observation.*

$ against a run : critical pressure condition

Run No	Atomizer	Metal			Gas		Observation		
		ΔT K	d mm	M gm/s	P kPa	m gm/s	O1	O2	O3
63	A67	150	5.5	250	475	18.5			+ $
64					500	19.5		+	
65	A69	150	5.5	250	675	26.3			+ $
66					700	27.9		+	
67					700	27.9			+
68	A612	150	5.5	250	1000	38.9			+
69					1500	56.2			+ $
70					1600	58.0		+	
71					700	27.9			+
72	A612	70	5.5	250	1000	38.9			+
73					1500	56.2			+ $
74					1600	58.0		+	
75					700	27.9			+
76	A612	110	5.5	250	1000	38.9			+
77					1500	56.2			+ $
78					1600	58.0		+	
79					700	27.9			+
80	A612	190	5.5	250	1000	38.9			+
81					1500	56.2			+
82	B45	150	5.5	250	550	30.7			+ $
83					600	33.9		+	
84	B47	150	5.5	250	700	39.5			+ $
85					800	44.5		+	
86					500	27.9			+
87					700	39.5			+
88	B49	150	5.5	250	1000	55.7			+
89					1100	61.3			+ $
90					1200	65.4		+	
91	B67	150	5.5	250	600	33.5			+ $
92					650	36.7		+	
93					1000	38.9	+		
94	A212	150	5.5	125	1500	56.2			+
95					1900	68.9			+
96	A45	150	5.5	125	450	17.5	+		$
97					500	19.5		+	

O1, O2. O3 : *Type of observation, namely incomplete solidification, deposition and complete solidification of droplets, respectively.*

\+ *against each run : Select the type of observation.*

$ against a run : critical pressure condition

Run No	Atomizer	Metal			Gas		Observation		
		ΔT K	d mm	M gm/s	P kPa	m gm/s	O1	O2	O3
98	A47	150	5.5	125	600	23.4	+		$
99					650	25.9		+	
100	A49	150	5.5	125	950	37.0	+		$
101					1000	38.9		+	
102	A67	150	5.5	125	400	15.6	+		$
103					450	17.5		+	
104	A27	150	5.5	48	900	35.1	+		$
105					1000	38.9		+	
106	A212	150	5.5	48	1500	56.2	+		
107					1900	68.9			+
108	A45	150	5.5	48	350	13.7	+		$
109					400	15.6		+	
110	A47	150	5.5	48	450	17.5	+		$
111					500	19.5		+	
112	A49	150	5.5	48	650	25.3	+		$
113					700	27.9		+	
114	A412	150	5.5	48	1300	50.6	+		$
115					1400	52.4		+	
115M	A412	150	5.5	48	1400	52.4		+	
116	A67	150	5.5	48	300	11.7	+		$
117					400	15.6		+	
118	A612	150	5.5	48	1000	38.9	+		$
119					1100	41.2		+	
120	A212	150	5.5	130	1500	56.2	+		
121					1900	68.9			+

O1, O2. O3 : *Type of observation, namely incomplete solidification, deposition and complete solidification of droplets, respectively.*

\+ *against each run : Select the type of observation.*

$ against a run : critical pressure condition

NOTE

Run 1 to 92 for lead, Run 93 to 103 for zinc, Run 104 to 119 for aluminum and Run 120 to 121 for tin.

δ was found to vary for all atomizers in between 0.0 to 2.1 kPa for the range of plenum pressures of the present study.

3.2.2 Atomization

Aluminum, lead, zinc and tin were atomized in the set-up given in Figure 3.3. For this purpose 500 gm of the respective metal was charged into the crucible. The liquid metal delivery tube was closed with the stopper rod and the metal was heated to the required temperature above its melting point. The stopper rod was lifted, and the liquid metal stream was atomized. In this way the behaviour of the different components of the atomization unit, namely atomizer and cooling chamber was studied at different plenum pressures for various combinations of atomizer and liquid metal related parameters. All these combinations are given in Table 3.3. In addition, powder characteristics was also studied.

3.2.2.1 Behaviour of Cooling Chamber

The behavior of cooling chamber was studied by atomizing different metals at different plenum pressures and observing each time the nature of material collected on the circular tray, as shown in Figure 3.3. The plenum pressure was noted at which the nature of the material on the tray was not completely in the powder form. The runs corresponding to these experiments are indicated under column 01 in Table 3.3 by '+' sign.

3.2.2.2 Behaviour of Atomizer

The behavior of each atomizer, mentioned in Table 3.1, is studied by observing deposition of liquid metal droplets on its surface at the end of each atomization run. The

plenum pressure at which the liquid metal droplets just found to be deposited on the surface of atomizer was noted. The value of plenum pressures prior to the value at which deposition was observed, is termed as critical plenum pressure in the present investigation. All these runs are identified in Table 3.3 under column 02 with '+' and in column 03 with '$' signs.

3.2.2.3 Powder Characteristics

All the powder collectives which were in the form of powder, produced during experiments described in Section 3.2.2.1 and 3.2.2.2 at or below the critical plenum pressure, were used to investigate the power characteristics. All these runs are indicated in Table 3.3 under column 03 with '+' and '$' sign.

To investigate the powder characteristics, the mass balance on each collective is made prior to sieve analysis. The mass balance is given by

$$M_i = M_C + M_R + M_l \qquad (3.1)$$

All symbols used together with their meanings are given in the nomenclature.

Total mass (M_C) collected on the tray was found to consist of a mixture of metal powder and the liquid metal remains. These remains were found to be in the form of large flakes of size greater than around 0.8 mm. It was considered that these flakes were fallen either at the start or toward the end of the run and hence this mass is assumed to be unatomized. Therefore, for the purpose of studying the powder characteristics, the mass retaining on 600 μm sieve was rejected.

Hence, mass for sieve analysis is

$$M_S = M_C - M_+ \qquad (3.2)$$

From the initial mass of the metal (M_i,) mass collected on the tray (M_C), remaining in the crucible (M_R) and mass of large flakes greater than 600 μm (M_+), M_l and M_S were determined by equation (3.1) and (3.2). All the values are given in Table 3.4 The 95% confidence limits of various terms in the equations are as follows:

M_C = 459 ± 1.2 gm

M_R = 26.6 ± 0.7 gm

M_+ = 22.2 ± 1.4 gm

M_l = 14.8 ± 0.8 gm

M_s = 436.4 ± 1.7 gm

The powder collective (M_S) was dry sieved in a mechanical shaker for 30 minutes duration by using the following sieves: 600, 420, 300, 211, 152, 105, 76, 53 and 38 micrometer, respectively. The amount of powder retained on each sieve was weighed. The morphology of powder particles in different size range was studied by scanning electron microscope (SEM) JEOL JXA 840A.

3.2.2.4 Maximum Size of Droplets Solidified in Flight

These experiments were done specifically to know the size of droplets solidified in flight in the same atomization unit (Figure 3.3) by fixing the tray arrangement. Since size of spherical shape particles can be determined exactly as compared to other shapes, therefore experimental parameters were selected such that atomization produces large fraction of spherical shape powder. For this purpose, powder collectives produced under experimental conditions of column 03 of Table 3.3 were examined under SEM for spherical shape. From these observations, type of metal and atomizer and liquid metal

Table 3.4: Mass balance for runs corresponding to complete solidification of droplets (observation 03 of table 3.3)

Run No.	Mc gm	Mr gm	M+ gm	Ml gm	Ms gm
1	453	28	10	19	443
3	457	30	15	13	442
5	459	24	14	17	445
6	452	29	14	19	438
8	459	29	14	12	445
9	463	21	18	16	445
10	464	22	21	14	443
11	458	30	20	12	438
13	457	25	23	17	434
15	460	24	12	16	448
15	467	23	11	10	456
17	460	28	35	12	425
17	461	25	39	14	422
18	479	13	11	8	468
18	478	12	14	10	464
19	458	23	40	19	418
20	446	32	39	22	407
21	462	23	15	15	447
22	458	24	29	18	429
23	463	28	31	9	432
23	454	27	12	19	442
25	458	21	12	21	446
25	461	26	26	13	435
26	463	27	32	10	431
26	454	29	22	17	432
27	466	22	24	12	442
27	472	19	34	9	438
29	463	23	21	14	442
30	465	17	25	18	440
30	462	25	11	13	451
31	462	22	20	16	442
31	452	29	13	19	439
32	461	21	10	18	451
32	462	27	17	11	445
34	453	28	14	19	439
35	461	28	12	11	449
35	466	24	12	10	454
35	466	25	19	9	447
36	467	24	26	9	441
36	460	26	22	14	438
37	460	28	23	12	437
37	464	26	32	10	432
38	456	30	28	14	428

Run No.	Mc gm	Mr gm	M+ gm	Ml gm	Ms gm
38	459	28	36	13	423
39	461	26	31	13	430
39	452	27	26	21	426
39	454	22	23	24	431
40	462	23	15	15	447
40	457	25	11	18	446
40	451	27	13	22	438
41	462	22	23	16	439
41	458	29	27	13	431
41	462	21	31	17	431
42	465	26	40	9	425
42	461	28	19	11	442
43	470	24	30	6	440
43	465	28	34	7	431
44	460	25	39	15	421
45	465	29	31	6	434
45	460	30	28	10	432
45	461	24	17	15	444
46	462	29	15	9	447
46	460	28	10	12	450
46	463	26	16	11	447
47	465	24	31	11	434
48	463	24	33	13	430
48	461	28	32	11	429
49	462	24	40	14	422
49	467	23	35	10	432
50	456	35	38	9	418
50	462	28	32	10	430
50	462	26	31	12	431
51	451	26	19	23	432
51	458	28	26	14	432
51	452	29	29	19	423
52	459	29	29	12	430
52	464	24	28	12	436
52	456	29	28	15	428
53	463	23	33	14	430
53	463	26	33	11	430
53	457	24	17	19	440
54	464	21	17	15	447
63	460	23	26	17	434
63	460	26	16	14	444
65	458	25	31	17	427
65	462	27	26	11	436

Run No.	Mc gm	Mr gm	M+ gm	Ml gm	Ms gm
67	453	25	21	22	432
67	447	32	16	21	431
68	459	26	18	15	441
68	462	32	12	6	450
68	460	31	12	9	448
69	451	30	9	19	442
69	449	33	15	18	434
69	447	25	20	28	427
71	454	24	16	22	438
71	449	28	16	23	433
71	447	32	18	21	429
72	469	24	26	7	443
72	439	41	17	20	422
72	448	35	17	17	431
73	461	28	18	11	443
73	468	22	24	10	444
73	444	33	26	23	418
75	450	29	24	21	426
75	444	32	25	24	419
75	443	35	26	22	417

Run No.	Mc gm	Mr gm	M+ gm	Ml gm	Ms gm
76	444	37	21	19	423
76	443	36	25	21	418
77	468	21	27	11	441
77	462	28	23	10	439
80	452	35	23	13	429
81	448	27	19	25	429
81	460	26	13	14	447
82	449	30	12	21	437
84	461	23	13	16	448
86	457	29	15	14	442
87	462	27	23	11	439
88	461	29	27	10	434
89	454	31	16	15	438
91	452	27	18	21	434
94	455	29	32	16	423
95	445	37	23	18	422
95	448	33	27	19	421
107	471	18	25	11	456
121	446	33	36	21	415
121	447	36	28	17	419

related parameters were determined to perform these experiments. 500 gm of liquid metal was atomized in the same way as described in Section 3.2.2.1. The droplets were collected on the various rotating trays positioned at different vertical distances. At the end of the experiment, SEM observations were made on the powder sample collected from each tray to determine the maximum size of the spherical powder particle.

CHAPTER - 4

RESULTS

The chapter describes the experimental results on dynamics of gas flow rate through atomizers, and atomization of liquid metals. All the measured values of Pilot pressure are given in Table 4.1 to 4.3. In the free fall atomization, velocity of atomization gas rather than Pilot pressure is a very useful parameter. Therefore, all the results reported in Table 4.1 to 4.3 were converted into velocity by equation B-4 derived in Appendix - B. In the following, results on velocity and their variation are presented for different plenum pressures as a function of parameters characterising the atomizer design. Description is also given about the results on atomization in terms of critical pressure for atomization, powder characteristics and size of spherical particles solidified during their flight.

4.1 GAS VELOCITY VARIATION

The velocity values had shown that the atomization gas field created by impingement of gas jets is dynamic in nature i.e. the gas field has large variation in velocities even when the atomizer is operated at constant pressure. In the following, these variations in velocities are classified and effect of each variable on the velocity variation is presented.

TABLE 4.1: Pitot pressure (kPa) as a function of plenum pressure at geometric point of atomizers of different types

Atomizer	Plenum pressure, kPa					
	200	400	700	1000	1500	1900
a45	-	-	9.6	25.6	67.6	-
	-	-	9.6	25.6	67.0	-
a412	-	-	1.3	3.9	8.2	-
a65	-	-	9.5	25.2	66.8	90.2
	-	-	9.5	25.0	67.4	94.0
a612	-	-	1.3	3.9	8.2	9.7
	-	-	1.3	3.9	8.2	9.7
A27	1.1	4.0	13.2	23.7	50.0	-
	1.1	4.0	13.2	23.7	49.0	-
A29	0.8	2.6	7.4	14.5	35.4	56.4
	0.8	2.6	7.4	14.5	36.2	56.1
A212	-	-	2.1	4.6	9.7	17.2
	-	-	2.1	4.6	9.7	17.2
A45	1.2	5.0	17.8	35.2	79.0	-
	1.2	5.0	17.8	36.0	80.1	-
	1.2	5.0	17.8	35.8	78.0	-
A47	1.1	4.0	13.2	23.7	51.6	-
	1.1	4.0	13.2	23.7	49.1	-
	1.1	4.0	13.2	23.7	49.3	-
A49	0.8	2.6	7.4	14.5	35.4	59.1
	0.8	2.6	7.4	14.5	37.0	57.1
	0.8	2.6	7.4	14.5	35.6	57.5
A412	-	-	2.1	4.6	9.7	17.1
	-	-	2.1	4.6	9.7	17.1
	-	-	2.1	4.6	9.7	17.1
A62	1.6	10.3	22.3	72.0	-	-
	1.6	10.6	25.0	72.4	-	-
	1.6	10.3	23.7	69.7	-	-
A65	1.2	5.0	17.8	35.0	82.2	-
	1.2	5.0	17.8	36.2	83.6	-
	1.2	5.0	17.8	36.2	81.4	-
A67	1.1	4.0	13.2	23.6	53.7	89.6
	1.1	4.0	13.2	23.6	51.8	87.1
	1.1	4.0	13.2	23.6	51.2	88.0

Atomizer	Plenum pressure, kPa					
	200	400	700	1000	1500	1900
A69	0.8	2.6	7.4	14.5	35.2	60.2
	0.8	2.6	7.4	14.5	35.8	58.1
	0.8	2.6	7.4	14.5	36.4	57.8
A612	-	-	2.1	4.6	9.7	17.0
	-	-	2.1	4.6	9.7	17.0
	-	-	2.1	4.6	9.7	17.0
b412	-	-	1.0	3.5	6.9	-
B47	-	-	8.2	18.0	38.4	-
	-	-	8.2	17.2	37.8	-
B49	-	-	6.8	13.6	30.0	-
	-	-	6.8	13.6	30.4	-
B412	-	-	1.9	3.8	8.1	-
	-	-	1.9	3.8	8.1	-
c412	-	-	1.0	3.1	-	-
C49	-	-	6.1	12.6	-	-
C412	-	-	1.6	3.5	-	-

Table 4.2: Pitot pressure (kPa) as a function of plenum pressure and distance measured along axis of atomizer of different types

Atomizer	P	Downstream distance from geometric point, mm						
	kPa	10	20	40	60	90	150	250
a412	1500	8.2	6.6	5.0	2.9	2.0	0.5	0.1
	1500	8.2	6.6	5.0	2.9	2.0	0.5	0.1
	1000	35.2	21.4	10.5	5.0	2.2	0.9	0.3
A45	1000	36.0	21.8	11.0	5.0	2.2	0.9	0.3
	1500	79.0	52.0	24.3	9.7	4.2	1.6	0.6
	1500	80.1	53.6	25.3	9.7	4.2	1.6	0.6
	1000	14.5	12.9	7.4	5.0	3.1	1.0	0.4
A49	1000	14.5	12.4	7.7	5.0	3.1	1.0	0.4
	1500	35.4	27.4	18.9	8.2	6.0	2.4	0.9
	1500	37.0	28.0	19.4	8.2	6.0	2.4	0.9
	700	2.1	1.8	1.6	1.4	1.2	0.4	0.2
	700	2.1	1.8	1.6	1.4	1.2	0.4	0.2
	1000	4.6	4.3	3.8	3.6	2.6	0.9	0.3
A412	1000	4.6	4.3	3.8	3.6	2.6	0.9	0.3
	1500	9.7	9.2	8.3	6.6	4.2	1.8	0.6
	1500	9.7	9.2	8.3	6.6	4.2	1.8	0.6
	1900	17.1	16.0	13.9	11.6	8.7	2.9	1.0
	1900	17.1	16.0	13.9	11.6	8.7	2.9	1.0
b412	1500	6.9	5.9	4.0	3.2	2.5	0.8	0.2
	1500	6.9	5.9	4.0	3.2	2.5	0.8	0.2
B412	1500	8.2	7.3	5.8	5.0	3.1	1.0	0.5
	1500	8.2	7.3	5.8	5.0	3.1	1.0	0.5

Atomizer	P kPa	Upstream distance from geometric point, mm					
		5	10	20	30	40	50
a412	1500	8.2	8.2	8.2	6.8	3.2	1.0
	1500	8.2	8.2	8.2	6.8	3.2	1.0
A45	1000	36.0	29.0	13.4	5.6	0.0	0.0
	1000	36.0	29.4	13.0	5.6	0.0	0.0
	1500	-	40.0	19.2	7.0	0.1	0.0
	1500	-	40.4	18.8	7.0	0.1	0.0
A49	1000	14.5	14.5	10.1	5.3	2.1	1.3
	1000	14.5	14.5	10.1	5.3	2.1	1.3
	1500	36.8	36.2	30.2	17.8	10.6	1.8
	1500	35.6	35.8	30.6	17.8	10.6	2.1
A412	700	2.1	2.1	2.1	1.4	0.4	0.0
	700	2.1	2.1	2.1	1.4	0.4	0.0
	1000	4.6	4.6	4.6	4.4	2.1	0.3
	1000	4.6	4.6	4.6	4.4	2.1	0.3
	1500	9.7	9.7	9.7	8.9	4.2	1.1
	1500	9.7	9.7	9.7	8.9	4.2	1.1
	1900	17.1	17.1	17.1	15.7	6.7	1.8
	1900	17.1	17.1	17.1	15.7	6.7	1.8
b412	1500	6.9	6.9	6.9	5.9	2.2	0.5
	1500	6.9	6.9	6.9	5.9	2.2	0.5
B412	1500	8.2	8.2	8.2	6.6	3.0	0.8
	1500	8.2	8.2	8.2	6.6	3.0	0.8

Table 4.3: Pitot pressure (kPa) as a function of plenum pressure and distance measured normal to axis ofatomizer of different types

Atomizer No.	Y mm	Plenum pressure, kPa			
		700	1000	1500	1900
a45	1	9.5	25.2	67.2	-
	1	9.5	25.2	67.0	-
	2	9.5	16.0	40.2	-
	2	9.5	16.0	39.8	-
	4	6.3	6.7	16.0	-
	6	4.2	3.0	6.8	-
	8	2.6	1.3	2.9	-
	10	1.8	0.5	1.3	-
a412	2	1.3	3.9	8.2	-
	4	1.3	3.4	5.4	-
	6	1.0	2.8	3.4	-
	8	0.8	2.0	2.4	-
	10	0.6	1.4	1.6	-
	12	0.5	1.0	1.0	-
A45	2	17.8	36.0	79.0	-
	4	10.8	22.0	42.0	-
	6	6.8	14.0	26.0	-
	10	2.0	5.0	10.0	-
A412	2	2.1	4.6	9.7	17.1
	4	2.1	4.6	9.7	17.1
	5	2.1	-	-	-
	6	1.8	3.4	8.6	14.4
	8	1.4	3.0	7.2	11.0
	12	1.0	2.1	5.0	8.0
B412	4	1.9	3.8	8.1	-
	8	1.9	3.3	6.3	-
	12	1.5	3.0	4.5	-
	16	1.3	1.8	1.9	-

4.1.1 GEOMETRIC POINT

4.1.1.1 Effect of Plenum Pressure

Figures 4.1 and 4.2 show velocity as a function of plenum pressure for different types of atomizers. Figure 4.1 is for A6 (solid lines) and a6 (dashed lines) atomizer types of different focal lengths and nozzle diameter but same apex angle and number of nozzles, whereas Figure 4.2 is for atomizers A2, A4 and B4 types of different apex angles, focal lengths and number of nozzles but same nozzle diameter.

It can be observed that the velocity is higher for all atomizers containing nozzle of 3 mm diameter as compared with that of 2 mm at all plenum pressures as shown in Figure 4.1. For example at a plenum pressure of 1500 kPa, the velocity of atomizer A612 is 125 m/s, whereas it is 115 m/s for atomizer a612.

In both Figures the atomizers of smaller focal lengths produce larger velocities as compared with that of greater focal lengths at all plenum pressures irrespective of apex angle, number and diameter of nozzles. The increase in velocity with increase in plenum pressure is faster in the initial range of plenum pressure as compared with that in later range. Consider the variation in velocity for atomizer A65 in Figure 4.1. The increase in velocity is 117 m/s (from 45 m/s to 162 m/s) for a 500 kPa change in plenum pressure in the initial range (200 kPa to 700 kPa). Whereas it is 73 m/s (225 m/s to 298 m/s) for a similar change in plenum pressure in the later range (1000 kPa to 1500 kPa). Similarly for atomizer A69 increase in velocity is 80 m/s (32 m/s to 112 m/s) when plenum pressure increases by 500 kPa (200 kPa to 700 kPa) but the increase is 68 m/s (152 m/s to 220 m/s) when plenum pressure increases by the same value of 500 kPa (1000 kPa to 1500 kPa).

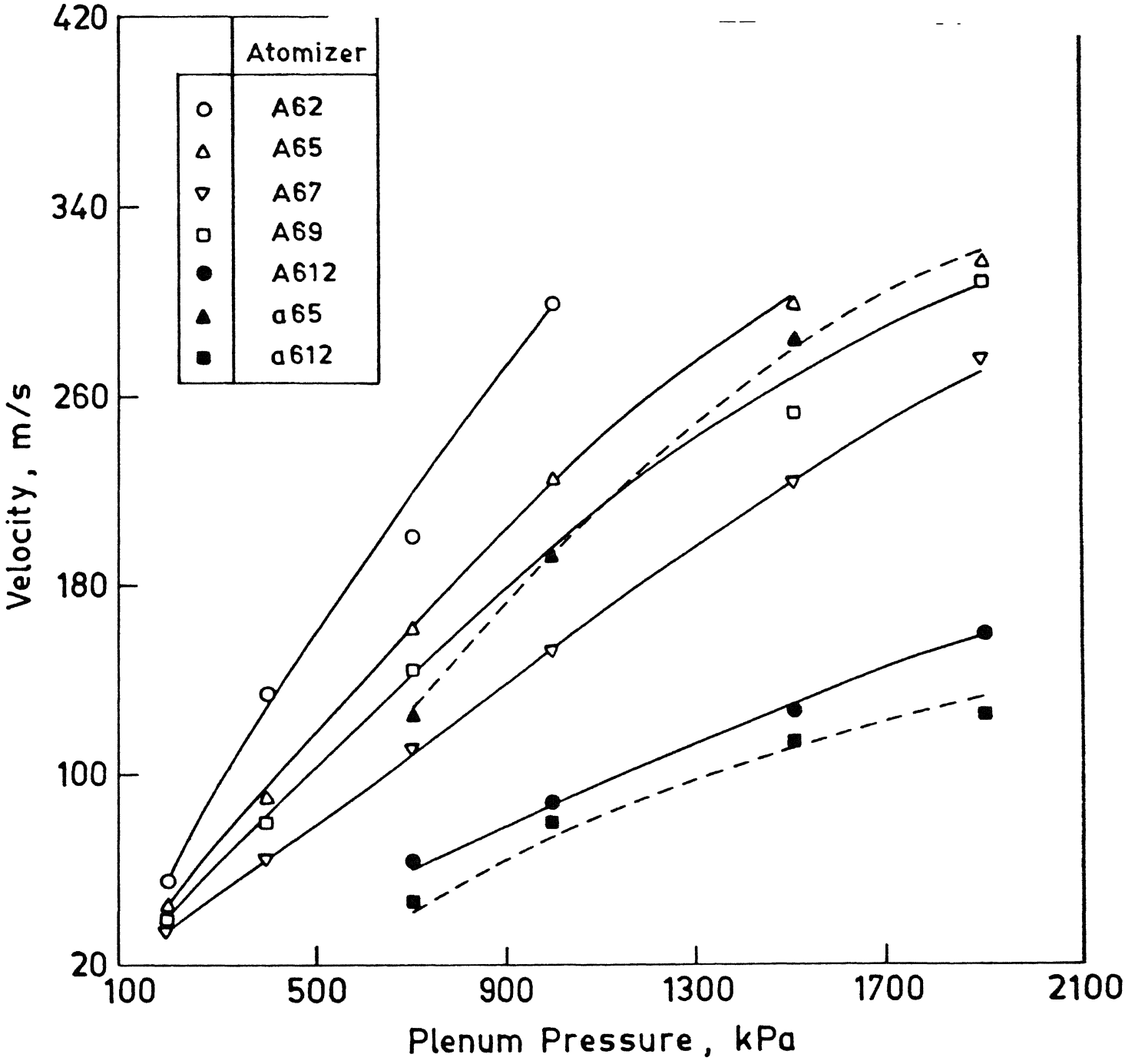

Figure 4.1 : Variation of air velocity at geometric point as a function of plenum pressure for atomizers of 60° apex angle

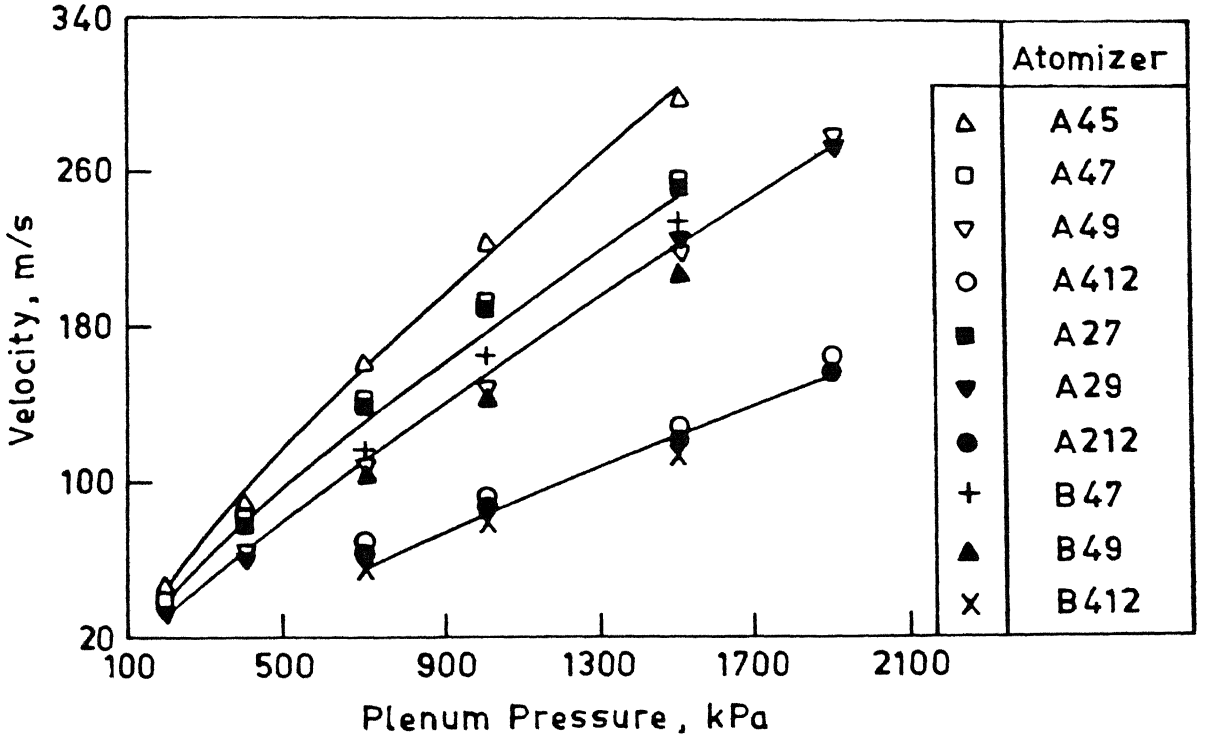

Figure 4.2 : Variation of air velocity at geometric point as a function of plenum pressure for atomizers of 20° and 40° apex angle

Thus, it appears from Figures 4.1 and 4.2 that the effect of change in plenum pressure on increase in velocity is smaller for atomizers of greater focal lengths as compared with that of smaller ones irrespective of the apex angle of the atomizer. Similar observations can be made for other atomizers at other ranges of lower and higher pressures.

The change in either apex angle or number of nozzles according to Figure 4.2 resulted in the behaviour similar to that reported above.

4.1.1.2 Effect of Focal Length

In the Figure 4.3 the velocity is shown as a function of focal length at various plenum pressures for atomizers of A6, A4 and A2 types having same number and diameter of nozzles, but different apex angles. It can be seen that the velocity increases with the decrease in focal length at all plenum pressures for all atomizers. Consider the velocity variation at 700 kPa and 1500 kPa for atomizer of A6 types. At 700 kPa plenum pressure, the velocity increases by 98 m/s (62 m/s to 160 m/s) by decreasing the focal length from 120 mm to 50 mm. Whereas increase in velocity is 173 m/s (125 m/s to 298 m/s) at 1500 kPa for the same reduction in focal length. Similar observations can be made at other plenum pressures. It appears that the increase in velocity as attained by decrease in focal length is higher at higher plenum pressures.

4.1.1.3 Effect of Apex Angle

Figure 4.4 shows the velocity of air as a function of apex angle of atomizers A6, A4 and A2 types of different focal lengths at various plenum pressures. The experimental results show that the velocity is almost independent of apex angles of atomizers at all plenum pressures.

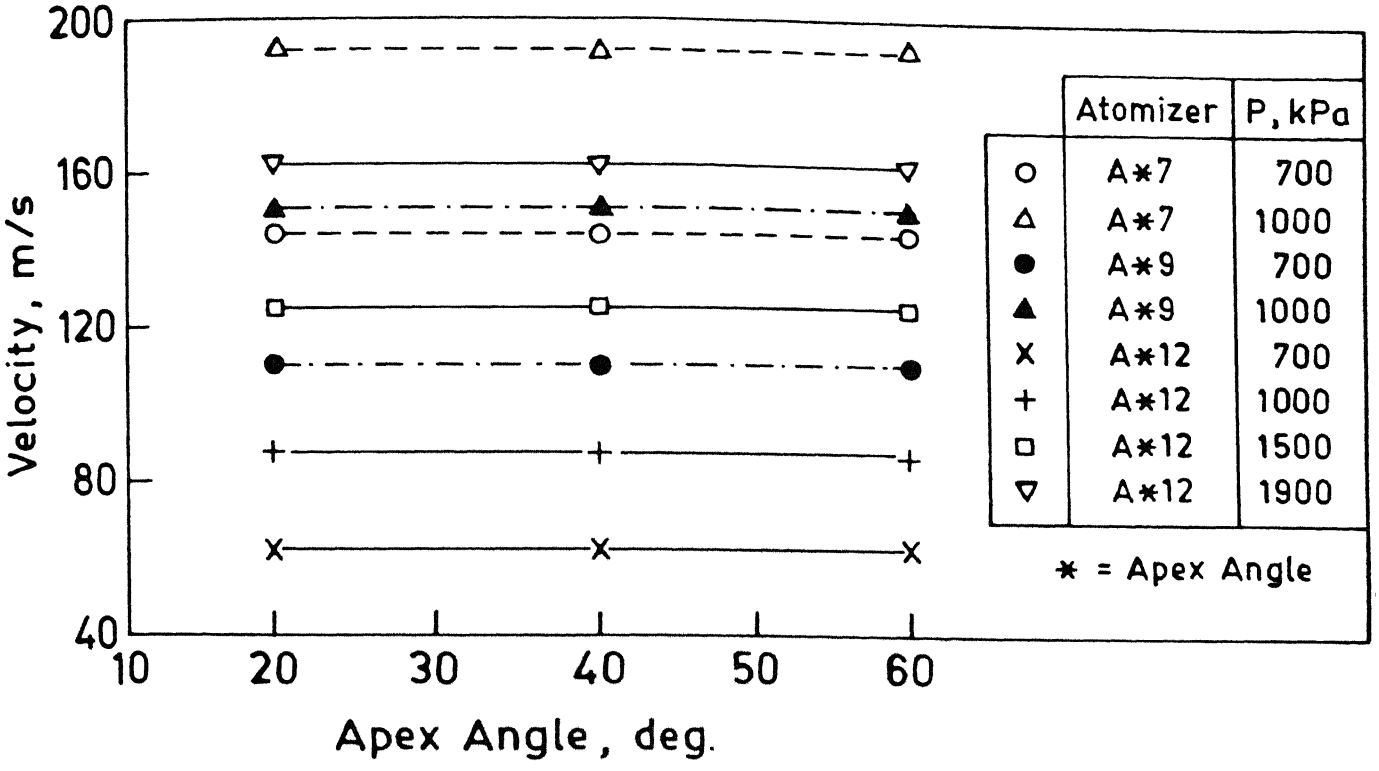

Figure 4.4 : Variation of air velocity with apex angle at the geometric point

4.1.1.4 Effect of Number of Nozzles

Figure 4.5 shows the variation of velocity as a function of number of nozzles at different plenum pressures for different types of atomizers having same apex angle and focal length. The variation is shown for atomizers of a, b, c type (nozzle diameter 2 mm, dashed lines) and A, B, C type (nozzle diameter 3 mm, solid lines). It can be seen that velocity is almost independent of the number of nozzles at all plenum pressures and nozzle diameters.

4.1.2 ALONG THE AXIS OF ATOMIZERS

Figures 4.6 and 4.7 show the variation of velocity with vertical distance measured along the axis of atomizer passing through the geometric point. In Figure 4.6 this variation is shown at different plenum pressures for atomizers A45, A49 and A412 type of different focal lengths (solid lines for 120 mm, dashed lines 90 mm and dotted dashed 50 mm). Whereas Figure 4.7 shows a similar plot at constant plenum pressure for atomizers A412, B412 and b412 types of different numbers and nozzle diameters. The vertical distances downstream of the geometric point are shown positive and those of upstream negative. The origin in both the Figures is the geometric point of all atomizers.

It can be seen in both the Figures that the velocity remains constant up to about 12±3 mm in both upstream as well as downstream of the geometric point. Beyond this distance, the velocity decays faster along the upstream side as compared with that of the downstream. For example, consider variation in velocity upstream and downstream of the geometric point of atomizer A412 operated at 1000 kPa plenum pressure. For the same vertical distance of 50 mm on both sides of the geometric point the upstream velocity

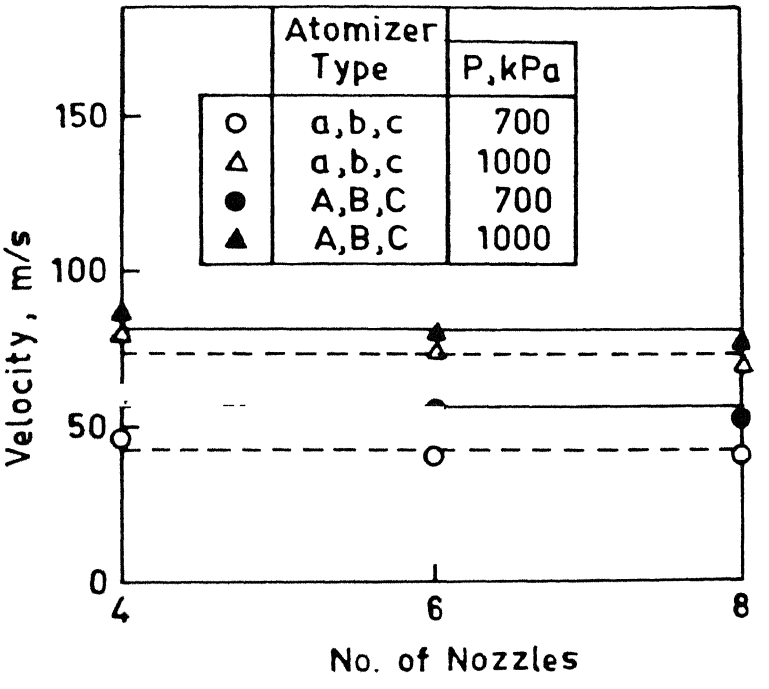

Figure 4.5 : Variation of air velocity with number of nozzles at the geometric point

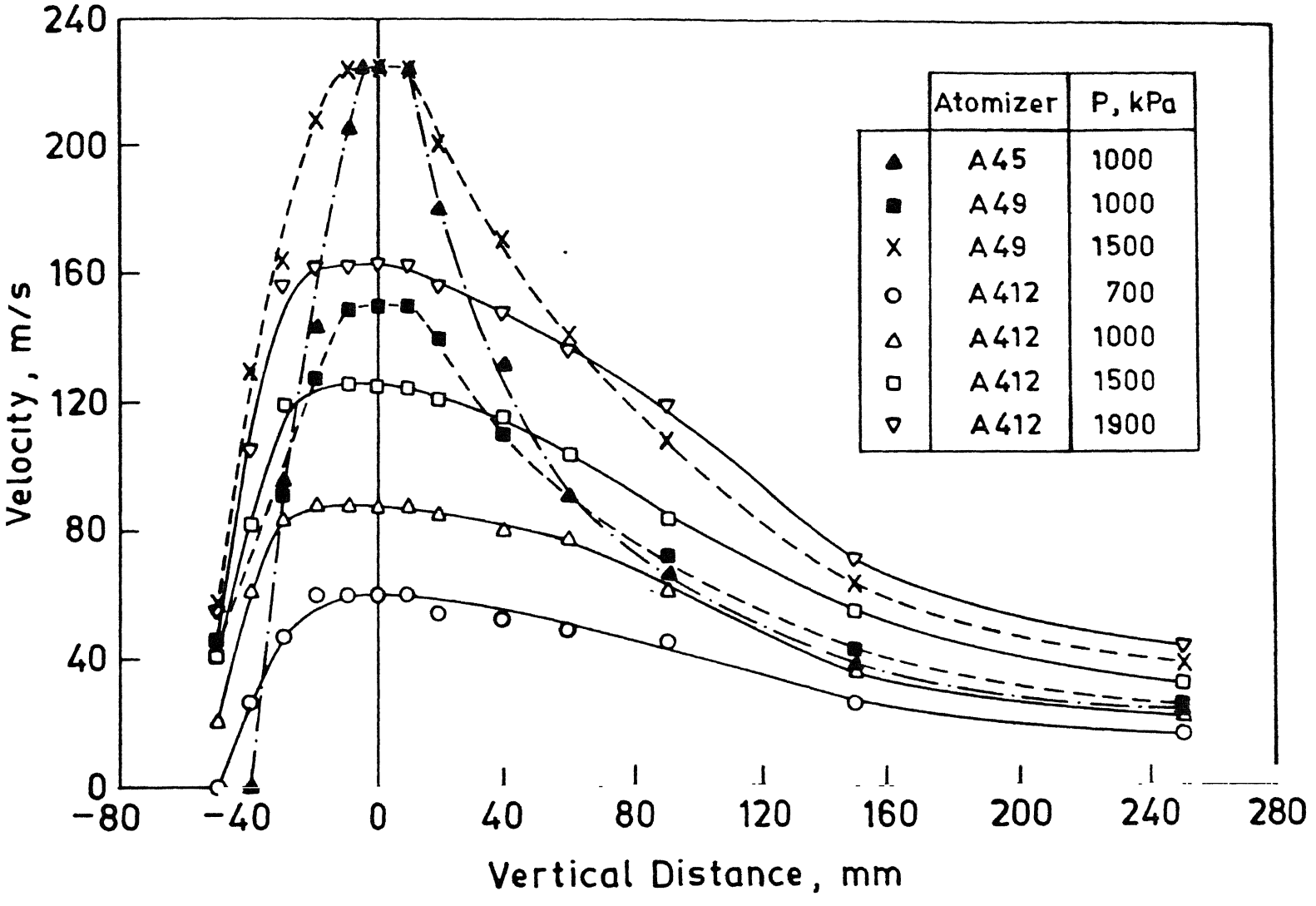

Figure 4.6 : Air velocity as a function of vertical distance measured from geometric point of atomizers containing four nozzles of 3 mm diameter

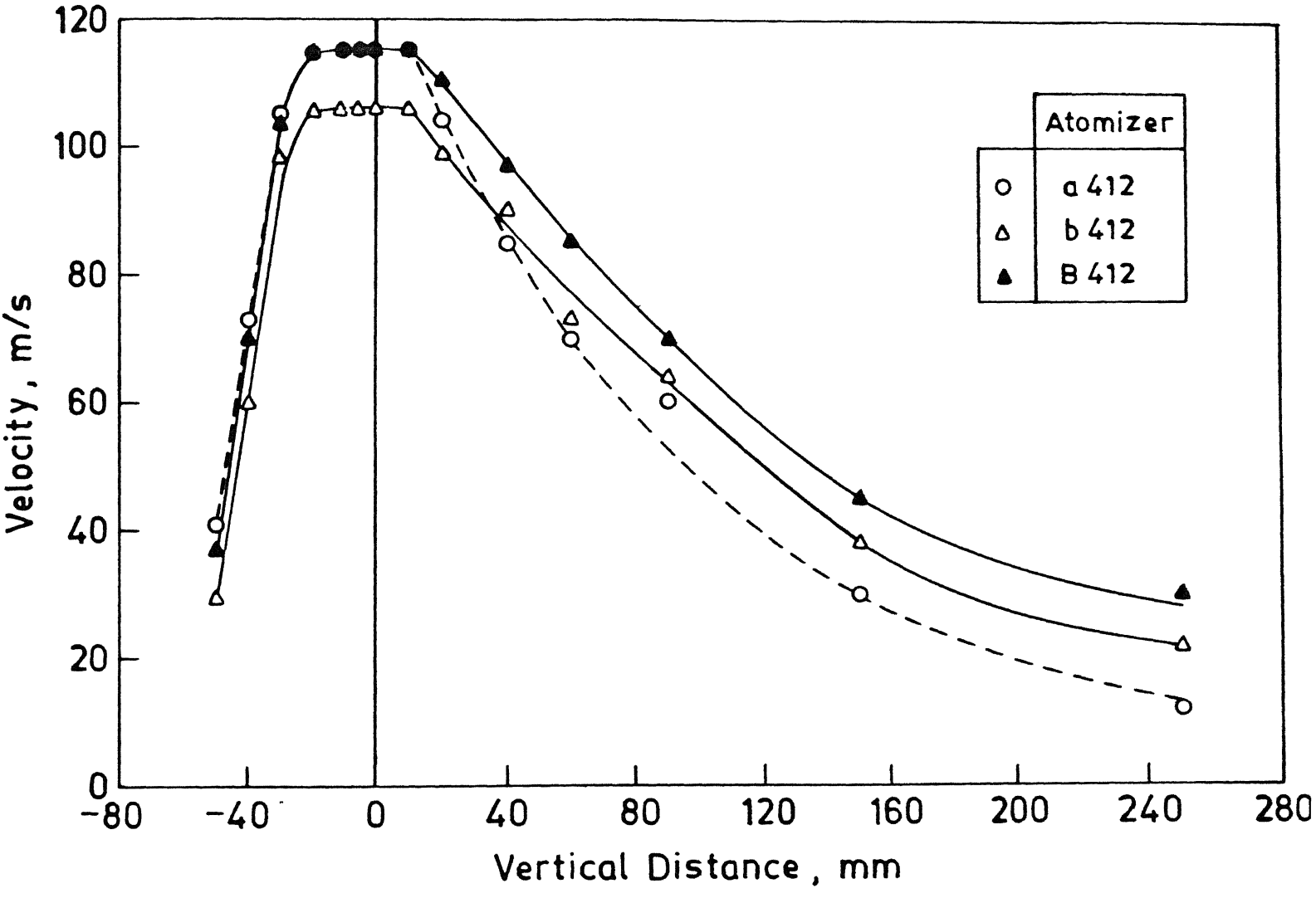

Figure 4.7 : Air velocity as a function of vertical distance measured from geometric point (P = 1500 kPa) of atomizers

decreases to a very small value, i.e. from 87 m/s (This velocity is at geometric point.) to 20 m/s whereas the downstream velocity decreases to a very small value, i.e. from 87 m/s to 80 m/s. Further, the upstream velocity becomes almost negligible at a short distance beyond 50 mm but the downstream velocity decays very slowly with the downstream distance as observed in Figure 4.6. Similar trend of variation of velocity produced by atomizers of other focal lengths with vertical distance can be seen in Figure 4.6 at other plenum pressures.

The decay of velocity with distance depends on the velocity at the geometric point (The velocity at geometric point is at Z=0 in the Figure). Higher velocity at the geometric point as attained by either larger plenum pressures, larger nozzle diameter or smaller focal lengths results in faster decrease in upstream and downstream velocity with distance as compared with that of smaller pressures and larger focal lengths. For example in Figure 4.6 consider atomizers A49 and A412 operating at a plenum pressure of 1500 kPa. The air velocity decreases by 103 m/s, i.e. from 223 m/s at geometric point to 120 m/s at a vertical distance of 80 mm for atomizer A49. Whereas, it decreases by 33 m/s, i.e. from 125 m/s at geometric point to 92 m/s at the same vertical distance of 80 mm for atomizer A412.

4.1.3 NORMAL TO THE AXIS OF ATOMIZER

Figures 4.8 to 4.10 show the variation of air velocity as a function of horizontal distance measured normal to atomizer axis from the geometric point for various atomizers operated at different plenum pressures. Figure 4.8 shows this variation for atomizers A412 (solid lines) and a412 (dashed lines) having different nozzle diameter but same focal

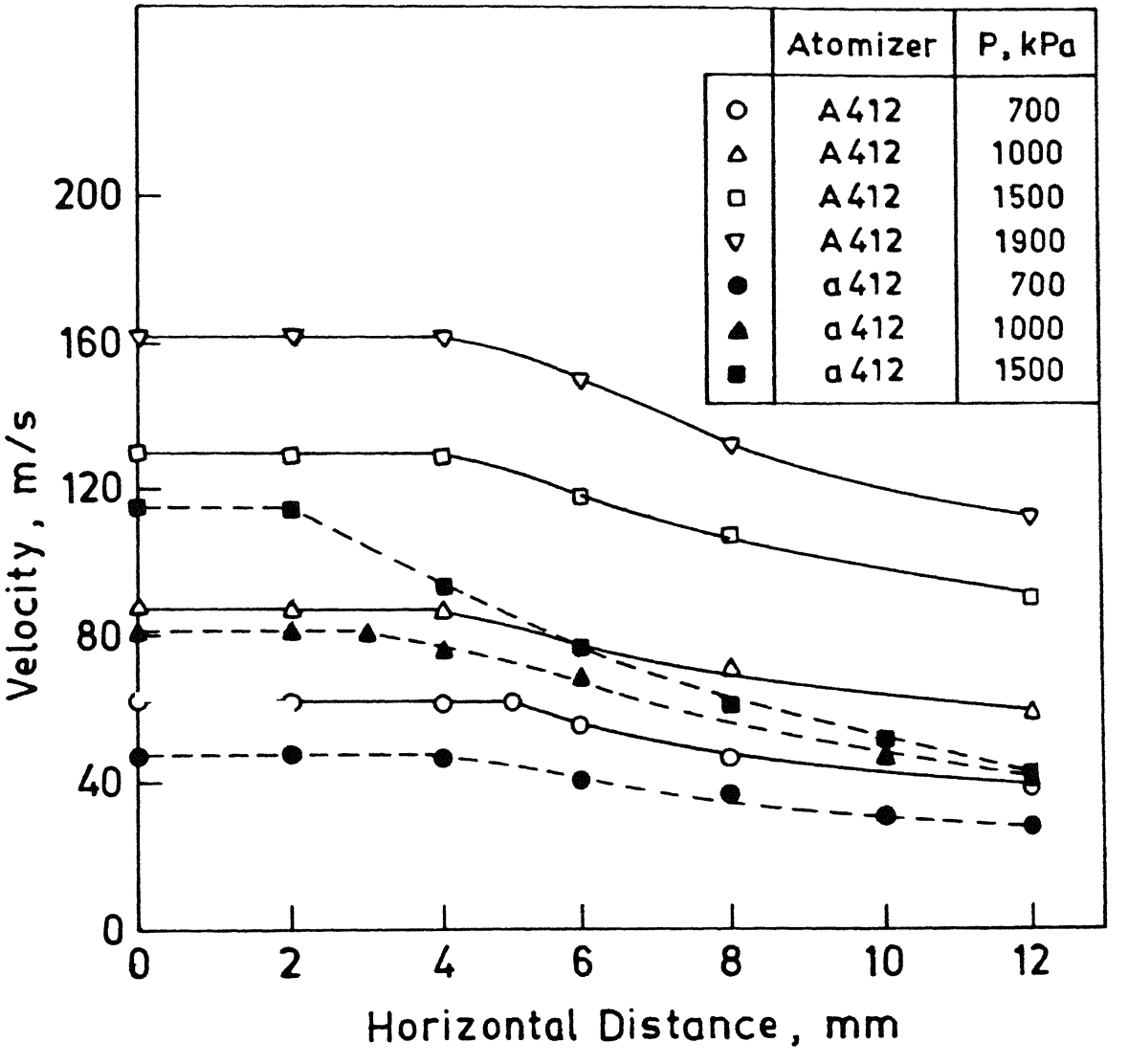

Figure 4.8 : Velocity of air as a function of horizontal distance from the geometric point of atomizers whose focal length is 120 mm

length, apex angle and number of nozzles. Figure 4.9 show this variation for atomizer B412 of the same characteristics parameters except number of nozzles which are equal to 6. Figure 4.10 is for atomizers A45 (solid line) and a45 (dashed lines) having same focal length, apex angle and number of nozzles but different nozzle diameter.

It can be seen that the velocity remains constant up to a distance of 1 mm to 8 mm for atomizers of different focal lengths, number and nozzle diameters operated at different plenum pressures. Beyond this distance the velocity decreases with increase in horizontal distance; the decrease, however, depends more on nozzle diameter than on plenum pressure irrespective of focal lengths of atomizers. For example, consider variation of velocities with horizontal distance in Figure 4.8 at 1500 kPa and 700 kPa plenum pressures. The decrease in velocity is 70 m/s (114 m/s to 90 m/s) for 3 mm nozzle diameter at 1500 kPa. The above values are 19 m/s (47 m/s to 28 m/s) and 22 m/s (62 m/s to 40 m/s) at 700 kPa plenum pressure. This suggests that smaller nozzle diameter of an atomizer for a given plenum pressure (or gas rate) produces lower velocities as compared with larger nozzle diameter. But the magnitude of decrease in velocity due to increase in horizontal distance occurs relatively faster for smaller nozzle diameter as compared with larger ones, and this effect is more pronounced at larger plenum pressures as compared with lower ones. Similar observations can be made for the atomizers of different number of nozzles (Figure 4.9) and focal lengths (Figure 4.10) operated at various plenum pressures.

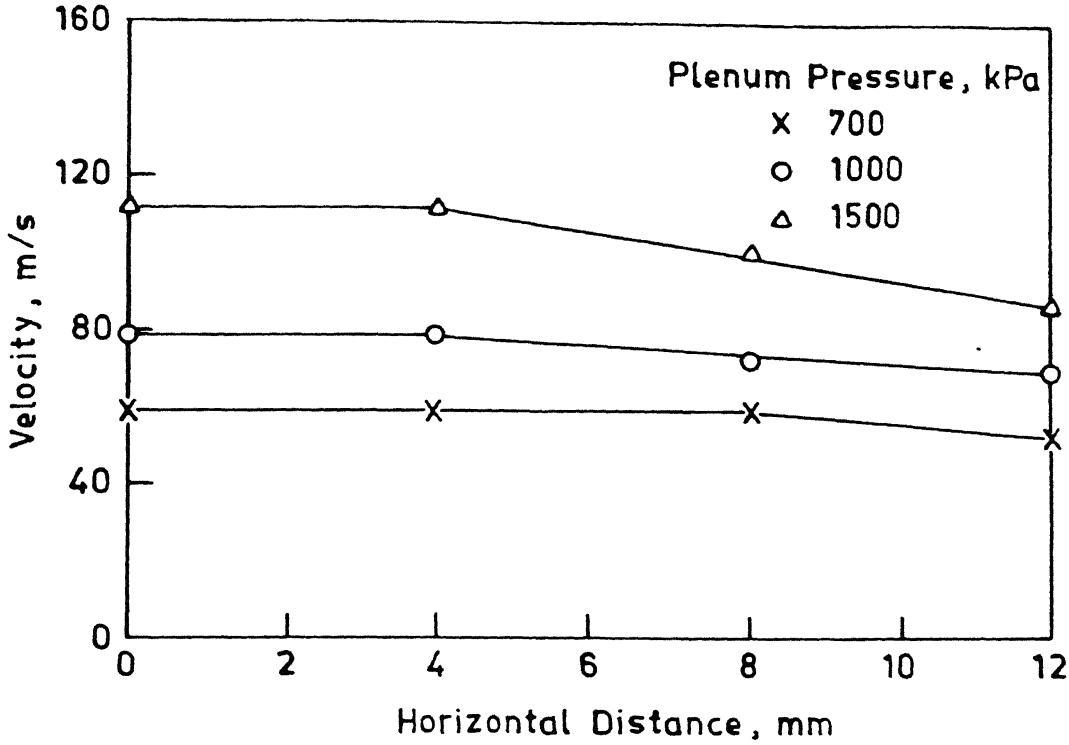

Figure 4.9 : Velocity of air as a function of horizontal distance from geometric point of an atomizer B412

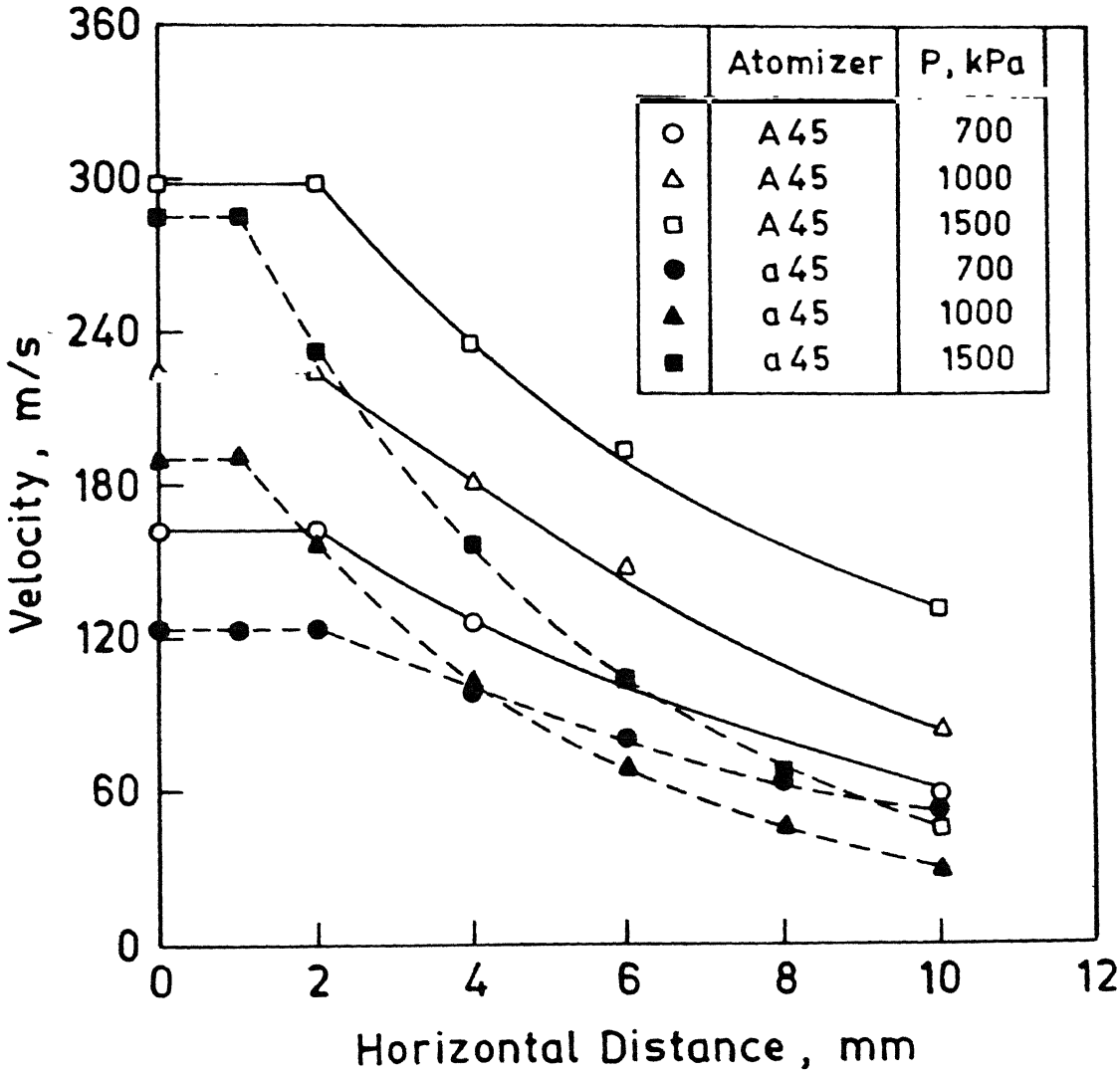

Figure 4.10 : Velocity of air as a function of horizontal distance from geometric point of an atomizer of different nozzle diameters (Focal length = 50 mm)

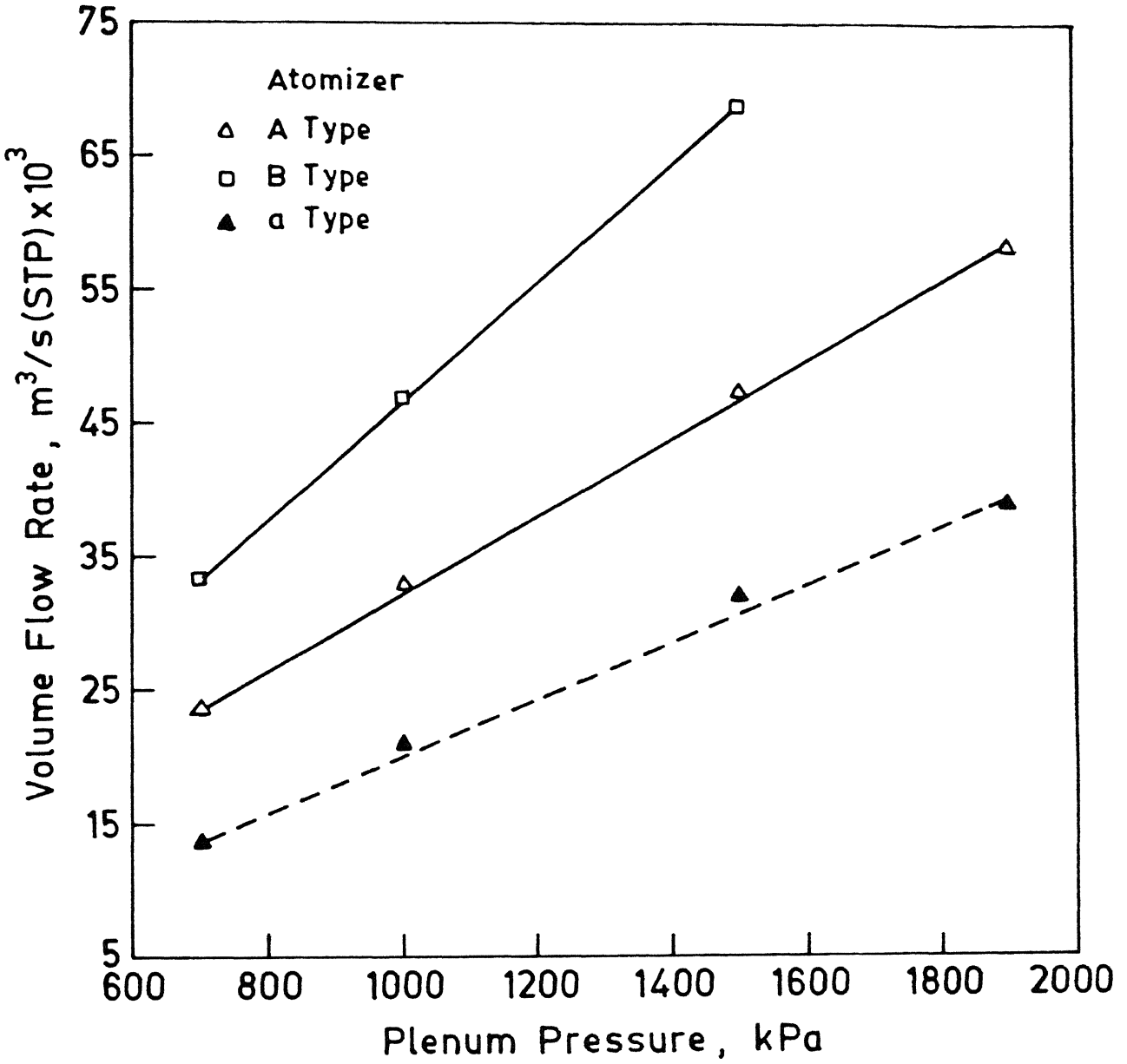

Figure 4.11 : Volume flow rate of air at STP (1 atm., 298 K) through atomizers as a function of plenum pressure

4.1.4 GAS FLOW RATE

Volume flow rate of air at STP (1 atm and 298 K) is plotted in Figure 4.11 as a function of plenum pressure for atomizers of A, B type (solid line) and a type (dashed line). The results show that the flow rate increases linearly with increase in plenum pressure for all atomizers of different number and diameters of nozzles.

4.2 ATOMIZATION

Any atomization unit, such as that in Figure 3.3 in relation to powder production must satisfy at least the following two requirements : The flying droplets should not hit on any surface of the unit, particularly atomizer and powder collection tray and at the same time they must be solidified completely before reaching the tray. Meeting of both the requirements is one of the necessary condition also to study powder characteristics as a function of parameters related to atomizer/liquid metal.

The results on atomization of aluminium, lead, tin and zinc had shown that both the requirements could be fulfilled simultaneously over a range of pressure for a given type of atomizer. The atomization runs with + signs in column O3 of Table 3.3 are for different pressures. Within the limits of plenum pressure and cooling chamber height, this range can be seen to be larger for lead than all other metals. It was observed that pressures below the lower limit of the range, though atomized the liquid stream but droplets were not solidified completely. Similarly, pressures above the upper limit of the range also atomized the liquid stream but a fraction of the droplets was found to be

deposited on the atomizer surface and the rest fraction solidified into powder. At the upper value of pressure within a pressure range for a given type of atomizer and metal, no deposition of droplets was observed on the atomizer surface (this value corresponds to $ sign in Table 3.3). This value of pressure is termed "critical pressure". At the critical pressure, most of the atomization runs resulted into complete solidification of all droplets before reaching at the bottom of the powder collecting tray. These runs are characterized by + and $ signs in the column O3 of Table 3.3.

As an example of the droplet deposition, Figure 4.12 is a photograph of the powder collective in the tray taken at the end of atomization run no. 61 which shows the influence of incomplete solidification of lead droplets on the powder yield. The powder collective can be seen to consist of the deposits of droplets (in the photograph it is white material at the centre of the tray) and loose powder (in the photo, it is at the periphery of the tray). This observation suggests the incomplete solidification of droplets during their fall in the cooling chamber. Similar type of observation was also made for atomized droplets of other metals at different pressures. A summary of the runs corresponding to the incomplete solidification is given in column O1 of Table 3.3 and experimental parameters are identified by '+' sign in the same Table.

Figure 4.13(a) is an example of the photograph of the atomizer A47 which was taken at the end of atomization of 500 gm lead to illustrate the effect of hitting of droplets on the atomizer surface. This run is 28 in Table 3.3. In this photograph, light bluish material can be seen to be present around the liquid metal delivery tube and extending upto gas nozzles. This material is identified as deposit of droplets. It must be mentioned

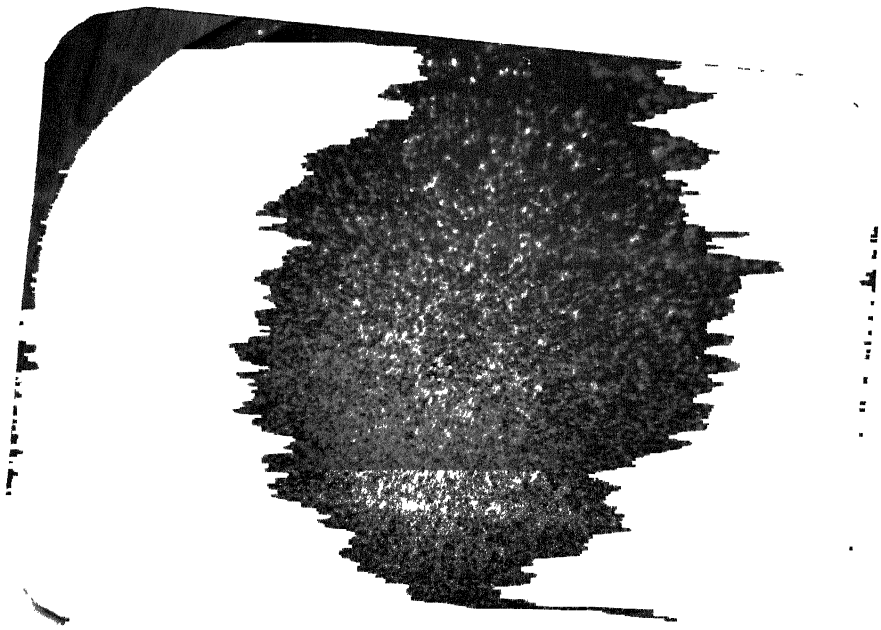

Figure 4.12 : Photograph of powder collection tray taken at the end of run no. 61

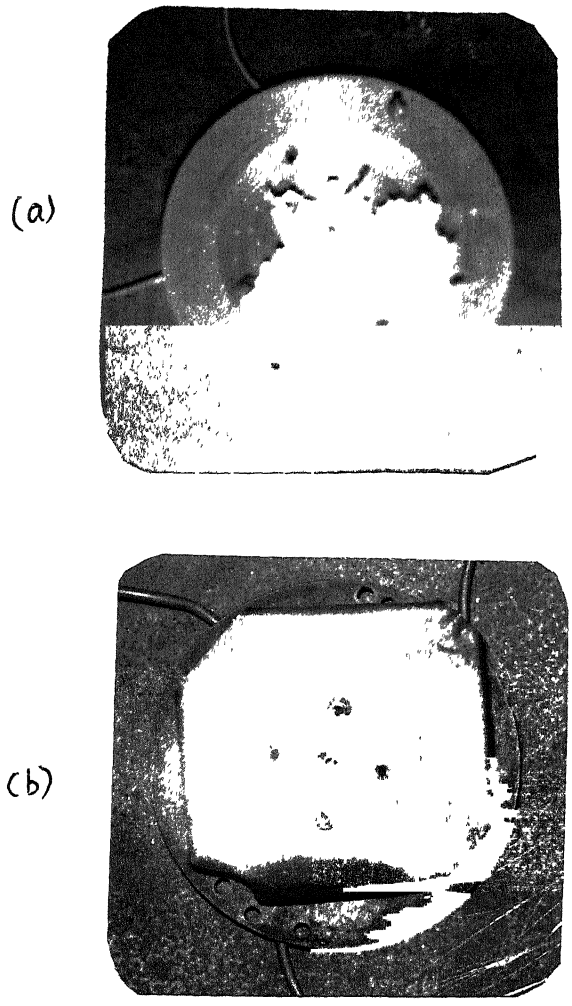

Figure 4.13 : Photographs of atomizer A47 taken at the end of run no. (a) 28 (b) 28 M.

Figure 4.14 : Photograph of atomizer A412 taken at the end of run no. 115 M

that this deposit occurs in a very short time of atomization (~2s). Other atomizers of Table 3.1 have also shown similar behviour, but at different plenum pressures for the atomization of different metals. A summary of runs corresponding to droplet deposition is given in column O2 of Table 3.3 and experimental parameters are identified by '+' sign in the same Table.

In order to illustrate the risk involved due to deposition on atomizer surface on atomization for a longer time, the atomizer of Figure 4.13(a) was employed to atomize 1500 gm more lead (Run No. 28M in Table 3.3) under same conditions without removing the deposits of run no. 28. The atomizer was observed at the end of atomization of 2000 gm lead. More deposition of droplets were found on the atomizer surface. Figure 4.1.3(b) is a photograph of the atomizer taken at the end of atomization of 2000 gm lead. Liquid metal delivery tube which is open for atomization run 28 (Figure 4.13a) can be seen to be blocked partially in photograph 4.13b.

Similarly, Figure 4.14 shows a photograph of the atomizer A412, which was taken at the end of the atomization run no. 115M. This run corresponds to the atomization of 2000 gm aluminum. It can be seen that the liquid delivery tube is blocked completely. The partial blockage of the gas nozzles was also observed though photograph does not show clearly.

From these observations it is asserted that in the free fall atomization, an atomizer should be operated preferably upto a plenum pressure at which the deposition of droplets does not take place on the atomizer surface. This pressure is termed as critical plenum pressure and its values correspond to the runs identified by $ sign in the column O3 of

Table 3.3 for different atomizers and metals. The same column O3 also identifies the runs with + signs which corresponds to complete solidification of the powder collectives produced by parameters given against each run of column O3.

The results in the following are organised in the two subsections; one deals with the variation of critical pressure and the other with powder characteristics.

4.2.1 CRITICAL PRESSURE

In the following, the variation of critical pressure for atomization is presented. This critical pressure may also be understood as an upper limit of pressure to operate the atomizer without running into the risk of droplet deposition related problems (at mentioned above) during atomization for a long time.

4.2.1.1 Effect of Focal Length

In Figure 4.15 critical pressure is plotted against focal length of the atomizer of A4 and B4 type for the atomization of lead (dashed line), zinc (dotted dashed) and aluminium (solid line) all superheated to 150 K, when the free fall distance of liquid stream is equal to focal length of atomizers. The diameters of liquid delivery tube are 3.5 mm and 5.5 mm. Each line separates the region of deposition of droplets on the atomizer surface with that from no-deposition one; i.e. for a given focal length of the atomizer, if the pressure is greater than that on the line, the atomization of the given liquid metal will precede with deposition of droplets on the surface of the atomizer (The type of deposit is shown in Figures 4.13 and 4.14). It can be observed that the critical pressure for all metals increases with increase in focal length for all atomizers. The critical pressure to atomize the liquid stream decreases in the following order, critical pressure of lead is greater than

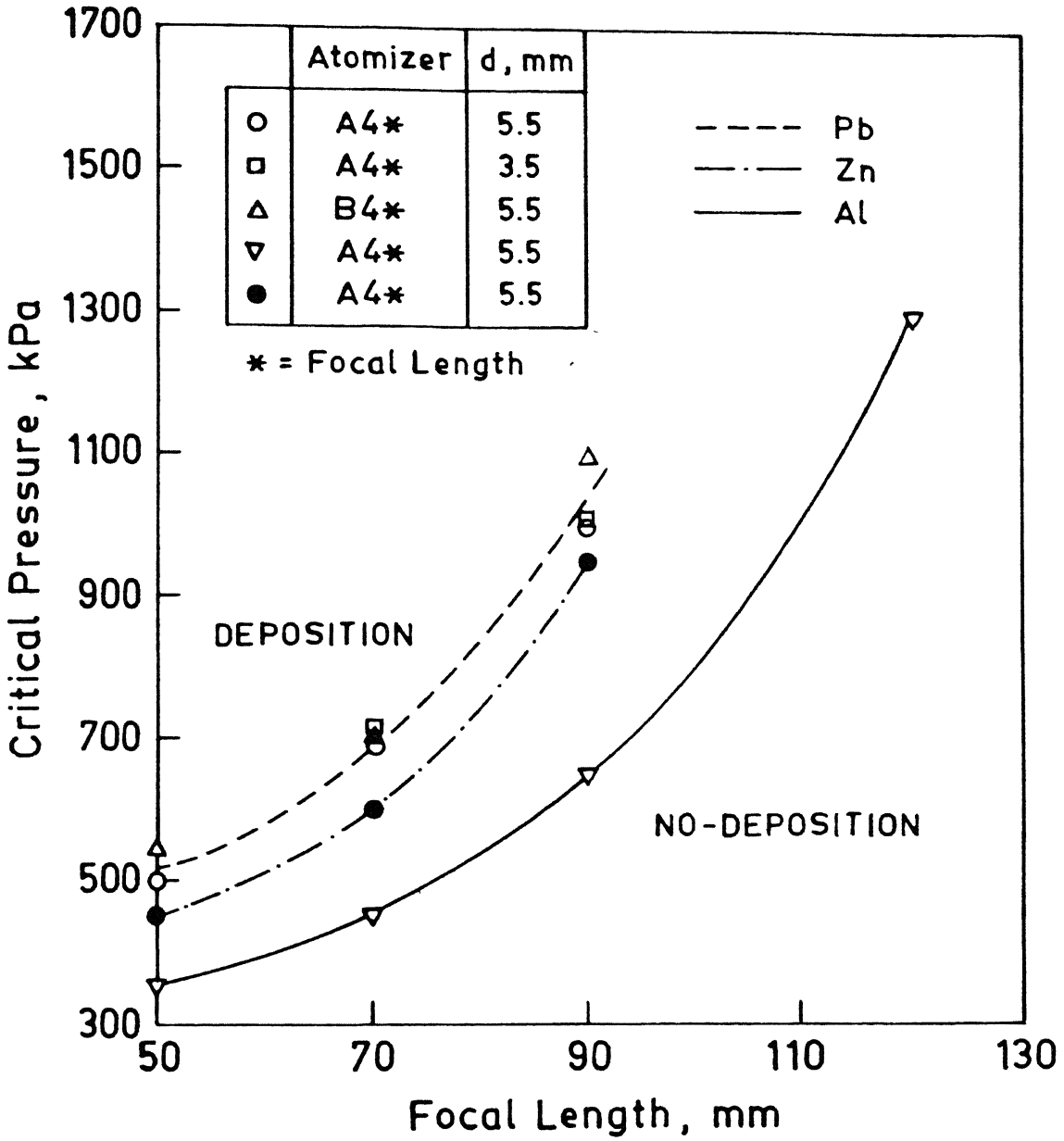

Figure 4.15 : Dependence of critical pressure on focal length of atomizer

that of zinc and zinc than that of aluminum. For example for the atomizer A49 the critical pressures for lead, zinc and aluminum are 1000 kPa, 950 kPa and 650 kPa, respectively. Further, it can be seen that the critical pressure is independent of the diameter of liquid delivery tube.

4.2.1.2 Effect of Superheat of Liquid Metal

The critical plenum pressure is plotted against superheat of liquid metal in Figure 4.16 for atomizers A65 (run nos. 57, 59 and 61), A612 (run No. 69, 73 and 77) of different focal lengths for atomization of lead (solid lines) and aluminum (dashed line). It can be seen that the critical plenum pressure does not change with change in superheat of liquid stream for all atomizers of different focal lengths.

4.2.1.3 Effect of Apex Angle

Figure 4.17 is a plot of critical pressure for atomization of lead and aluminium vs. apex angle of the atomizers of different nozzle diameters characterised by A type (run No. 15, 27, 63, 104, 111 and 116) and a type (run Nos. 1, 6 and 13) of same focal length. Increase in apex angle of atomizer of all types decreases the critical pressure required for the atomization of both metals. The critical pressure for a type atomizer is higher as compared to A type atomizer. For example, the critical pressure for a47 atomizer is 800 kPa whereas for A47 atomizer it is 700 kPa for the atomization of lead.

4.2.2 POWDER CHARACTERISTICS

All the powder collectives produced in the atomization unit of Figure 3.3 are analysed for their size and size distribution, surface area and morphology. As seen in Table 3.3 (Column O3), aluminium, tin and zinc could be atomized into powder for a very

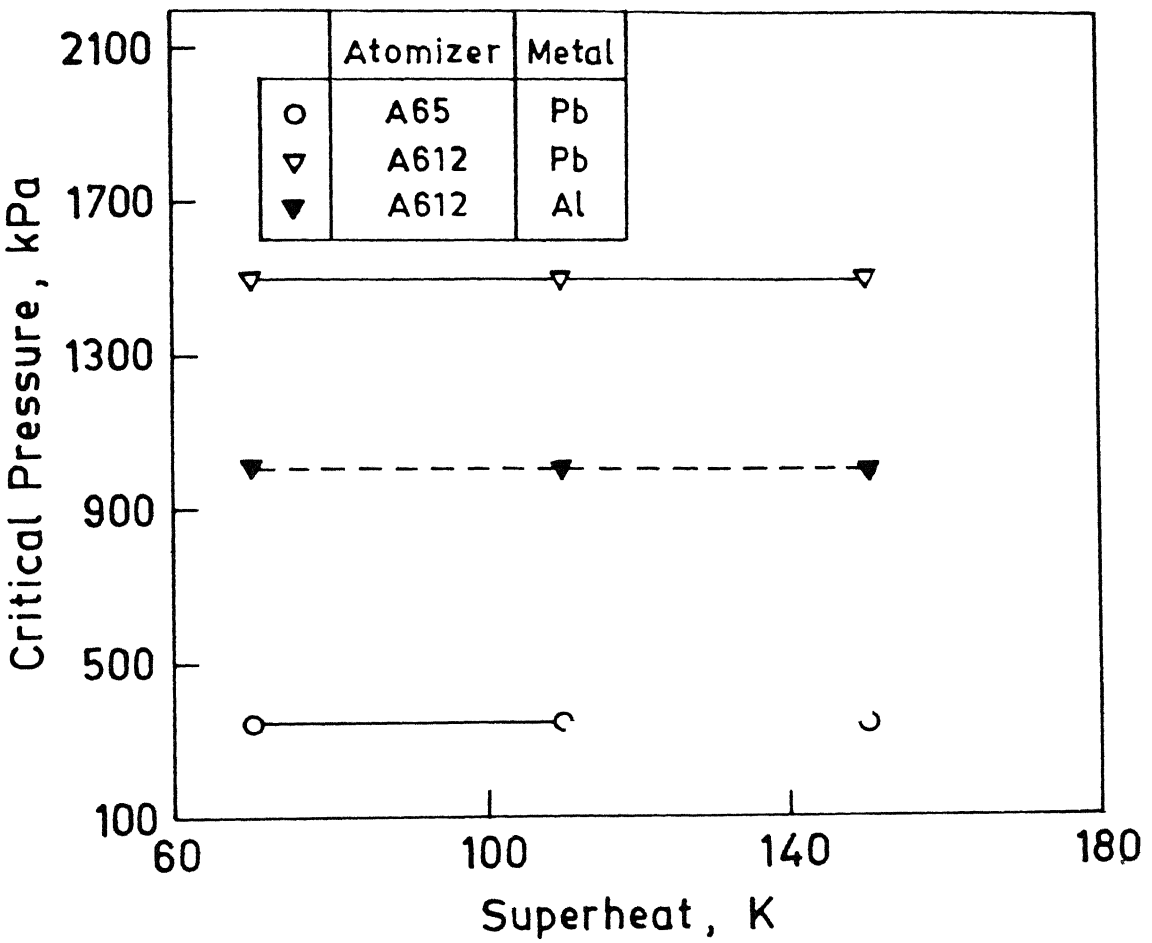

Figure 4.16 : Dependence of critical pressure on superheat of liquid metal

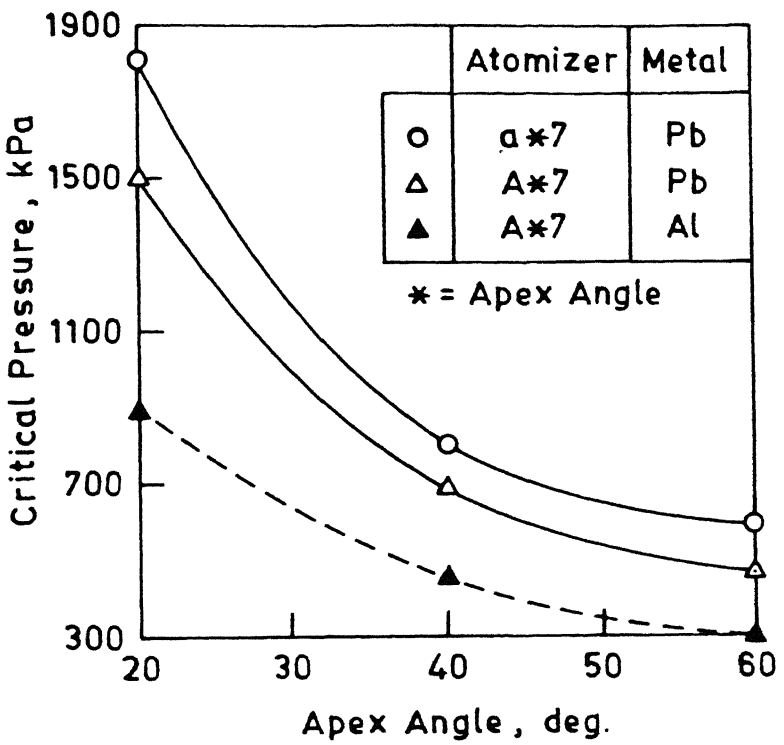

Figure 4.17 : Dependence of critical pressure on apex angle of the atomizer.

limited range of plenum pressures. Whereas lead is atomized into powder for a wide range of plenum pressures. All the results on sieve analysis of powder collectives are given in Table 4.4. In the following, the results on powder characteristics are given for lead only.

4.2.2.1 Size and Size Distribution

The results on the sieve analysis of all runs corresponding to the type of observation O3 including those at critical pressures are given in Table 4.4. Table shows that all the powder collectives are within the size varying from 38 μm to 600 μm. The commutative mass % passing through each sieve is plotted in Figure 4.18 to 4.30 on log normal probability paper against particle size for all run of the present study. The distribution of points was found to be closely approximated by the straight lines which suggested the use of log-normal distribution function to represent the data.

The straight lines on the Figures can be drawn by viewing the points, and from the straight lines the characteristic parameters of the distribution function, namely mass median size and the geometric standard deviation can also be determined as described elsewhere[2]. In the present study a slightly different approach is used to draw the straight lines. From the results of the sieve analysis reported in Table 4.4, the mass median size (X_g) and the geometric (σ_g) are calculated by the following equations[2] :

$$\ln X_g = \frac{\sum W \ln x}{\sum W} \qquad (4.1)$$

and

Table 4.4 : Sieve analysis data corresponding to observation 03 of table 3.3 of complete solidification of droplets

Run No =	1		= 3		= 5		= 6	
size range (um)	mass (%)	cumu.% passing	mass (%)	cumu.% passing	mass (%)	cumu.% passing	mass (%)	cumu.% passing
600 - 420	0.6	100.0	2.3	100.0	5.3	100.0	0.5	100.0
420 - 300	0.7	99.4	9.4	97.7	11.0	94.7	4.9	99.5
300 - 211	1.9	98.7	18.2	88.3	18.9	83.7	14.2	94.7
211 - 152	4.3	96.8	21.5	70.1	23.9	64.7	21.8	80.4
152 - 105	9.9	92.5	21.1	48.6	20.2	40.9	20.2	58.6
105 - 76	10.9	82.7	13.0	27.5	11.2	20.7	18.3	38.4
76 - 53	19.8	71.7	8.5	14.5	6.2	9.5	10.6	20.1
53 - 38	17.7	51.9	4.4	6.0	2.4	3.3	5.8	9.5
< 38	34.2	34.2	1.6	1.6	0.9	0.9	3.7	3.7
	= 8		= 9		= 10		= 11	
600 - 420	7.5	100.0	4.8	100.0	3.0	100.0	2.0	100.0
420 - 300	18.1	92.5	9.3	95.2	4.4	97.0	4.6	98.0
300 - 211	21.9	74.3	19.4	85.9	10.1	92.7	8.7	93.4
211 - 152	24.4	52.5	22.3	66.5	22.0	82.6	14.6	84.8
152 - 105	15.8	28.0	21.8	44.2	24.9	60.6	20.7	70.2
105 - 76	6.8	12.3	11.3	22.3	20.3	35.7	20.6	49.5
76 - 53	3.6	5.5	7.6	11.0	9.2	15.4	13.7	28.9
53 - 38	1.1	1.8	2.4	3.5	4.6	6.2	8.3	15.3
< 38	0.7	0.7	1.0	1.0	1.6	1.6	7.0	7.0
	= 13		= 15		= 15		= 17	
600 - 420	6.8	100.0	0.4	100.0	0.2	100.0	0.7	100.0
420 - 300	14.3	93.2	0.6	99.6	0.5	99.8	5.6	99.3
300 - 211	22.9	78.9	1.4	99.0	0.9	99.3	15.8	93.7
211 - 152	23.8	56.0	3.6	97.6	3.0	98.3	24.6	77.9
152 - 105	17.2	32.2	8.6	94.0	8.5	95.3	16.0	53.4
105 - 76	9.3	15.0	13.4	85.4	14.0	86.8	19.3	37.4
76 - 53	4.1	5.7	20.0	72.0	19.7	72.8	7.9	18.1
53 - 38	1.1	1.6	17.6	52.0	20.0	53.1	4.7	10.2
< 38	0.6	0.6	34.4	34.4	33.1	33.1	5.6	5.6
	= 17		= 18		= 18		= 19	
600 - 420	0.5	100.0	0.2	100.0	0.2	100.0	0.1	100.0
420 - 300	5.4	99.5	1.2	99.8	1.2	99.8	0.3	99.9
300 - 211	15.5	94.1	7.0	98.6	7.2	98.5	2.3	99.6
211 - 152	24.5	78.6	17.1	91.5	16.7	91.3	10.4	97.4
152 - 105	16.7	54.1	15.0	74.4	14.9	74.6	11.2	86.9
105 - 76	18.7	37.4	27.9	59.4	27.5	59.7	25.6	75.7
76 - 53	7.9	18.7	10.5	31.5	10.8	32.2	12.3	50.2
53 - 38	5.0	10.7	9.2	21.0	9.6	21.3	13.9	37.9
< 38	5.7	5.7	11.8	11.8	11.8	11.8	24.0	24.0

Run No =	20		= 21		= 22		= 23	
size range (um)	mass (%)	cumu.% passing	mass (%)	cumu.% passing	mass (%)	cumu.% passing	mass (%)	cumu.% passing
600 - 420	0.5	100.0	0.8	100.0	6.3	100.0	2.3	100.0
420 - 300	0.6	99.5	2.2	99.2	10.2	93.7	6.1	97.7
300 - 211	1.4	98.9	2.9	97.0	20.9	83.5	17.5	91.6
211 - 152	5.8	97.5	5.9	94.1	21.1	62.6	22.6	74.1
152 - 105	8.7	91.8	13.6	88.2	21.6	41.6	23.2	51.6
105 - 76	27.7	83.0	18.3	74.6	12.3	20.0	14.7	28.3
76 - 53	8.8	55.4	17.8	56.3	5.6	7.7	9.3	13.6
53 - 38	16.1	46.6	15.8	38.5	1.4	2.1	3.5	4.3
< 38	30.5	30.5	22.7	22.7	0.7	0.7	0.8	0.8
	= 23		= 25		= 25		= 26	
600 - 420	2.9	100.0	7.5	100.0	7.8	100.0	3.8	100.0
420 - 300	6.1	97.1	15.4	92.5	13.7	92.2	9.3	96.2
300 - 211	15.1	91.0	21.0	77.1	20.7	78.6	16.5	86.9
211 - 152	21.8	75.9	24.3	56.1	23.8	57.8	22.6	70.5
152 - 105	23.5	54.1	16.1	31.7	16.8	34.0	23.9	47.8
105 - 76	15.9	30.6	9.1	15.7	10.1	17.2	12.9	23.9
76 - 53	10.6	14.7	4.4	6.5	5.2	7.2	6.8	11.0
53 - 38	3.1	4.1	1.2	2.1	1.1	2.0	2.9	4.2
< 38	1.0	1.0	0.9	0.9	0.8	0.8	1.3	1.3
	= 26		= 27		= 27		= 29	
600 - 420	4.0	100.0	2.2	100.0	2.9	100.0	2.4	100.0
420 - 300	9.0	96.0	6.8	97.8	6.8	97.1	6.0	97.6
300 - 211	16.0	86.9	11.4	91.1	11.8	90.3	13.0	91.6
211 - 152	22.1	70.9	18.4	79.7	19.1	78.4	19.1	78.6
152 - 105	23.3	48.8	22.3	61.3	23.1	59.3	20.5	59.5
105 - 76	13.8	25.5	18.2	39.0	17.7	36.2	17.0	39.0
76 - 53	7.0	11.7	13.1	20.8	11.1	18.5	14.7	22.0
53 - 38	3.4	4.7	5.3	7.7	5.4	7.4	5.3	7.3
< 38	1.3	1.3	2.4	2.4	2.1	2.1	2.0	2.0
	= 30		= 30		= 31		= 31	
600 - 420	7.9	100.0	6.6	100.0	3.5	100.0	4.0	100.0
420 - 300	14.3	92.1	14.3	93.4	6.6	96.5	6.3	96.0
300 - 211	21.3	77.8	20.8	79.1	13.5	89.9	13.3	89.7
211 - 152	24.4	56.6	25.0	58.2	19.8	76.4	19.4	76.4
152 - 105	16.3	32.1	17.1	33.2	22.1	56.5	24.3	57.0
105 - 76	9.9	15.9	9.4	16.2	15.9	34.4	17.4	32.7
76 - 53	4.4	5.9	5.0	6.7	13.4	18.5	10.8	15.4
53 - 38	1.0	1.5	1.0	1.7	4.0	5.1	3.8	4.6
< 38	0.5	0.5	0.7	0.7	1.1	1.1	0.8	0.8

Run No =	32		= 32		= 34		= 35	
size range (um)	mass (%)	cumu.% passing	mass (%)	cumu.% passing	mass (%)	cumu.% passing	mass (%)	cumu.% passing
600 - 420	1.1	100.0	1.0	100.0	0.5	100.0	9.0	100.0
420 - 300	2.3	98.9	3.0	99.0	1.0	99.5	18.4	91.0
300 - 211	7.2	96.6	7.7	96.0	5.4	98.5	29.5	72.6
211 - 152	19.0	89.4	15.9	88.3	19.1	93.1	21.6	43.1
152 - 105	22.3	70.4	21.0	72.4	24.8	73.9	9.3	21.5
105 - 76	21.7	48.1	20.5	51.4	22.0	49.1	8.0	12.2
76 - 53	14.8	26.4	17.2	30.9	15.3	27.1	2.6	4.2
53 - 38	8.1	11.6	8.9	13.6	7.1	11.8	1.0	1.6
< 38	3.5	3.5	4.7	4.7	4.7	4.7	0.6	0.6
	= 35		= 35		= 36		= 36	
600 - 420	8.9	100.0	9.5	100.0	1.2	100.0	1.3	100.0
420 - 300	18.3	91.1	18.7	90.5	8.9	98.8	9.4	98.7
300 - 211	31.7	72.8	32.9	71.8	23.1	89.9	22.7	89.3
211 - 152	19.9	41.1	18.6	38.9	32.0	66.8	30.9	66.6
152 - 105	9.2	21.2	8.8	20.3	13.8	34.8	14.3	35.7
105 - 76	7.9	12.0	7.8	11.5	13.9	21.1	14.7	21.4
76 - 53	2.4	4.1	2.4	3.8	3.6	7.2	3.0	6.7
53 - 38	0.9	1.7	0.9	1.4	1.9	3.6	2.0	3.7
< 38	0.7	0.7	0.5	0.5	1.7	1.7	1.7	1.7
	= 37		= 37		= 38		= 38	
600 - 420	0.9	100.0	0.4	100.0	0.7	100.0	0.8	100.0
420 - 300	2.4	99.1	1.6	99.6	1.2	99.3	1.5	99.2
300 - 211	10.0	96.7	4.8	98.0	2.1	98.1	2.2	97.8
211 - 152	25.5	86.7	25.1	93.2	14.3	96.0	14.0	95.6
152 - 105	17.9	61.2	21.2	68.2	16.0	81.7	16.0	81.6
105 - 76	23.4	43.3	27.5	46.9	28.4	65.7	28.4	65.6
76 - 53	9.9	20.0	8.4	19.5	17.4	37.3	17.1	37.1
53 - 38	5.1	10.1	5.8	11.1	9.1	19.9	9.2	20.1
< 38	5.0	5.0	5.3	5.3	10.8	10.8	10.8	10.8
	= 39		= 39		= 39		= 40	
600 - 420	0.7	100.0	1.0	100.0	1.1	100.0	1.6	100.0
420 - 300	9.5	99.3	9.5	99.0	9.1	98.9	9.0	98.4
300 - 211	24.1	89.7	23.6	89.5	22.4	89.8	21.8	89.3
211 - 152	31.0	65.6	31.0	65.9	29.1	67.4	29.0	67.6
152 - 105	15.3	34.6	16.2	34.9	18.4	38.3	17.7	38.6
105 - 76	9.3	19.3	9.2	18.8	9.9	19.9	14.0	20.9
76 - 53	5.2	10.0	5.2	9.6	5.4	10.0	3.8	6.9
53 - 38	2.4	4.8	2.4	4.4	2.5	4.6	1.7	3.1
< 38	2.5	2.5	2.0	2.0	2.2	2.2	1.5	1.5

Run No =	40		= 40		= 41		= 41	
size range (um)	mass (%)	cumu.% passing	mass (%)	cumu.% passing	mass (%)	cumu.% passing	mass (%)	cumu.% passing
600 - 420	1.5	100.0	1.3	100.0	2.4	100.0	2.3	100.0
420 - 300	9.1	98.5	8.2	98.7	11.1	97.6	11.1	97.7
300 - 211	22.3	89.4	22.9	90.5	20.6	86.5	19.5	86.6
211 - 152	29.7	67.1	32.1	67.6	28.0	65.9	28.6	67.1
152 - 105	16.9	37.4	16.1	35.5	18.8	37.9	19.3	38.5
105 - 76	13.4	20.5	13.1	19.5	11.0	19.1	11.0	19.1
76 - 53	4.2	7.1	4.0	6.4	5.4	8.2	5.7	8.1
53 - 38	1.8	3.0	1.5	2.4	2.0	2.7	1.9	2.4
< 38	1.2	1.2	0.8	0.8	0.7	0.7	0.5	0.5
	= 41		= 42		= 42		= 43	
600 - 420	2.4	100.0	5.9	100.0	6.3	100.0	1.2	100.0
420 - 300	10.1	97.6	15.6	94.1	14.5	93.7	3.0	98.8
300 - 211	19.9	87.5	22.1	78.5	21.4	79.2	6.3	95.8
211 - 152	29.2	67.6	25.2	56.5	26.9	57.9	20.6	89.6
152 - 105	18.5	38.4	19.2	31.2	17.8	30.9	18.6	68.9
105 - 76	11.5	19.9	7.8	12.1	9.1	13.1	26.2	50.3
76 - 53	6.1	8.3	3.1	4.3	3.1	4.0	11.2	24.1
53 - 38	1.8	2.2	0.8	1.2	0.6	0.9	6.9	13.0
< 38	0.4	0.4	0.4	0.4	0.3	0.3	6.1	6.1
	= 43		= 44		= 45		= 45	
600 - 420	1.1	100.0	2.6	100.0	0.2	100.0	0.4	100.0
420 - 300	2.9	98.9	3.3	97.4	2.3	99.8	2.5	99.6
300 - 211	7.7	96.0	6.8	94.1	8.9	97.5	9.2	97.1
211 - 152	20.0	88.3	23.2	87.3	27.5	88.6	26.7	87.9
152 - 105	18.8	68.3	19.6	64.1	18.9	61.1	18.6	61.2
105 - 76	26.5	49.5	25.5	44.5	25.6	42.2	25.2	42.6
76 - 53	10.1	23.0	9.1	19.0	8.8	16.7	8.9	17.4
53 - 38	6.9	12.9	5.8	9.8	4.7	7.9	5.3	8.5
< 38	5.9	5.9	4.0	4.0	3.1	3.1	3.3	3.3
	= 45		= 46		= 46		= 46	
600 - 420	0.4	100.0	0.7	100.0	0.6	100.0	0.7	100.0
420 - 300	2.4	99.6	3.0	99.3	2.8	99.4	2.8	99.3
300 - 211	8.3	97.3	9.4	96.3	9.0	96.5	9.4	96.5
211 - 152	28.7	89.0	22.6	86.8	23.1	87.5	23.2	87.1
152 - 105	18.2	60.3	19.5	64.2	19.6	64.4	19.5	64.0
105 - 76	24.6	42.1	26.6	44.7	26.7	44.8	26.6	44.5
76 - 53	8.9	17.5	8.5	18.0	9.0	18.1	8.8	17.9
53 - 38	5.4	8.6	5.2	9.5	4.9	9.1	4.9	9.0
< 38	3.2	3.2	4.3	4.3	4.3	4.3	4.2	4.2

Run No =	47		= 48		= 48		= 49	
size range (um)	mass (%)	cumu.% passing	mass (%)	cumu.% passing	mass (%)	cumu.% passing	mass (%)	cumu.% passing
600 - 420	0.3	100.0	0.3	100.0	0.3	100.0	1.0	100.0
420 - 300	3.8	99.7	3.6	99.7	3.8	99.7	6.0	99.0
300 - 211	10.5	95.8	15.3	96.1	15.5	95.9	15.9	93.0
211 - 152	24.8	85.4	24.6	80.7	24.7	80.4	25.2	77.1
152 - 105	19.3	60.5	16.9	56.1	16.3	55.7	18.4	51.9
105 - 76	22.6	41.3	21.7	39.2	21.0	39.4	19.2	33.5
76 - 53	9.2	18.7	7.4	17.5	7.5	18.4	6.9	14.3
53 - 38	4.5	9.5	5.9	10.1	6.4	10.9	4.0	7.4
< 38	5.1	5.1	4.3	4.3	4.5	4.5	3.4	3.4
	= 49		= 50		= 50		= 50	
600 - 420	1.3	100.0	0.2	100.0	0.6	100.0	0.8	100.0
420 - 300	6.3	98.7	0.3	99.8	1.2	99.4	0.7	99.2
300 - 211	16.0	92.3	1.2	99.5	2.4	98.2	2.1	98.4
211 - 152	24.9	76.3	10.6	98.3	13.9	95.8	9.7	96.4
152 - 105	18.2	51.4	16.2	87.7	17.0	81.8	16.2	86.7
105 - 76	19.0	33.2	28.8	71.5	26.2	64.8	25.1	70.5
76 - 53	6.7	14.2	20.3	42.6	18.0	38.6	20.5	45.4
53 - 38	4.1	7.5	10.1	22.3	10.6	20.7	12.7	24.9
< 38	3.3	3.3	12.2	12.2	10.1	10.1	12.2	12.2
	= 51		= 51		= 51		= 52	
600 - 420	0.3	100.0	0.8	100.0	0.5	100.0	1.0	100.0
420 - 300	1.0	99.7	1.0	99.2	1.3	99.5	1.7	99.0
300 - 211	1.5	98.7	1.4	98.1	2.9	98.1	2.0	97.3
211 - 152	12.4	97.2	9.6	96.7	6.8	95.2	11.2	95.3
152 - 105	17.5	84.8	19.3	87.1	22.9	88.4	17.8	84.1
105 - 76	26.0	67.3	25.6	67.9	25.2	65.5	23.3	66.3
76 - 53	19.1	41.3	20.8	42.2	20.7	40.3	20.4	43.0
53 - 38	11.2	22.2	12.6	21.5	11.7	19.7	14.1	22.6
< 38	11.0	11.0	8.9	8.9	8.0	8.0	8.5	8.5
	= 52		= 52		= 53		= 53	
600 - 420	0.7	100.0	0.7	100.0	2.6	100.0	2.1	100.0
420 - 300	1.2	99.3	1.7	99.3	5.1	97.4	5.3	97.9
300 - 211	3.3	98.1	4.1	97.5	8.9	92.3	9.6	92.6
211 - 152	13.0	94.8	9.4	93.4	14.9	83.4	14.7	82.9
152 - 105	16.5	81.8	18.5	84.0	19.3	68.5	18.3	68.2
105 - 76	22.6	65.3	23.9	65.5	17.9	49.2	17.5	49.9
76 - 53	19.4	42.7	20.9	41.6	17.6	31.4	16.3	32.4
53 - 38	14.8	23.4	12.4	20.7	7.0	13.8	8.7	16.0
< 38	8.6	8.6	8.3	8.3	6.9	6.9	7.3	7.3

Run No =	53		= 54		= 63		= 63	
size range (um)	mass (%)	cumu.% passing	mass (%)	cumu.% passing	mass (%)	cumu.% passing	mass (%)	cumu.% passing
600 - 420	1.9	100.0	1.3	100.0	7.2	100.0	7.3	100.0
420 - 300	4.7	98.1	2.8	98.7	14.1	92.8	13.3	92.7
300 - 211	10.3	93.3	8.7	95.9	22.9	78.6	21.0	79.4
211 - 152	14.6	83.0	18.8	87.3	23.1	55.8	23.3	58.4
152 - 105	20.1	68.3	23.2	68.5	18.9	32.6	20.3	35.1
105 - 76	15.8	48.3	21.0	45.3	9.5	13.7	10.8	14.7
76 - 53	16.3	32.5	14.4	24.3	3.4	4.2	3.3	4.0
53 - 38	9.9	16.2	7.3	9.9	0.5	0.8	0.5	0.7
< 38	6.2	6.2	2.6	2.6	0.3	0.3	0.2	0.2
	= 65		= 65		= 67		= 67	
600 - 420	3.4	100.0	3.8	100.0	16.3	100.0	16.3	100.0
420 - 300	7.1	96.6	8.7	96.2	22.7	83.7	21.7	83.7
300 - 211	16.0	89.5	17.7	87.6	21.8	61.0	22.1	62.1
211 - 152	22.6	73.5	22.4	69.9	21.4	39.2	22.6	39.9
152 - 105	25.9	50.8	23.1	47.5	8.5	17.8	8.5	17.4
105 - 76	15.8	25.0	13.9	24.4	4.6	9.4	4.6	8.9
76 - 53	7.2	9.2	8.0	10.4	2.7	4.8	2.7	4.4
53 - 38	1.5	2.0	2.0	2.5	1.0	2.1	0.9	1.6
< 38	0.5	0.5	0.5	0.5	1.1	1.1	0.8	0.8
	= 68		= 68		= 68		= 69	
600 - 420	6.2	100.0	1.1	100.0	6.0	100.0	3.6	100.0
420 - 300	13.5	93.8	9.8	98.9	11.8	94.0	5.7	96.4
300 - 211	22.1	80.3	25.1	89.2	20.9	82.2	12.4	90.7
211 - 152	26.7	58.2	31.3	64.0	28.7	61.2	23.3	78.2
152 - 105	14.3	31.5	15.0	32.7	15.1	32.5	19.4	54.9
105 - 76	8.4	17.2	8.8	17.7	8.8	17.4	14.6	35.6
76 - 53	5.6	8.8	4.8	8.9	4.8	8.6	12.6	21.0
53 - 38	1.5	3.2	2.1	4.1	2.1	3.8	3.9	8.4
< 38	1.7	1.7	1.9	1.9	1.7	1.7	4.5	4.5
	= 69		= 69		= 71		= 71	
600 - 420	0.9	100.0	1.7	100.0	9.9	100.0	8.8	100.0
420 - 300	2.2	99.1	3.0	98.3	30.5	90.1	29.2	91.2
300 - 211	8.7	96.9	9.1	95.3	24.2	59.6	22.8	62.0
211 - 152	26.6	88.2	24.2	86.2	19.5	35.4	22.4	39.2
152 - 105	22.9	61.6	23.4	61.9	7.8	15.8	8.1	16.8
105 - 76	17.3	38.7	17.6	38.5	4.2	8.0	4.3	8.7
76 - 53	11.6	21.4	11.8	20.9	2.2	3.8	2.6	4.4
53 - 38	5.3	9.8	4.9	9.2	0.8	1.7	0.9	1.7
< 38	4.5	4.5	4.3	4.3	0.8	0.8	0.8	0.8

Run No =	71		= 72		= 72		= 72	
size range (um)	mass (%)	cumu.% passing	mass (%)	cumu.% passing	mass (%)	cumu.% passing	mass (%)	cumu.% passing
600 - 420	9.9	100.0	2.0	100.0	2.6	100.0	2.4	100.0
420 - 300	29.2	90.1	14.7	98.0	13.5	97.4	13.1	97.6
300 - 211	21.4	60.9	20.4	83.4	19.0	83.9	19.1	84.5
211 - 152	22.7	39.5	29.3	63.0	28.4	64.8	29.2	65.4
152 - 105	8.2	16.8	15.5	33.6	16.6	36.5	16.7	36.1
105 - 76	4.4	8.7	9.1	18.1	9.7	19.8	9.7	19.5
76 - 53	2.3	4.3	5.5	9.1	6.0	10.1	5.8	9.8
53 - 38	1.0	2.0	1.8	3.6	2.2	4.1	2.0	3.9
< 38	1.1	1.1	1.7	1.7	1.9	1.9	1.9	1.9
	= 73		= 73		= 73		= 75	
600 - 420	1.0	100.0	1.4	100.0	1.5	100.0	11.7	100.0
420 - 300	5.5	99.0	3.1	98.6	4.2	98.5	24.8	88.3
300 - 211	13.1	93.5	6.5	95.5	7.6	94.4	25.7	63.6
211 - 152	26.8	80.4	19.8	89.0	20.4	86.8	22.1	37.9
152 - 105	20.6	53.6	24.6	69.2	23.6	66.4	8.1	15.7
105 - 76	15.5	32.9	18.5	44.5	17.7	42.8	4.4	7.6
76 - 53	9.8	17.5	13.5	26.0	12.4	25.1	2.1	3.2
53 - 38	3.8	7.6	6.4	12.5	6.3	12.7	0.5	1.1
< 38	3.8	3.8	6.1	6.1	6.4	6.4	0.6	0.6
	= 75		= 75		= 76		= 76	
600 - 420	12.2	100.0	11.7	100.0	5.6	100.0	7.7	100.0
420 - 300	23.2	87.8	25.5	88.3	14.8	94.4	13.5	92.3
300 - 211	25.2	64.6	23.8	62.7	20.7	79.6	19.1	78.8
211 - 152	22.9	39.4	22.9	38.9	25.3	58.9	26.7	59.7
152 - 105	7.8	16.4	8.0	16.1	14.7	33.5	15.0	33.0
105 - 76	4.2	8.6	4.3	8.1	8.5	18.8	8.8	18.0
76 - 53	2.6	4.4	2.2	3.8	6.2	10.3	5.8	9.2
53 - 38	0.9	1.8	0.9	1.6	2.0	4.2	1.6	3.4
< 38	0.9	0.9	0.8	0.8	2.2	2.2	1.8	1.8
	= 77		= 77		= 79		= 79	
600 - 420	3.6	100.0	3.0	100.0	16.2	100.0	10.7	100.0
420 - 300	6.5	96.4	6.0	97.0	22.0	83.8	25.5	89.3
300 - 211	11.5	89.9	10.8	91.0	21.3	61.8	25.8	63.8
211 - 152	21.6	78.3	21.6	80.2	21.9	40.5	21.0	38.0
152 - 105	19.7	56.7	20.4	58.6	8.5	18.6	8.4	17.1
105 - 76	14.8	37.1	15.4	38.2	4.6	10.1	4.5	8.6
76 - 53	13.6	22.2	13.8	22.8	3.5	5.5	2.3	4.1
53 - 38	4.2	8.7	4.4	9.0	0.9	2.0	0.9	1.8
< 38	4.5	4.5	4.6	4.6	1.1	1.1	0.9	0.9

Run No =	80	= 80	= 80	= 81

size range (um)	mass (%)	cumu.% passing	mass (%)	cumu.% passing	mass (%)	cumu.% passing	mass (%)	cumu.% passing
600 - 420	1.4	100.0	1.3	100.0	2.6	100.0	2.1	100.0
420 - 300	9.0	98.6	7.0	98.7	12.8	97.4	6.2	97.9
300 - 211	18.4	89.6	17.6	91.7	19.0	84.6	10.1	91.7
211 - 152	31.0	71.2	29.1	74.1	28.6	65.6	18.4	81.6
152 - 105	18.4	40.2	20.1	45.1	16.9	37.0	20.8	63.2
105 - 76	10.7	21.9	11.8	25.0	9.9	20.1	15.7	42.4
76 - 53	6.8	11.1	7.5	13.2	6.1	10.2	15.0	26.8
53 - 38	2.5	4.3	3.5	5.7	2.2	4.1	6.2	11.8
< 38	1.8	1.8	2.1	2.1	1.9	1.9	5.6	5.6
	= 81		= 82		= 84		= 86	
600 - 420	0.9	100.0	3.7	100.0	1.7	100.0	8.9	100.0
420 - 300	2.3	99.1	6.5	96.3	5.0	98.3	18.0	91.1
300 - 211	7.6	96.9	14.2	89.8	14.0	93.4	22.2	73.1
211 - 152	24.2	89.3	20.4	75.6	24.7	79.4	25.0	50.9
152 - 105	24.4	65.1	23.0	55.2	16.1	54.8	16.4	25.9
105 - 76	18.3	40.7	18.4	32.2	20.0	38.7	5.2	9.5
76 - 53	10.8	22.4	9.3	13.8	11.0	18.6	2.9	4.3
53 - 38	5.5	11.6	3.4	4.4	3.7	7.7	0.9	1.5
< 38	6.1	6.1	1.1	1.1	4.0	4.0	0.5	0.5
	= 87		= 88		= 89		= 91	
600 - 420	3.0	100.0	1.3	100.0	1.2	100.0	6.2	100.0
420 - 300	9.6	97.0	2.0	98.7	2.6	98.8	16.8	93.8
300 - 211	17.8	87.4	5.0	96.7	7.3	96.2	21.5	76.9
211 - 152	21.8	69.6	24.0	91.7	15.7	88.8	22.7	55.4
152 - 105	22.9	47.8	21.8	67.7	21.2	73.2	18.2	32.7
105 - 76	12.8	24.9	24.2	45.9	20.4	52.0	8.9	14.5
76 - 53	7.8	12.1	11.1	21.7	17.6	31.6	4.7	5.5
53 - 38	3.0	4.3	6.2	10.6	9.2	14.0	0.5	0.9
< 38	1.3	1.3	4.4	4.4	4.8	4.8	0.4	0.4
	= 94		= 95		= 95		= 107	
600 - 420	1.0	100.0	0.7	100.0	0.6	100.0	2.4	100.0
420 - 300	2.8	99.0	1.2	99.3	0.7	99.4	5.0	97.6
300 - 211	6.2	96.2	3.3	98.1	3.0	98.6	8.1	92.7
211 - 152	13.6	90.0	12.6	94.9	9.5	95.6	14.2	84.6
152 - 105	17.7	76.3	16.3	82.2	20.0	86.1	18.6	70.5
105 - 76	22.8	58.6	24.1	65.9	22.9	66.1	25.8	51.9
76 - 53	17.4	35.8	18.2	41.9	15.9	43.1	9.9	26.0
53 - 38	9.8	18.4	9.7	23.7	12.6	27.3	8.2	16.2
< 38	8.6	8.6	14.0	14.0	14.7	14.7	7.9	7.9

Run No = 121 = 121

size range (um)	mass (%)	cumu.% passing	mass (%)	cumu.% passing
600 - 420	0.3	100.0	0.3	100.0
420 - 300	0.5	99.7	0.8	99.7
300 - 211	2.2	99.2	2.2	98.9
211 - 152	7.7	96.9	5.2	96.7
152 - 105	14.3	89.2	13.9	91.5
105 - 76	16.6	74.8	20.1	77.7
76 - 53	14.1	58.2	13.6	57.6
53 - 38	15.5	44.1	16.3	43.9
< 38	28.6	28.6	27.6	27.6

$$\ln \sigma_g = \sqrt{\frac{\sum W(\ln X - \ln X_g)^2}{\sum W}} \qquad (4.2)$$

All the values of X_g and σ_g are given in Table 4.5.

The calculated values of X_g and σ_g, and $X_{84.1}$ which is determined by

$$X_{84.1} = X_g \times \sigma_g \qquad (4.3)$$

the straight lines are drawn on the Figures. It can be seen in all Figures that for all runs the cumulative mass percent passing values are uniformly distributed about the straight lines. The results confirm the validity of the log normal distribution function.

In the log normal distribution function, X_g and σ_g are the two characteristic parameters whose variation is important with atomizer design and liquid related parameters in order to calculate the mass fraction of a given size produced during atomization by using log normal equation. In the following the variation of mass median size and geometric standard deviation is given.

4.2.2.2 Mass Median Size

A. ***Plenum Pressure***

It can be seen in Table 4.5 that increase in pressure decreases X_g for all types of atomizers irrespective of their focal lengths, apex angles and number and diameter of nozzles, but at critical pressure, the value of X_g is minimum, which depends on the aforementioned parameters of atomizers. The minimum value in the following presentation is termed as critical mass median size (X_c) of a powder collective produced by an atomizer operated at critical pressure. It must be noted that the critical mass median size of a powder collective is due to the condition imposed on the operation of the

Table 4.5: The mass median size (X_g), geometric standard deviation (σ_g) and specific surface area (S) of all runs corresponding to observation 03 of table 3.3

Run No.	X μm	σ_g	S cm^2/gm
1	53	2.03	121.7
3	149	1.86	42.6
5	170	1.81	36.9
6	125	1.87	51.5
8	202	1.76	30.7
9	163	1.82	38.4
10	131	1.79	47.0
11	107	2.01	62.3
13	192	1.75	32.1
15	51	1.92	122.5
15	52	1.98	122.8
17	128	1.95	52.1
17	127	1.95	52 7
18	91	1.98	72.8
18	91	1.99	73.1
19	66	2.03	100.0
20	58	2.04	112.5
21	67	2.09	99.7
22	174	1.79	35.6
23	146	1.77	42.0
23	143	1.79	43.2
25	192	1.80	32.7
25	187	1.81	33.5
26	156	1.81	40.0
26	154	1.83	40.8
27	128	1.88	49.8
27	132	1.88	48.0
29	129	1.88	49.3
30	192	1.77	32.1
30	188	1.77	33.0
31	138	1.85	45.3
31	141	1.82	43.9
32	109	1.82	57.3
32	104	1.88	61.0
34	104	1.78	59.8
35	217	1.74	28.6
35	219	1.74	28.5
35	223	1.72	27.6
36	166	1.73	37.3

Run No.	X μm	σ_g	S cm^2/gm
36	166	1.74	37.4
37	117	1.86	54.8
37	109	1.78	57.3
38	85	1.89	74.9
38	86	1.9	74.9
39	164	1.78	38.8
39	166	1.76	38.0
39	162	1.78	39.1
40	165	1.72	37.3
40	166	1.71	36.8
40	168	1.67	35.8
41	170	1.73	36.0
41	169	1.71	35.8
41	168	1.71	35.9
42	195	1.70	30.9
42	194	1.69	30.9
43	107	1.89	60.1
43	109	1.89	59.3
44	118	1.86	53.8
45	120	1.75	51.4
45	120	1.77	51.9
45	120	1.76	51.8
46	117	1.82	54.0
46	116	1.81	54.0
46	117	1.82	53.6
47	120	1.86	53.8
48	125	1.87	51.6
48	124	1.89	52.3
49	136	1.85	47.2
49	138	1.86	46.9
50	78	1.82	80.5
50	85	1.88	74 7
50	78	1.89	81.4
51	81	1.86	77.6
51	82	1.82	75 8
51	84	1.80	73.4
52	84	1.87	75.2
52	84	1.89	75.0
52	86	1.87	73.7

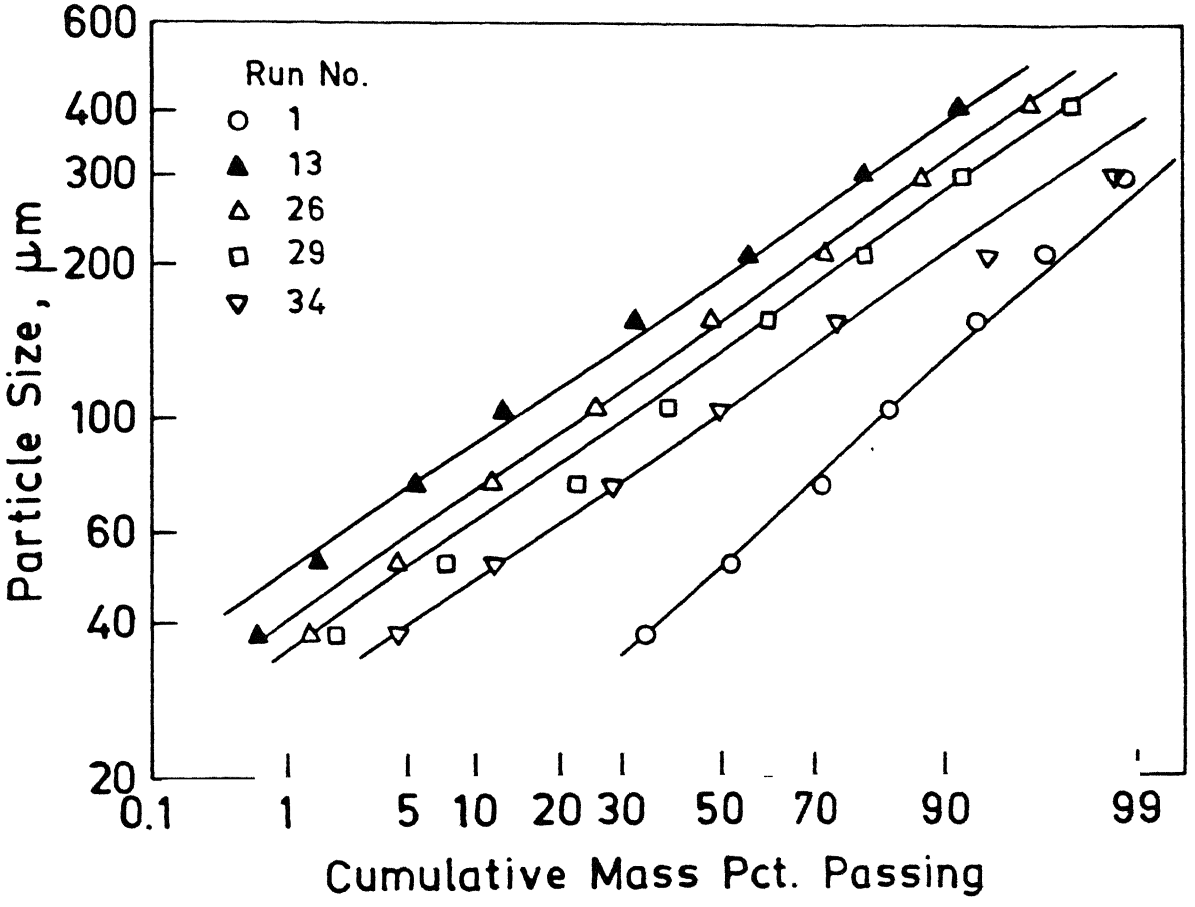

Figure 4.18 : Cumulative mass percent passing against particle size for different power collectives

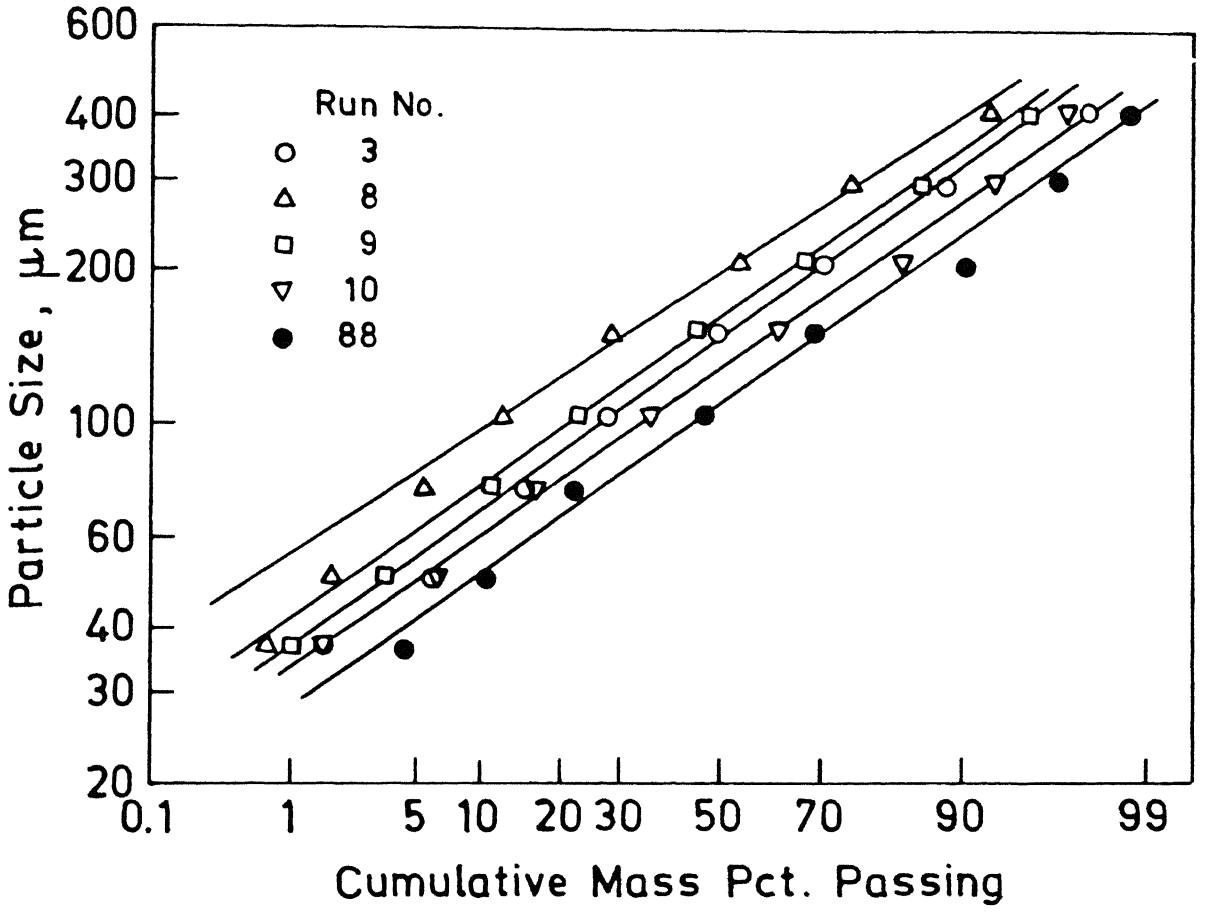

Figure 4.19 : Cumulative mass percent passing against particle size for different power collectives

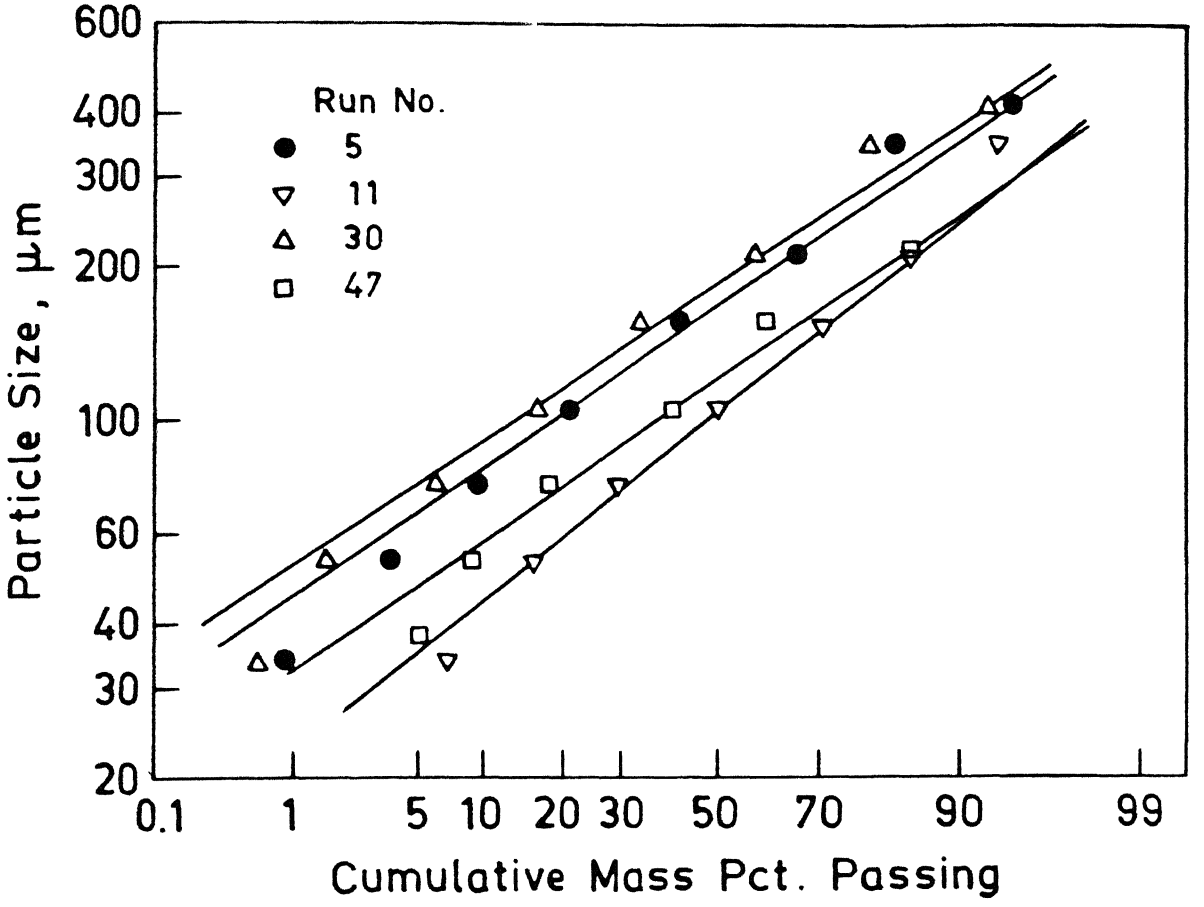

Figure 4.20 : Cumulative mass percent passing against particle size for different power collectives

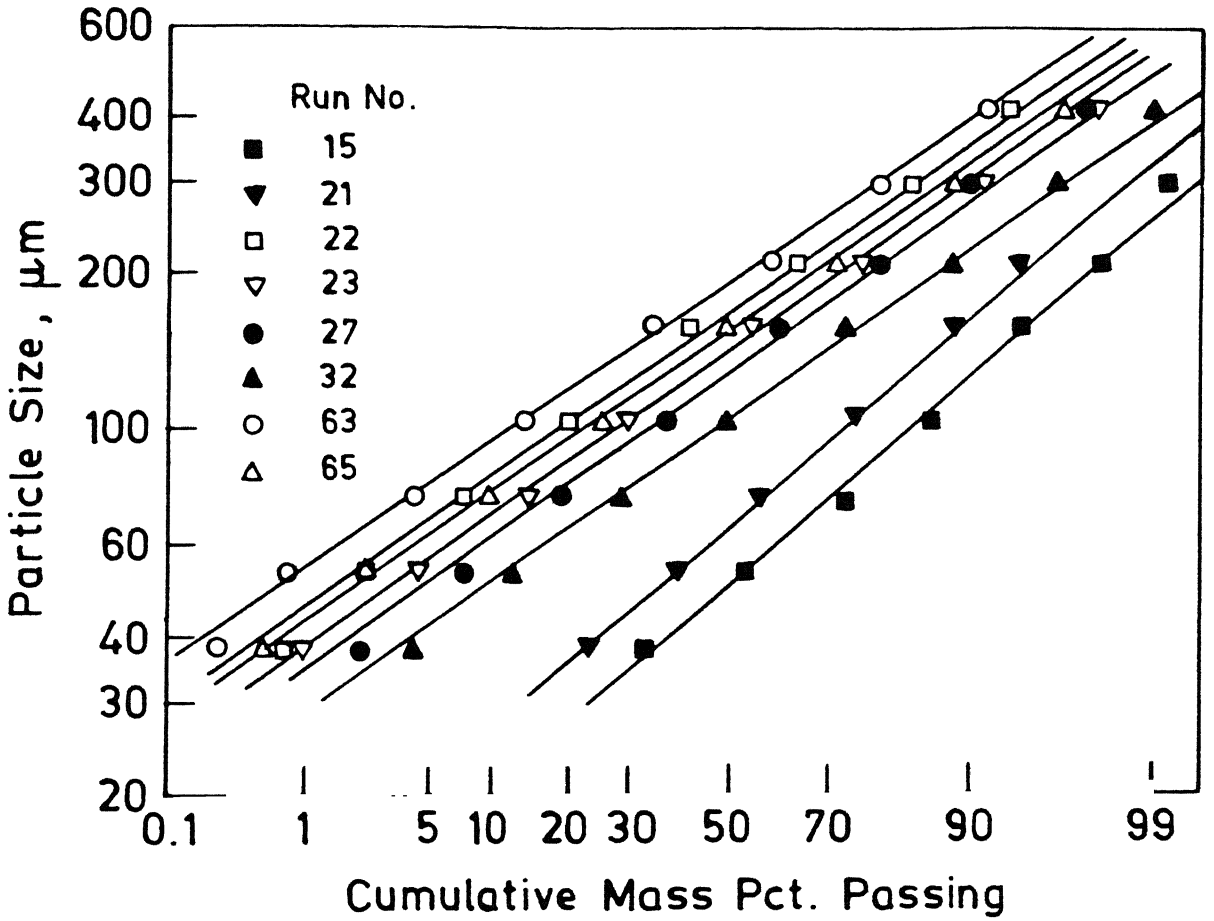

Figure 4.21 : Cumulative mass percent passing against particle size for different power collectives

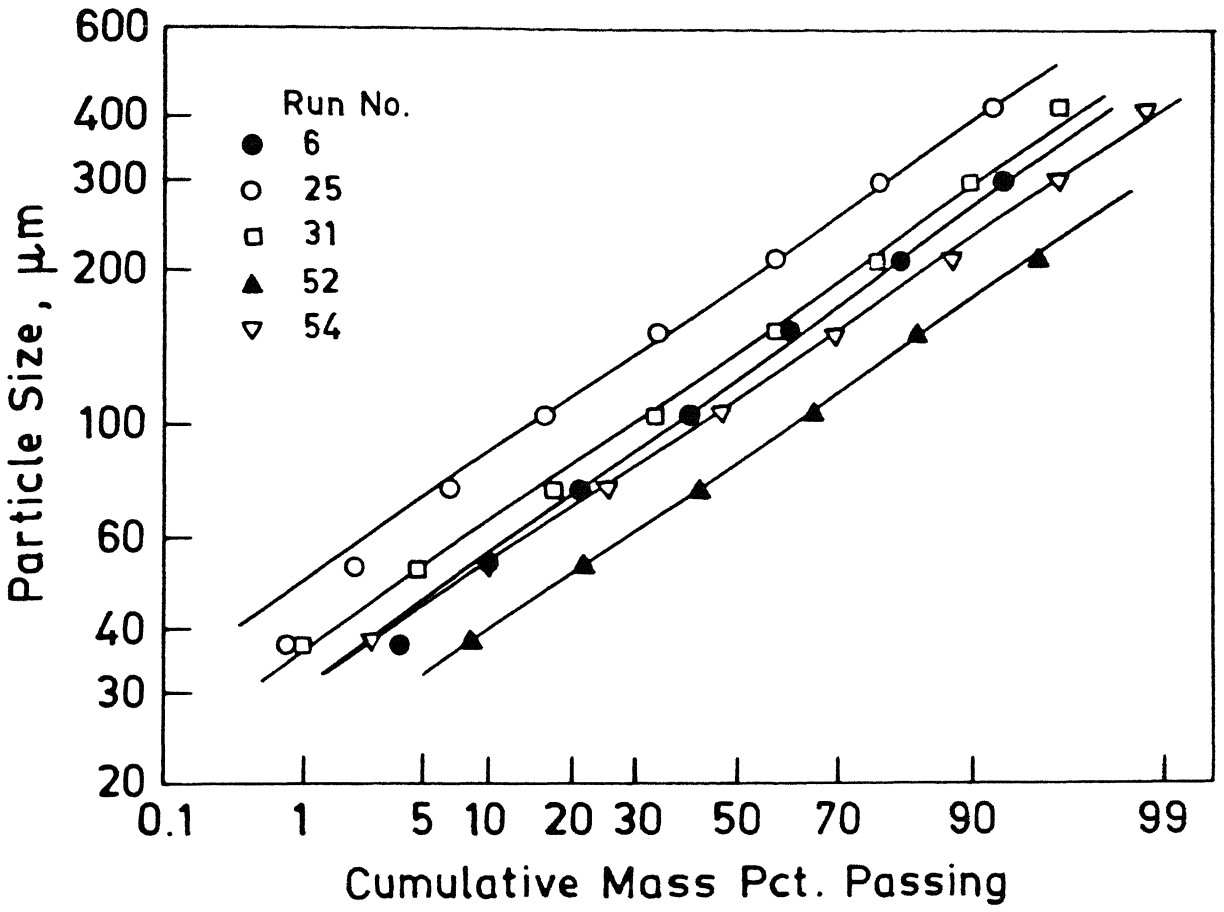

Figure 4.22 : Cumulative mass percent passing against particle size for different power collectives

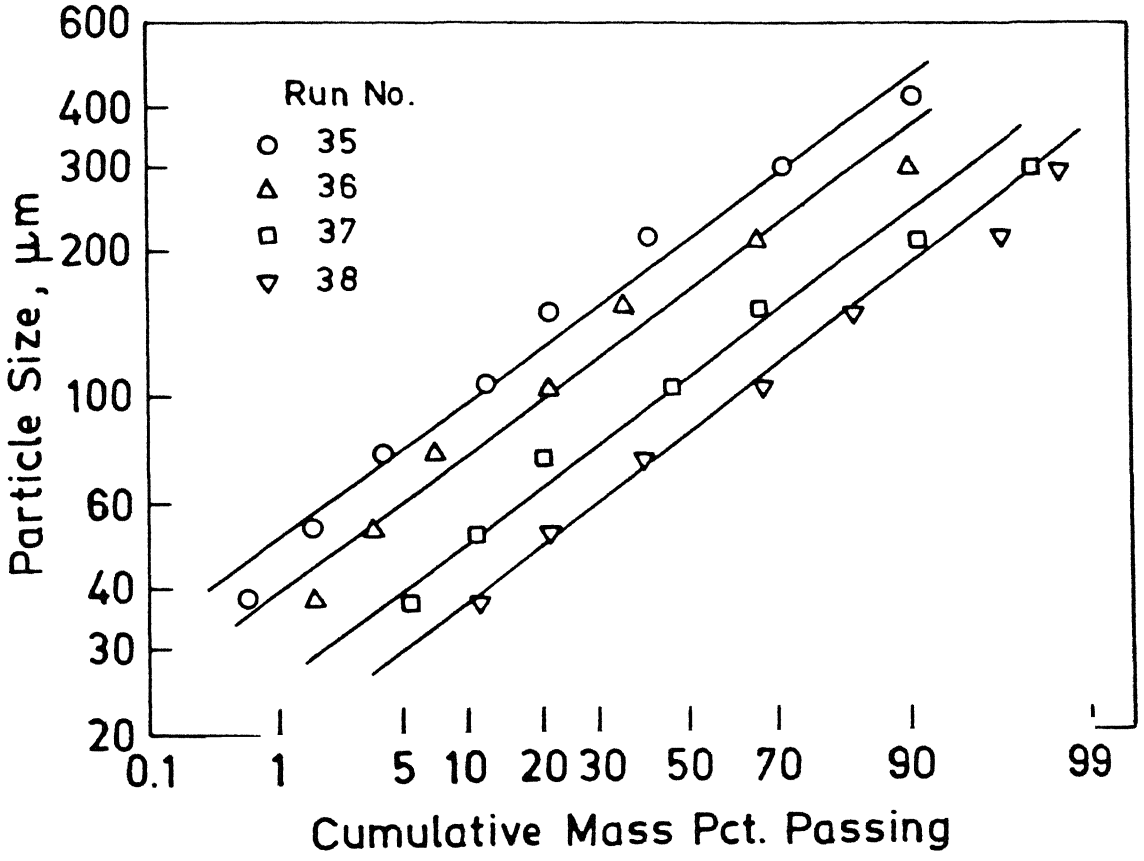

Figure 4.23 : Cumulative mass percent passing against particle size for different power collectives

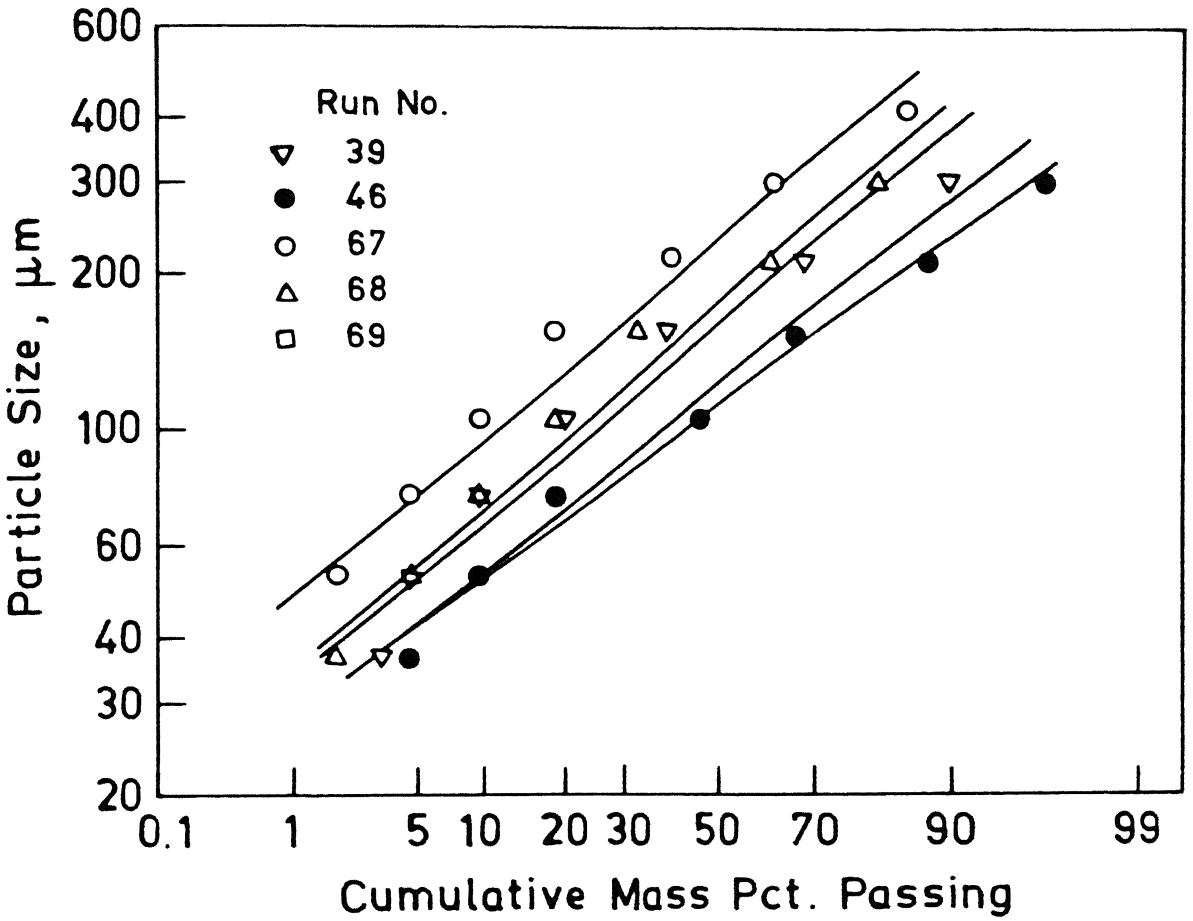

ure 4.24 : Cumulative mass percent passing against particle size for different power collectives

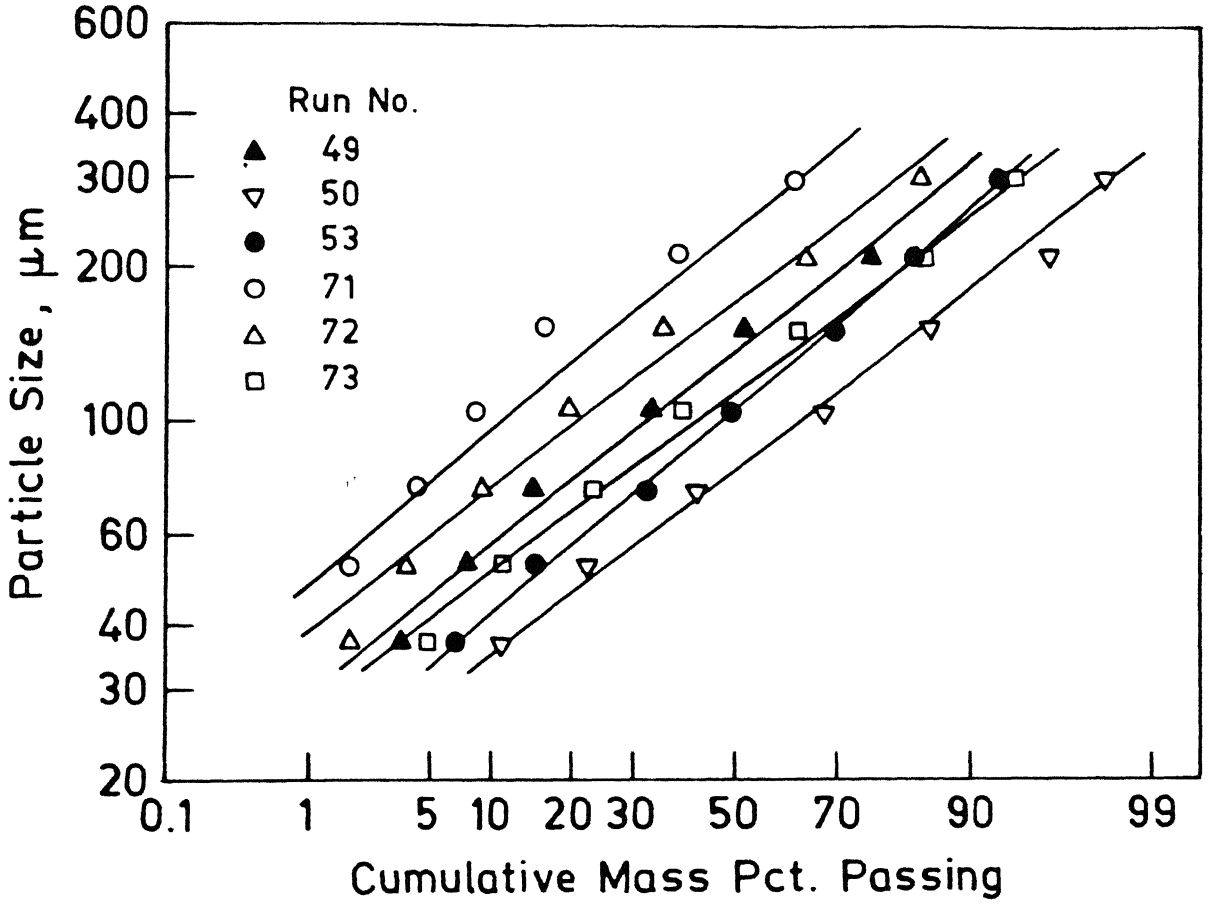

Figure 4.25 : Cumulative mass percent passing against particle size for different power collectives

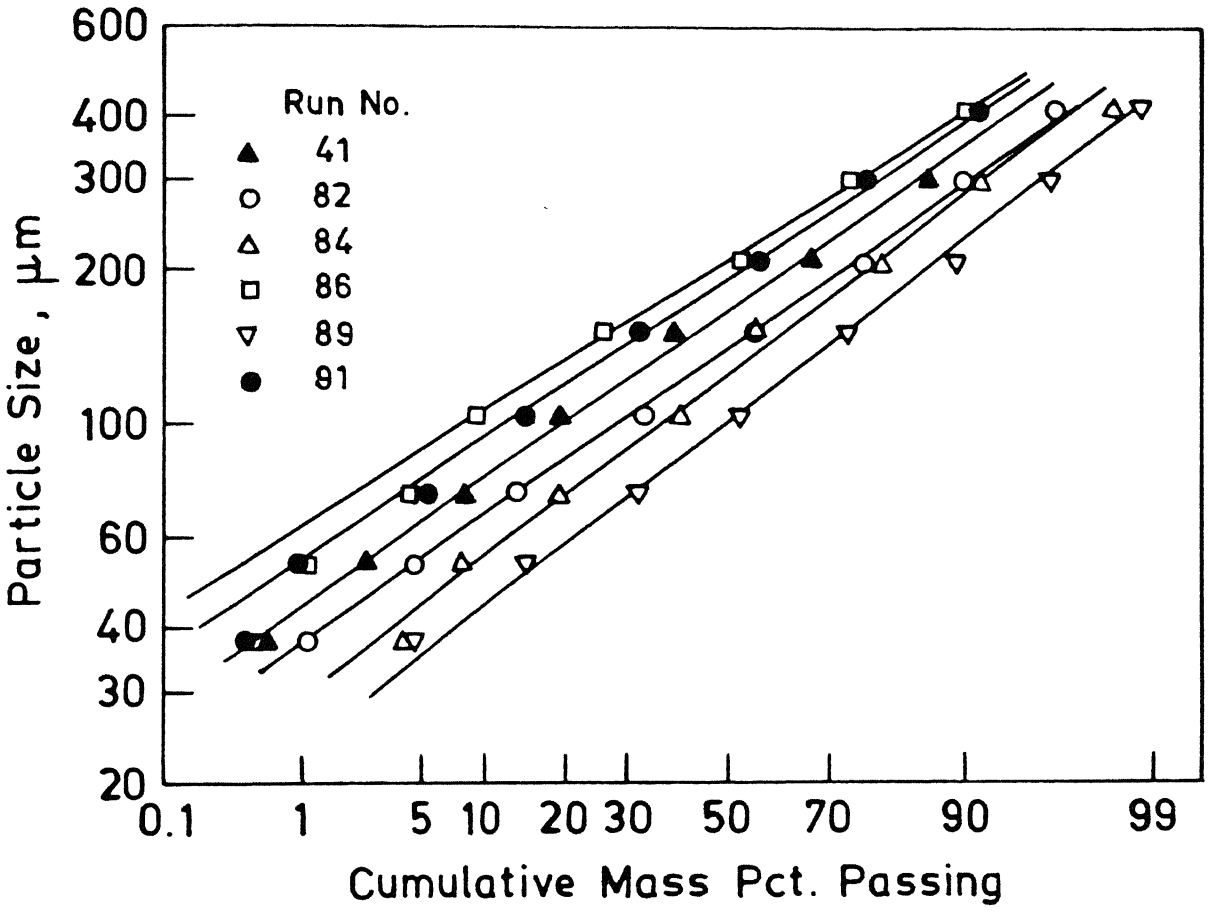

Figure 4.26 : Cumulative mass percent passing against particle size for different power collectives

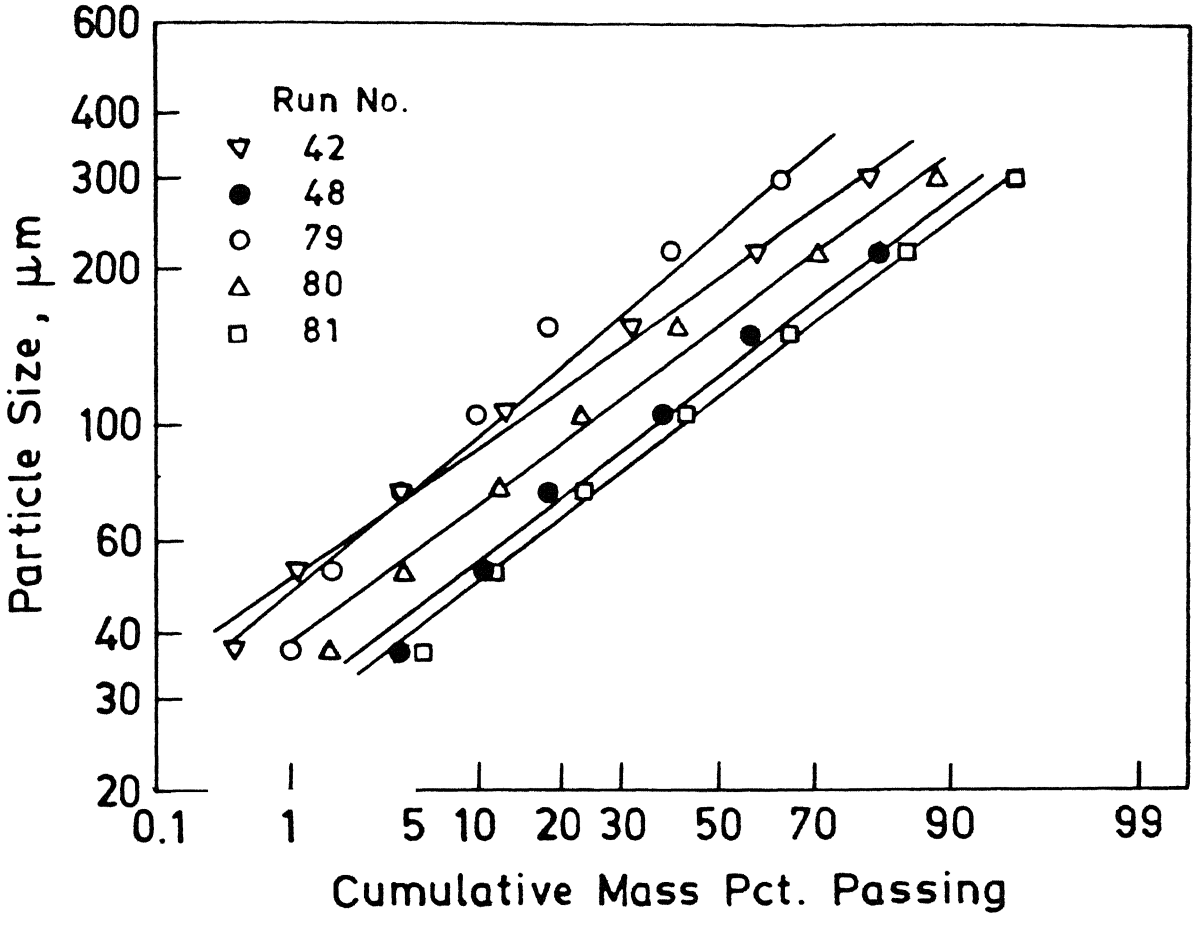

Figure 4.27 : Cumulative mass percent passing against particle size for different power collectives

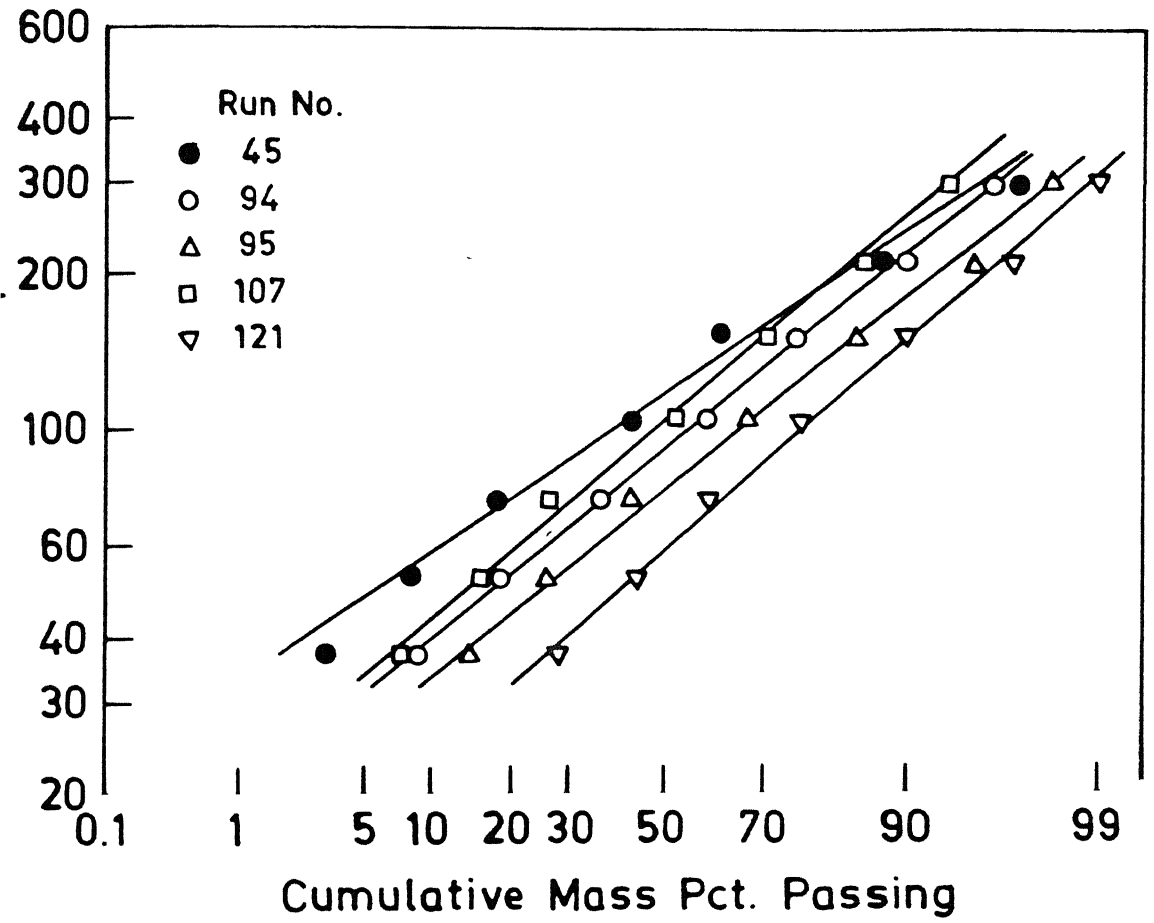

ure 4.28 : Cumulative mass percent passing against particle size for different power collectives

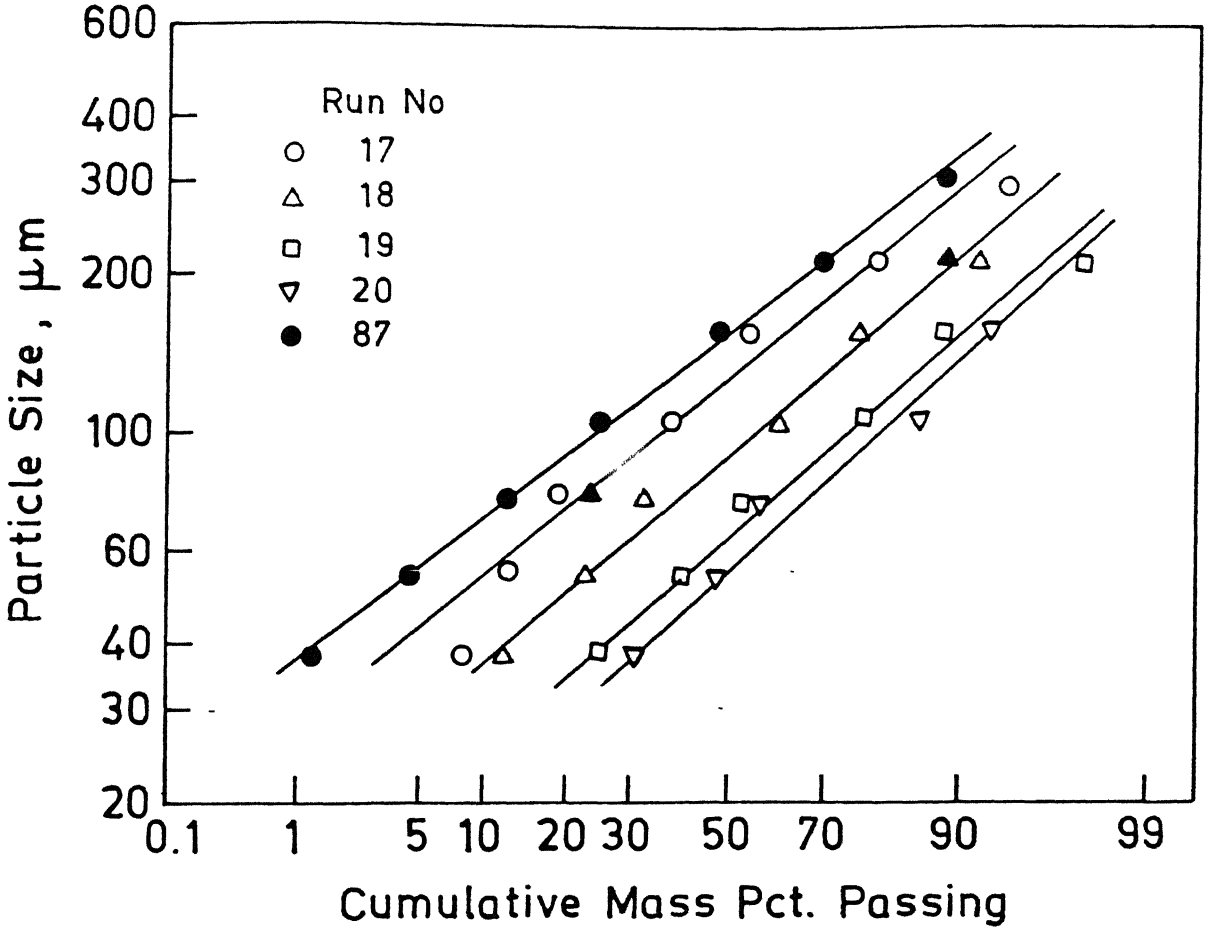

re 4.29 : Cumulative mass percent passing against particle size for different power collectives

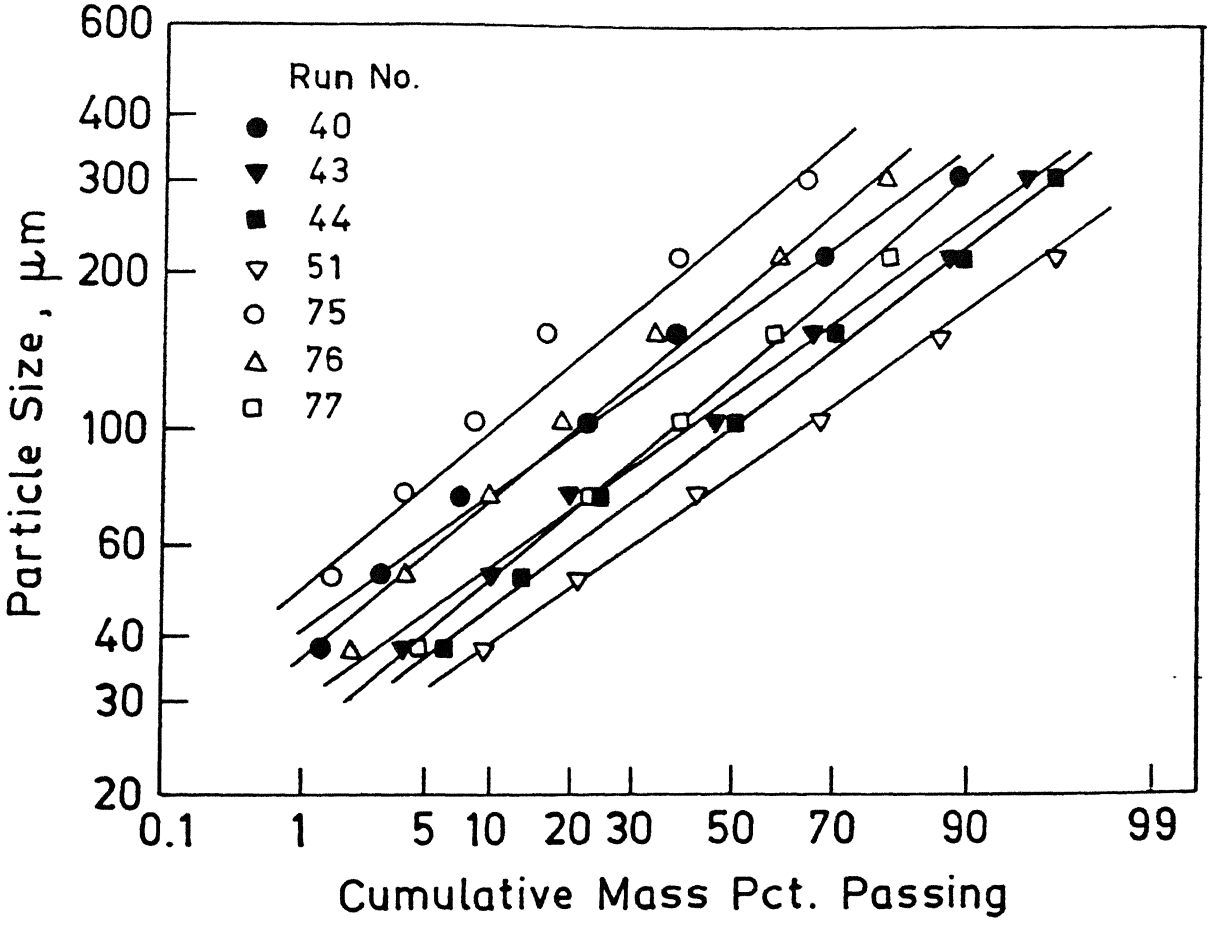

igure 4.30 : Cumulative mass percent passing against particle size for different power collectives

atomizer (Condition is no deposition of droplets on the atomizer surface). This condition limits the operation of an atomizer above a particular pressure which is termed critical pressure or maximum pressure.

Figure 4.31 shows the variation of critical mass median size with critical plenum pressure (solid lines) for different atomizers of A6, A4, a4 and B4 type of different focal lengths, apex angles number and nozzle diameter. Superimposed in this Figure also the values of focal lengths of different atomizers (dashed lines) for different critical pressures. The arrows on the Figure indicate the corresponding axes.

The increase in critical pressure caused either by increase in focal length or nozzle diameter decreases the critical mass median size. (Say for the A6 type atomizers increase in focal length from 83 mm to 110 mm, critical pressure increases from 600 kPa to 1200 kPa and critical mass median size decreases from 165 μm to 128 μm).

Further, the increase in apex angle increases critical mass median size. The cumulative effect is that the increase in critical pressure caused either by greater focal length or smaller apex angle or smaller nozzle diameter decreases the critical mass median size.

In the Figure 4.32, the effect of plenum pressure on mass median size is presented by plotting X_g/X_c versus P/P_c for different types of atomizers, namely A47, A49, B49, A412 and a412 of same apex angle. At the ratio $P/P_c = 1$, X_g/X_c is also equal to 1. Thus the point corresponding to $P/P_c = 1$ and $X_g/X_c = 1$ in the Figure 4.32 becomes a single point for all atomizers. Since P_c is fixed for a given type of atomizer and all the atomization experiments are conducted upto P_c, therefore increase in P will increase the

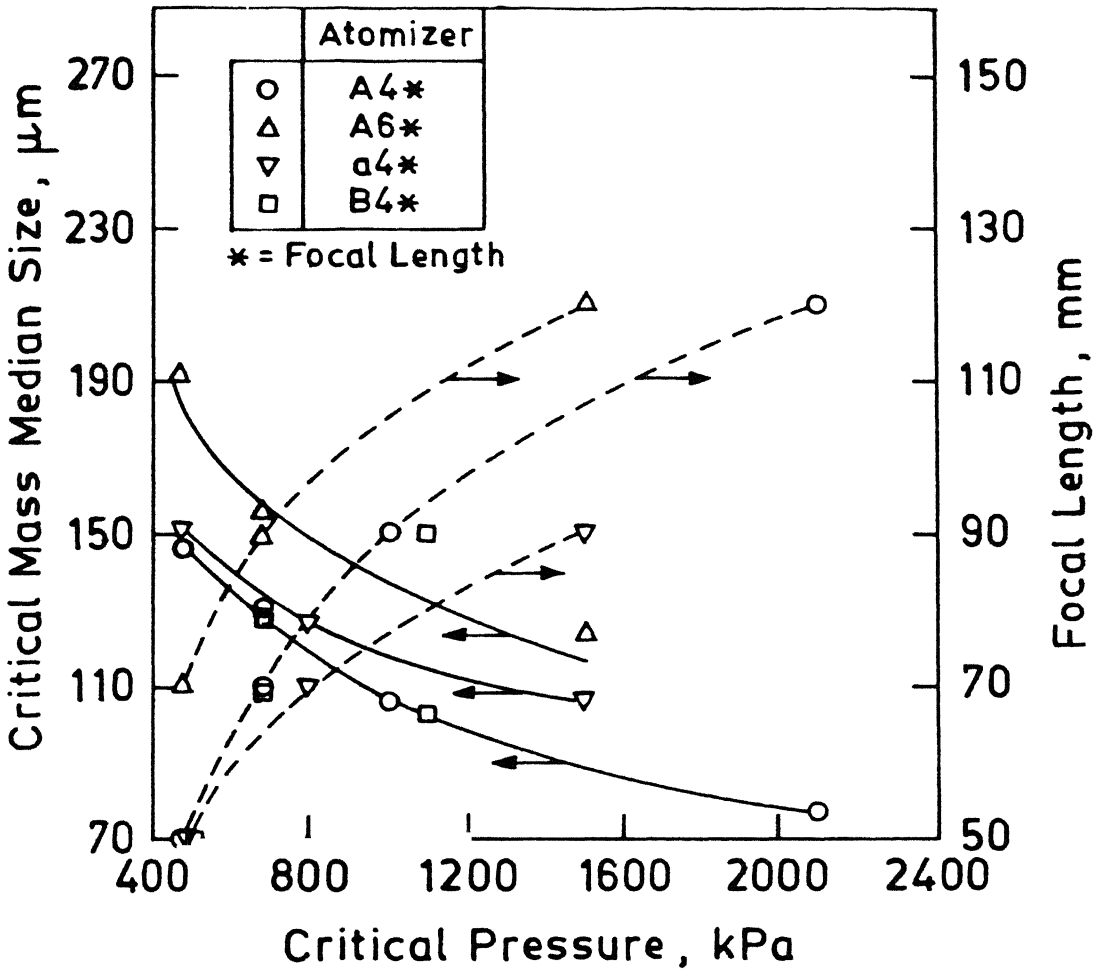

Figure 4.31 : Variation of critical mass median size and focal length with critical pressure

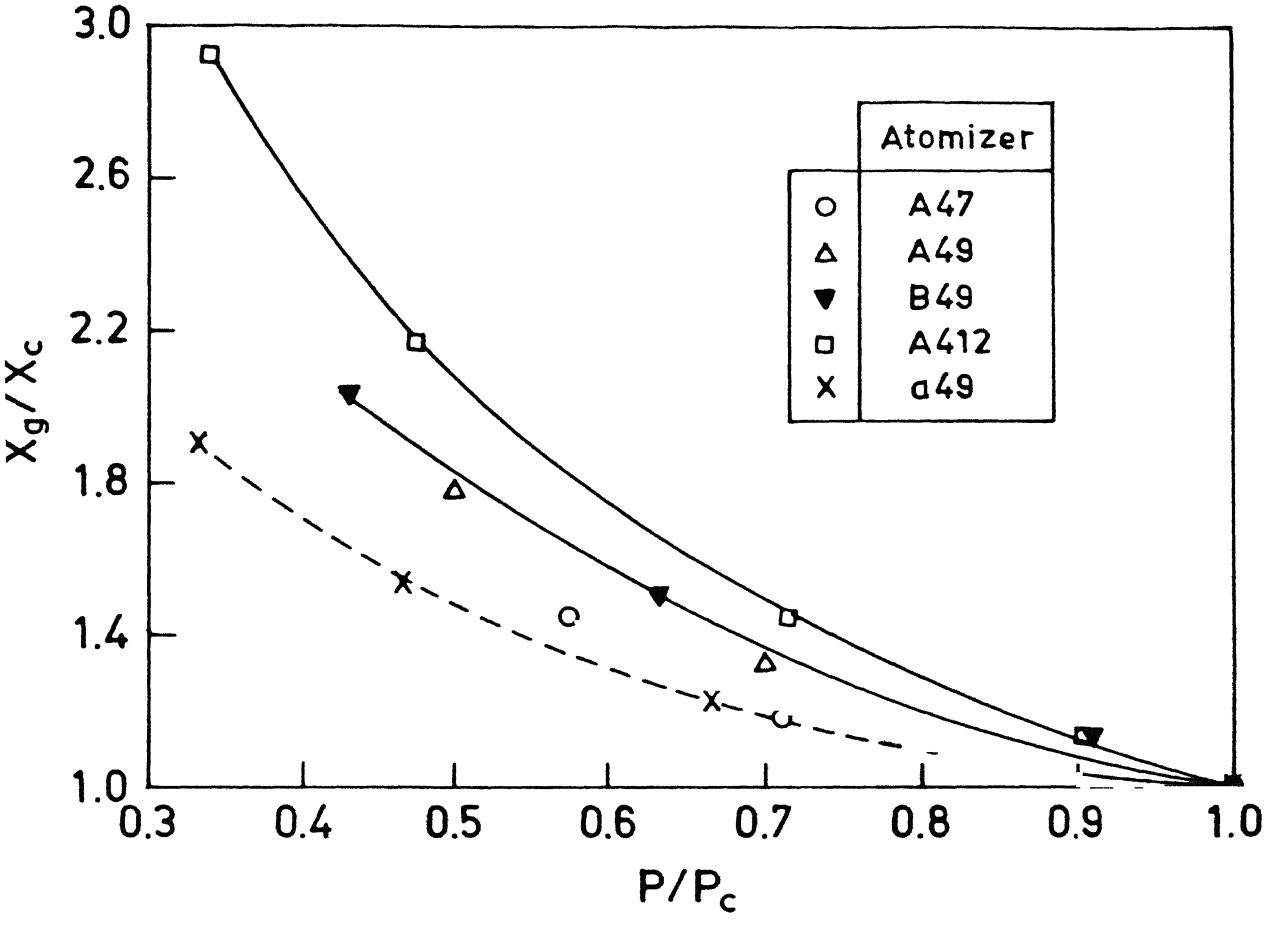

Figure 4.32 : Relationship between variation of the ratio X_g/X_c with P/P_c

ratio P/P_c to the maximum value 1 for all atomizers. The above imposed condition of P_c automatically sets-up a minimum value of X_c, hence increase in P will decrease the ratio X_g/X_c in accordance with the objective of higher pressure employed in atomization.

It can be seen in the Figure that increase in pressure decreases the mass median size for all types of atomizers. The results further indicate that collectives of different X_g can be produced by controlling the pressure.

B. ***Focal Length***

The variation of mass median size with focal length is shown in Figure 4.33 for atomizers a4 and A4 type containing nozzle of different diameter at different plenum pressures (all these plenum pressures are lower than critical pressures). It can be observed that the mass median size decreases by decreasing the focal length of the atomizer at all plenum pressures. The mass median size is smaller for the atomizers A4 type (3 mm nozzle diameter) as compared to that of a4 type (2 mm nozzle diameter), operated at same plenum pressure. For example, consider atomizers A47 and a47 operated at 500 kPa plenum pressure, the mass median sizes are 155 μm and 170 μm respectively.

C. ***Liquid Metal Superheat***

Figure 4.34 is a plot of mass median size versus superheat of liquid metal for an atomizer A612 operated at different plenum pressures (run No. 67-69, 71-73, 75-77 and 79-81). It can be observed that the mass median size of power collective at each plenum pressure is independent of superheat of liquid metal.

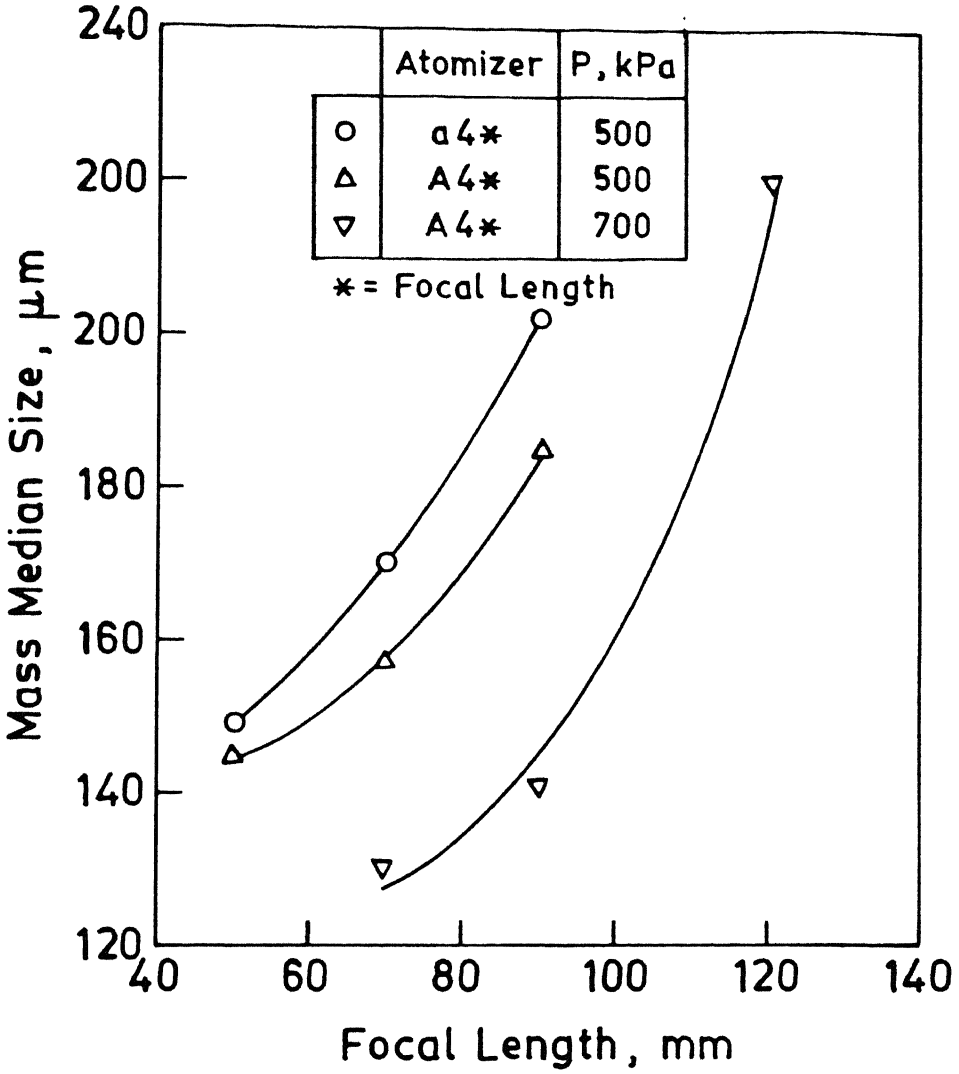

Figure 4.33 : Variation of mass median size with focal length of atomizer

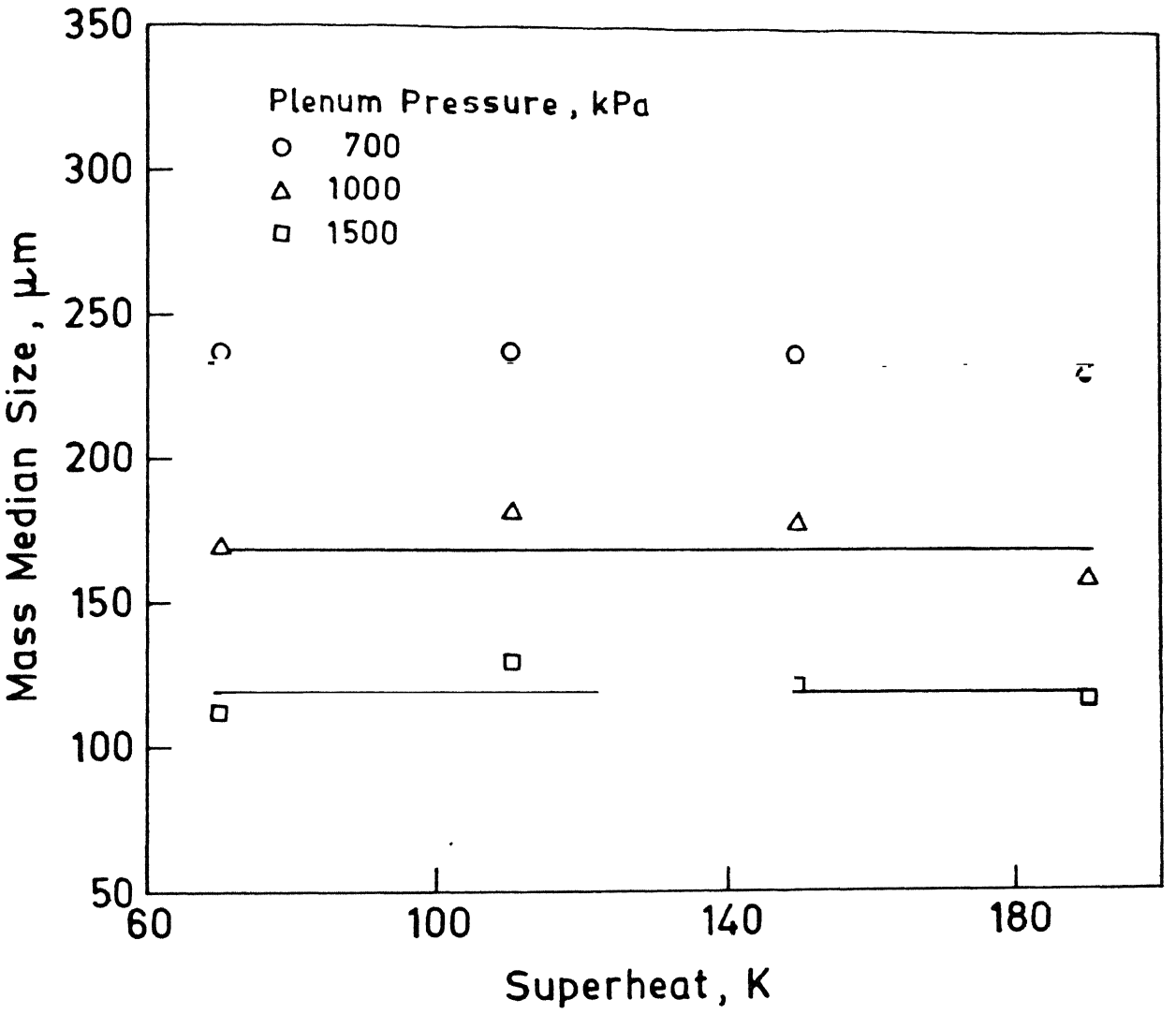

Figure 4.34 : Effect of superheat of liquid metal on mass median size for atomizer A412

D. *Apex Angle*

The variation of mass median size with apex angle is shown in Figure 4.35 for atomizers A212, A412 and A612 operated at different plenum pressures (run No. 17-19, 35-37 and 67-69). It can be observed that the mass median size at each plenum pressure, initially increases rapidly and then slowly with the increase in apex angle. For example, consider variation of X_g at 100 kPa with the apex angle, the mass median size increases by 77 μm by increasing the apex angle from 20° to 40° while it increases only 11 μm by further increase in apex angle from 40° to 60°.

E. ***Liquid Delivery Tube Diameter***

The mass median size is plotted in Figure 4.36 as a function of delivery tube diameter for atomizer A412 operated at different plenum pressures (run No. 36-53). It can be observed that the mass median size is almost independent of liquid delivery tube diameter up to 9.0 mm but beyond 9 mm, the mass median size tends to increase with the increase of liquid delivery tube diameter.

4.2.2.3 Geometric Standard Deviation

It can be seen in Table 4.5 that the geometric standard deviation of all powder collectives produced by varying atomizer and liquid related parameters varies within a very narrow range.

In the open technical literature, very few studies are available on atomization of liquid metals to produce metal powder by using atomizers of free fall type[4,5,8-16]. But

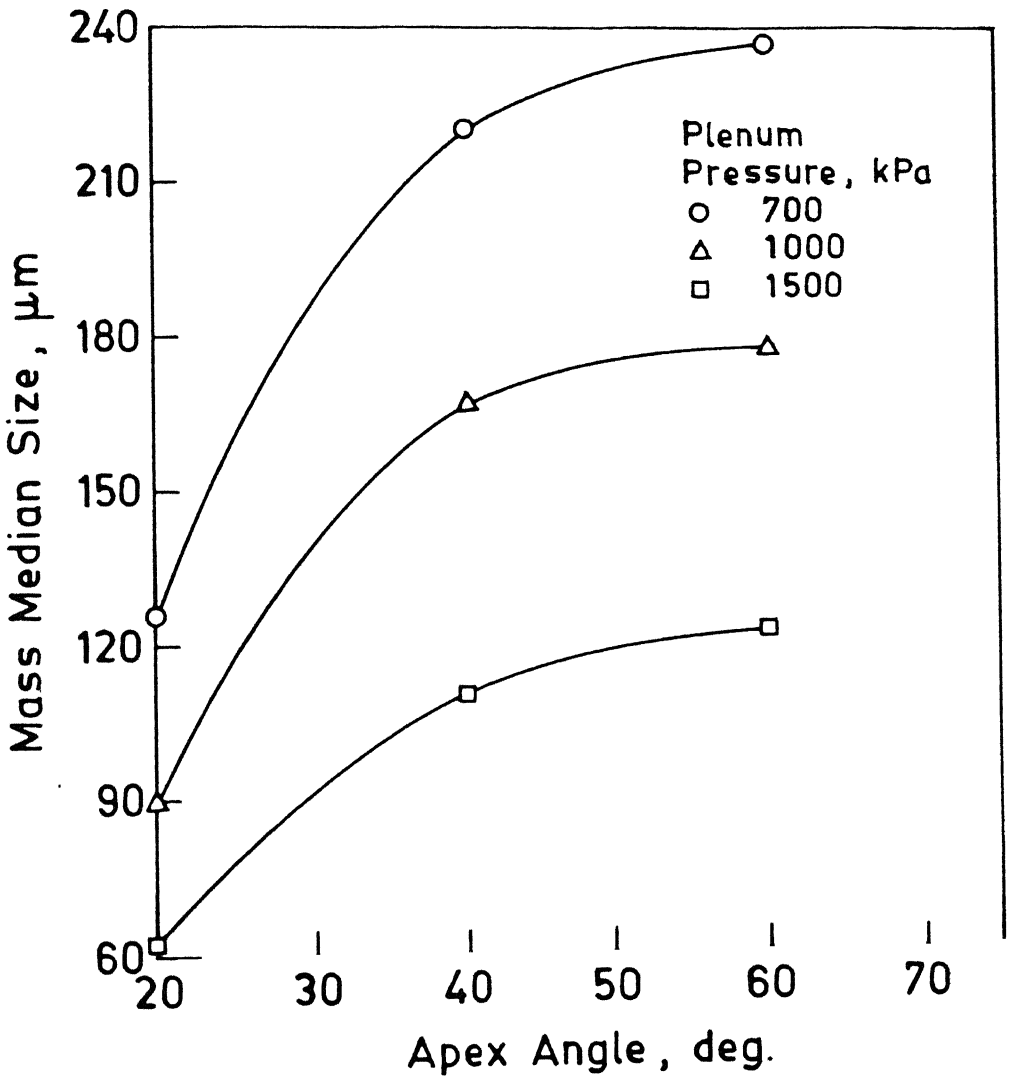

Figure 4.35 : Variation of mass median size with apex angle of atomizer

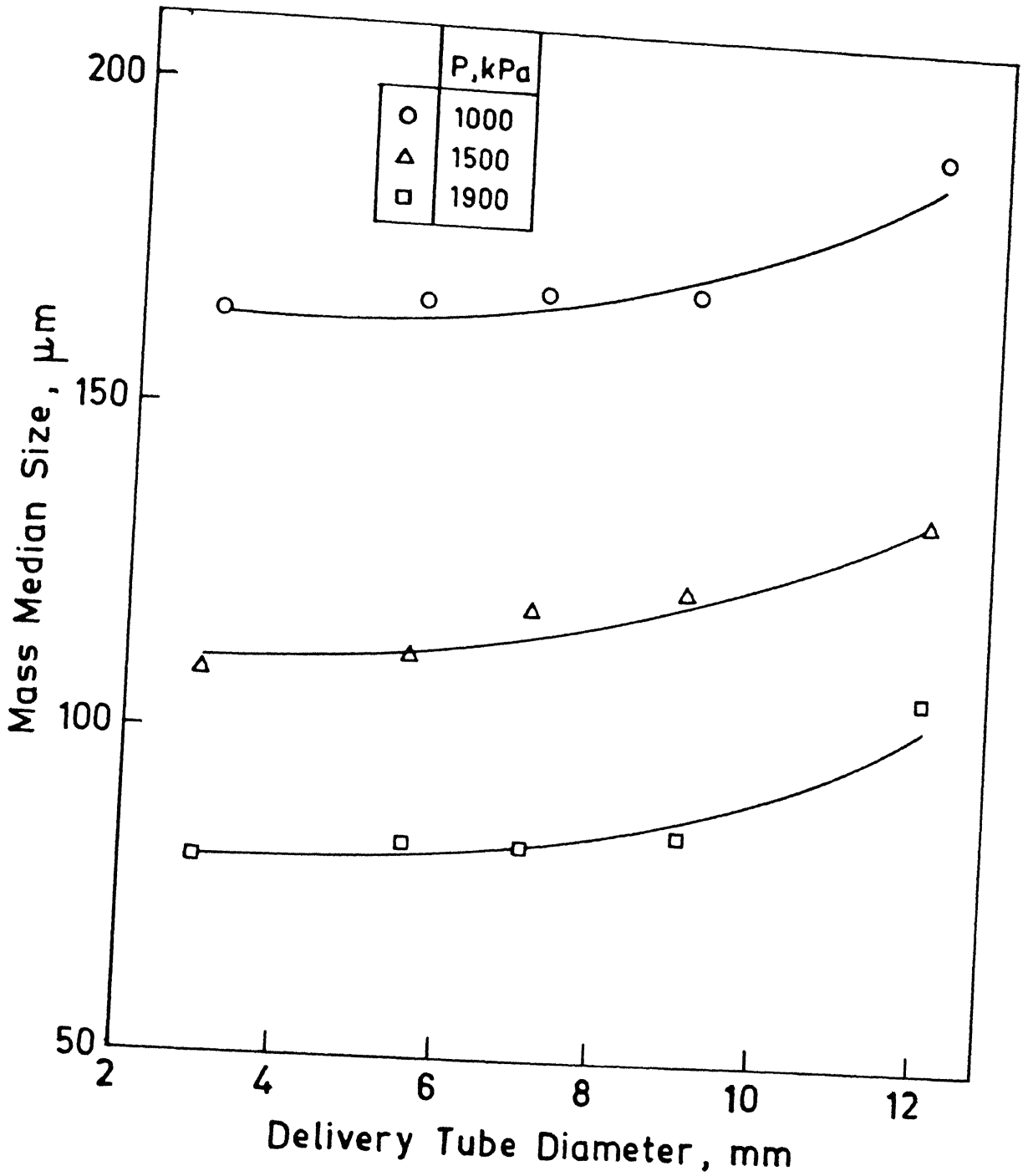

Figure 4.36 : Effect of metal delivery tube diameter on mass median size for atomizer A-412

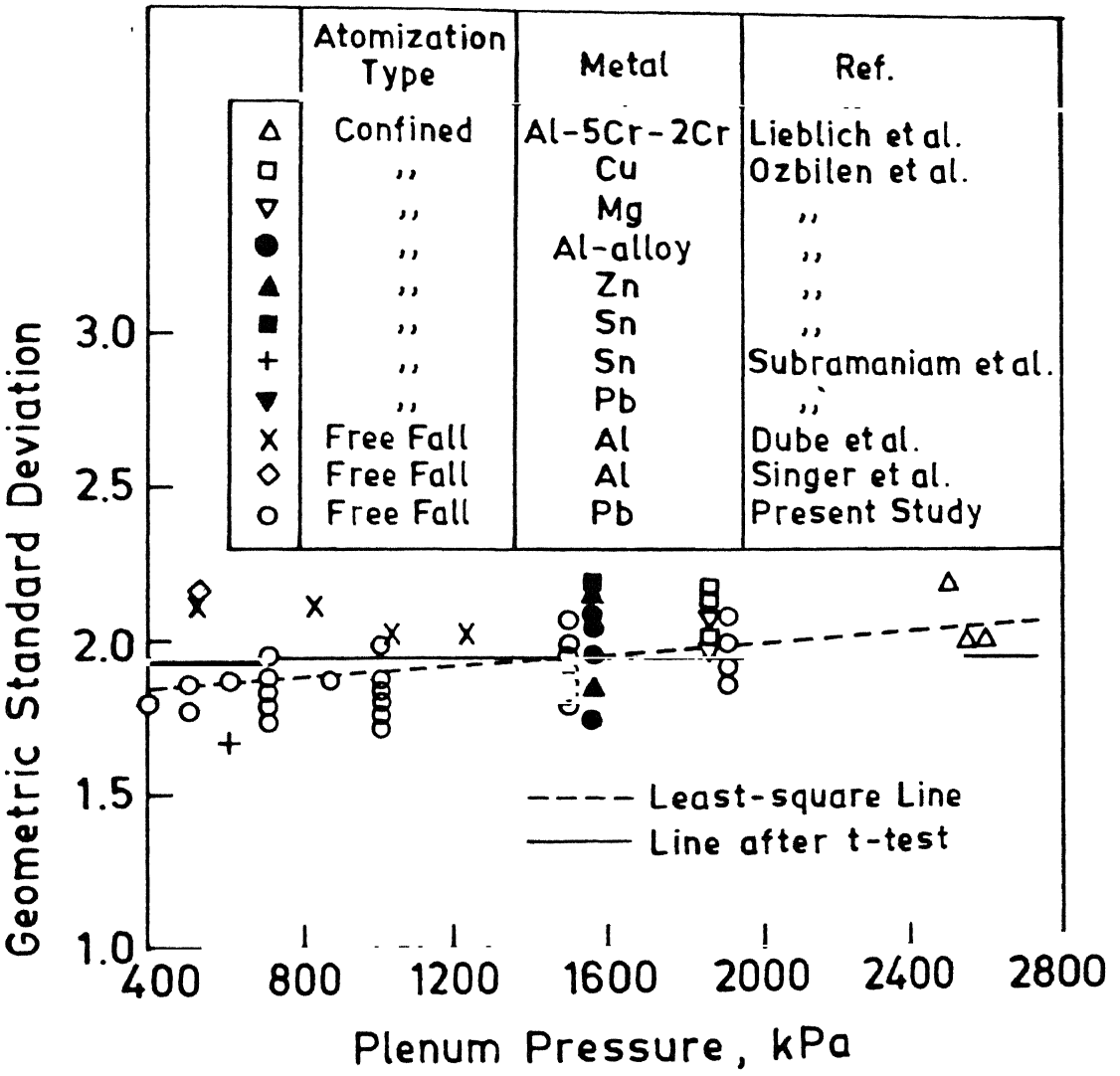

Figure 4.37 : Effect of plenum pressure on geometric standard deviation of powder collectives

several studies are available on confined type atomization to produce metal powder[2,19,20,21,27-31]. According to some studies, the geometric standard deviation varies within the range 2 to 2.4, whereas others have reported constant values.

In the Figure 4.37, all the available values of σ_g including the present one are plotted against plenum pressure. The least square analysis has given the following equation:

$$\sigma_g = 6.396 \times 10^{-5} P + 1.85 \qquad (4.4)$$

where, plenum pressure, P is in kPa. This line is shown as dashed line in the Figure. The slope of the regression line (equation 4.4) is tested by t-test. This test has yielded the test value $t_{exp} = 1.82$. This test value is compared with the 95% confidence level of the t-distribution is $t_{95} = 1.96$ for the experimental data of the present study. It can be seen that $t_{exp} < t_{95\%}$ which suggest, that the slope of the eq (4.4) can be neglected and σ_g can be taken as independent of pressure and is shown in the Figure by solid line passing through the mean value, $\sigma_g = 1.95$.

4.2.2.4 Specific Surface Area

It has been shown in Figure 4.18 to 4.30 that all the results on sieve analysis of powder collectives follow log normal distribution. According to log normal distribution the specific surface area of a collective consisting of spherical particles is given by[26] :

$$S_w = \exp\left[\ln \frac{\sigma}{\rho_m} - \ln X_g + 0.5 \ln^2 \sigma_g\right] \qquad (4.5)$$

According to equation 4.5 the specific surface area depends on ρ_m, X_g and σ_g. It has already been shown in Section 4.2.3.3 (Figure 4.37) that the geometric standard

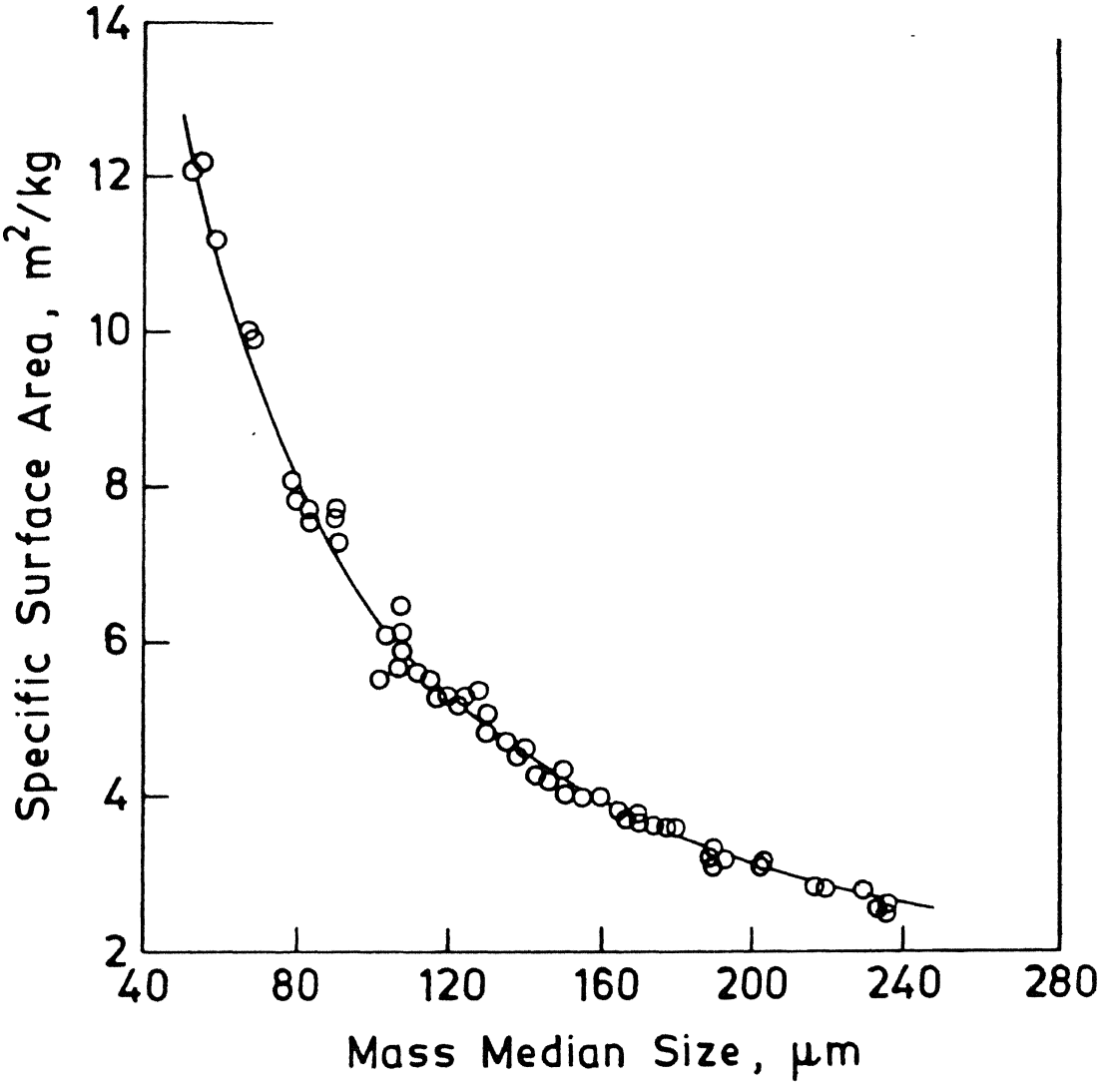

Figure 4.38 : Variation of specific surface area of powder collectives with mass median size

deviation, σ_g of all collectives of the present study (see Table 4.4 for all collective) neither depends on atomizer nor liquid metal related parameters. The constant value of geometric standard deviation is determined to be 1.95. Using this value of σ_g and ρ_m = 11370 kg/m^3 the S_w is plotted as solid line in Figure 4.38 against X_g for all the runs from 1 to 91 of the present study.

Independent to equation 4.5, the specific surface area is calculated for each size range of powder particles assuming spherical shape;

$$S_i = \frac{6M_i}{d_i \rho_m} \tag{4.6}$$

Total area of the powder collective is

$$S = \sum_{i=1}^{n} S_i = \frac{1}{\rho_M} \sum_{i=1}^{n} \frac{6M_i}{d_i} \tag{4.7}$$

where n denotes the total number of size ranges in a given powder collective. All the values calculated from equation (4.7) are given in Table 4.5. These values are shown on the Figure 4.42. It can be seen that the calculated values of surface area from sieve analysis are distributed very good along the line, representing the equation (4.5). Thus equation (4.5) represents very good the specific surface area of all the collective of the present study.

4.2.3 MORPHOLOGY OF POWDER

In this section the particle shape, porosity and surface texture are described for runs corresponding to 03 type of observation (see Table 3.3). The morphology of powder particle was studied for the powder collected in different sieve size ranges (Sieve analysis is given in Table 4.4). The observations were made to study the effect of plenum

pressure, apex angle, focal length, number of nozzles, diameter of delivery tube, superheat of liquid metal and type of metal.

4.2.3.1 Shape

Each collective of powder was found to contain particles of mixed shape. Some collectives contain mixture of spherical and rounded particles, whereas others contain particles of spherical, rounded and irregular shape. According to these two types of collectives, all runs were divided in two groups A and B as reported in Table 4.6. Group A contains runs corresponding to collectives containing spherical and rounded particle while that of Group B containing spherical, rounded and irregular particles. All observations are reported with run number and the corresponding mass median size of powder collective. From comparison of the particles shape of powder collectives of groups A and B it was observed that the shape of particles of powder collectives depend on the apex angle and superheat of liquid metal. The shape of particles was also found to depend on the size range within a powder collective.

A. ***Effect of Apex Angle***

Figures 4.39 (a, b and c) shows photographs of lead powder particles within the size range 76 - 211 μm produced by atomizers (A212, A412 and A612) having different apex angles 20°, 40° and 60°. These runs are 18, 36 and 68 respectively in table 4.6. The liquid metal was superheated to 150 K. It can be seen that the proportion of spherical powder particles in the photographs b and c is more as compared to other shapes. Whereas proportion of rounded and irregular shape is more in photograph a, which is for atomizer of apex angle 20°.

Table 4.6 : Shape of powder particles in different size ranges

A.	Run No	9	27	31	35	36	37	39	67	68	69	87
	$X_{g,\mu m}$	163	130	139	220	166	113	164	239	177	123	155

Size Range μm	Shape
< 38	Large proportion of particles were spherical and remaining were rounded.
38-53	-do-
53-76	-do-
76-105	About equal distribution of spherical and rounded particles.
105-152	-do-
152-211	Some near spherical and remaining rounded.
211-300	-do-
300-420	Few near spherical and remaining rounded
420-600	-do-

B.	Run No	54	71	72	73	75	76	77	79	80	81	18	19	20	21	95	107	121	15
	$X_{g,\mu m}$	80	237	171	117	238	181	127	235	158	115	91	66	58	67	80	106	61	52

Size Range μm	Shape, Porosity, Shrinkage
< 38	Major number rounded and irregular, and few spherical.
38-53	-do
53-76	-do
76-105	-do
105-152	-do
152-211	-do
211-300	Rounded and irregular
300-420	-do
420-600	-do

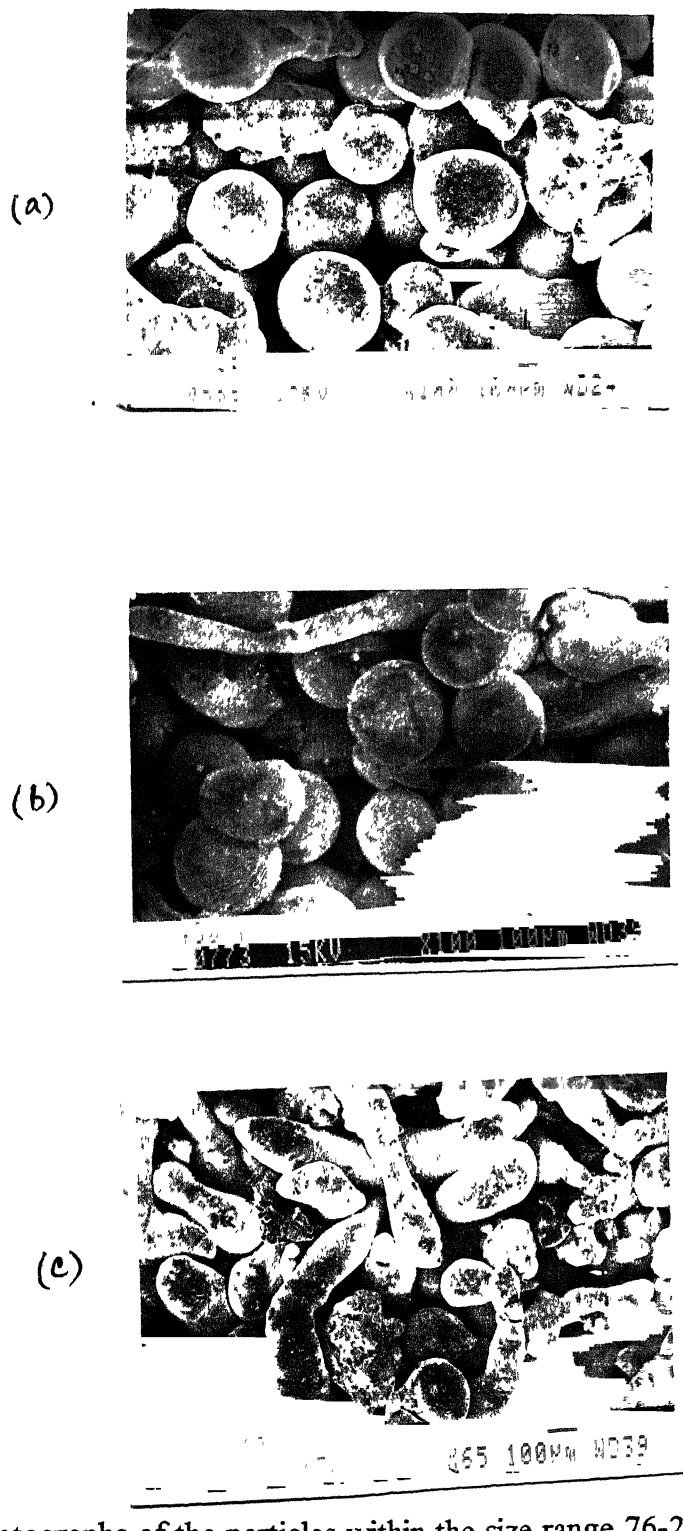

Figure 4.39 : SEM photographs of the particles within the size range 76-211 μm produced by atomizers of different apex angles (a) 60° (Run No. 18) (b) 40° (Run No. 36) (c) 20° (Run No. 68)

B. ***Effect of Superheat of Liquid Metal***

Figure 4.40 (a, b, c and d) shows photographs of lead powder particles (76-211 μm) produced by an atomizer A612 at different superheat of liquid metal corresponding to run No. 69 (150K), 73 (70K), 77 (110K) and 81 (190K), respectively. It can be observed that except at superheat of 150 K, the particles are rounded and irregular shape. Only at a superheat of 150 K large proportion of particles are spherical and remaining ones are rounded.

C. ***Effect of Particle Size Range***

Figures 4.41 (a, b and c) shows SEM photographs of lead powder particles in different size ranges, viz. <38 μm, 105-152 μm and 211-300 μm corresponding to run No. 37. It can be seen in photograph a that large proportion of powder particles in the size range <38 μm is spherical. In the 105-152 μm range about equal proportion of spherical and rounded particles can be seen in photograph b. As size range increased to 211-300 μm, photograph c shows that few particles are nearly spherical whereas others rounded shape. The shape of powder particles corresponding to the above runs is summarized in Table 4.6 for all sieve size ranges. It can be observed that the proportion of spherical particle in a size range is decreasing by increasing the particle size.

D. ***Effect of Type of Metal***

Figure 4.42 (a, b, c) show photographs of zinc (run No. 95), aluminum (run No. 107) and tin (run N0. 121) powder produced at superheat of 150 K by an atomizer A212.

(a)

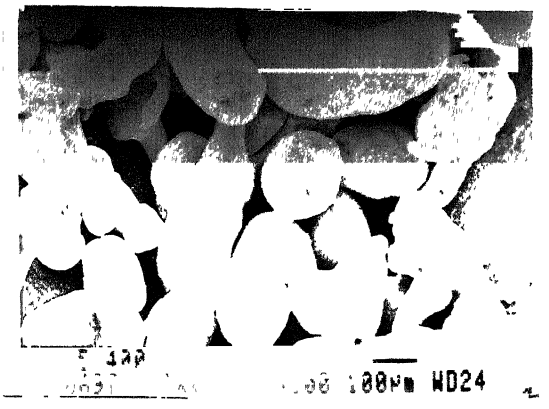

(b)

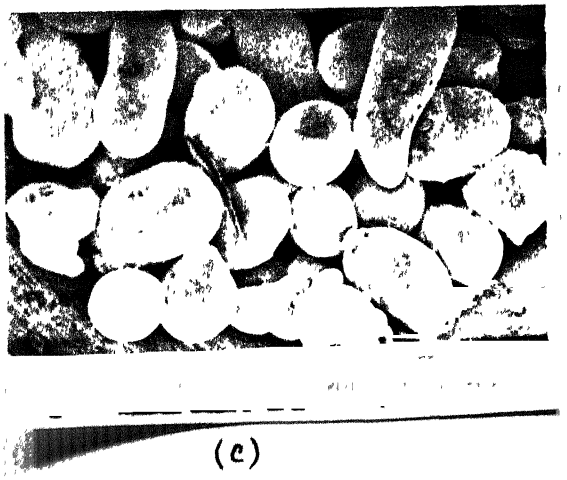

(c)

(d)

Figure 4.40 : SEM photographs of the particles within the size range 76-211 µm produced by atomizers of different apex angles (a) 70 K (Run No. 73) (b) 110 K (Run No. 77) (c) 150 K (Run No. 69) (d) 190 K (Run No. 81)

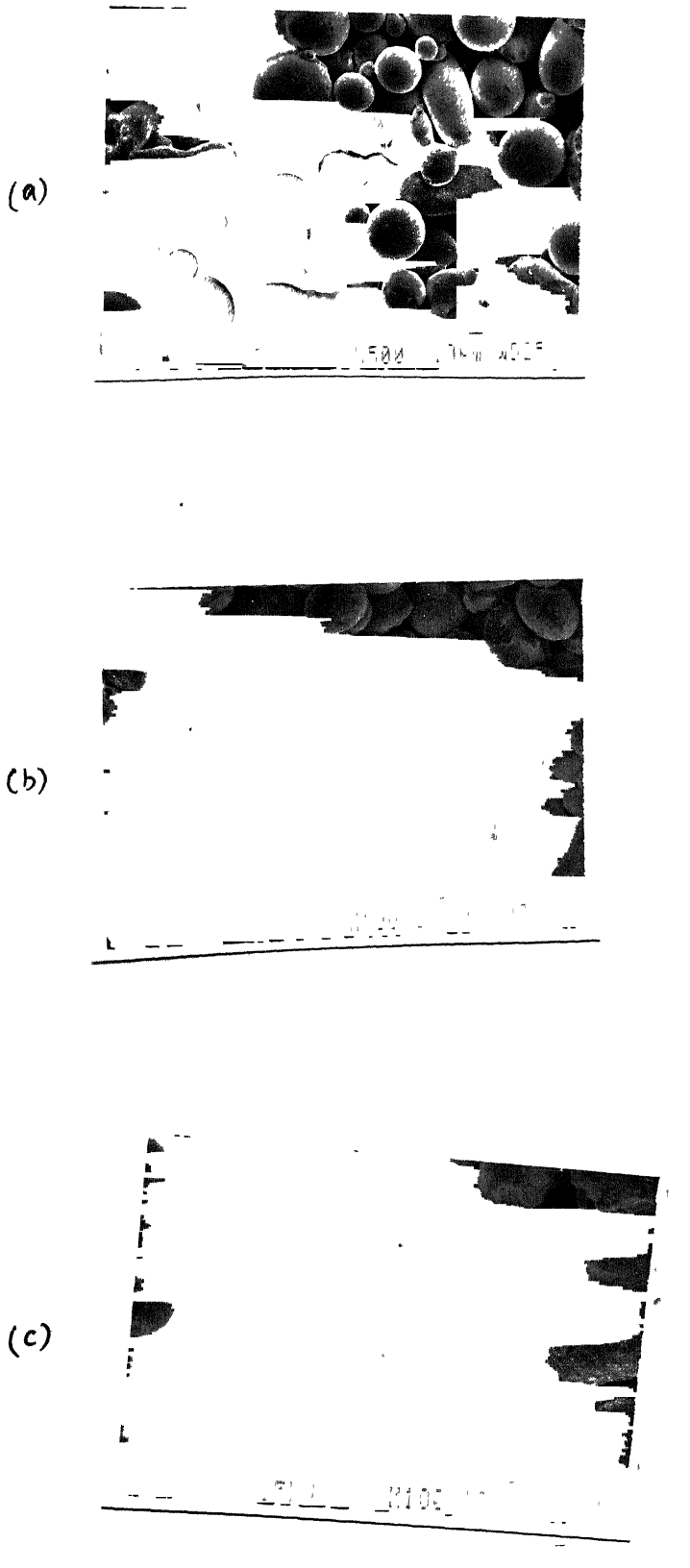

Figure 4.41 : SEM photographs of the particles (Run No. 37) lying in different size range of a collective (a) < 38 μm (b) 105-152 μm (c) 211-300 μm

(a)

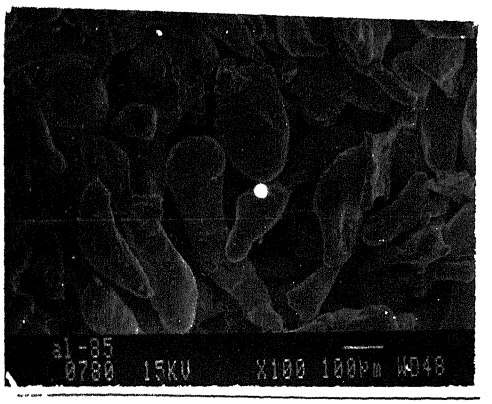

(b)

(c)

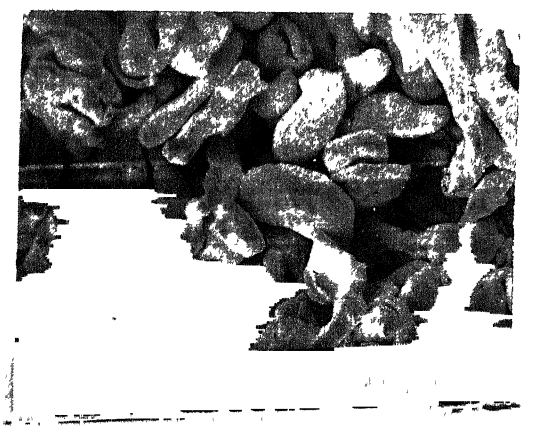

Figure 4.42 : SEM photographs of particles within size range 76-211 µm of different metals (a)

Most of the particles can be seen to be irregular and rounded. This suggests that these particles did not get sufficient time to spherodize before complete solidification.

4.2.3.2 Porosity and Surface Shrinkage

Figure 4.43(a) (for lead) and (b) (for aluminium) show SEM photographs of the surface of particle. It can be observed that there are some dark black spots on the photographs. These spots show the presence of porosity in powder particle of both metals. Similar type of porosity was observed in powder particles produced for all runs.

Figure 4.44(a) shows the surface of a particle which is rough and has some waviness. This type of surface may be due to the solidification shrinkage of Pb and Al which indicate that the liquid metal existing at the surface solidify at the end of solidification process. The surface shrinkage as well as porosity can also be seen in Figure 4.44(b).

4.2.4 SIZE OF SPHERICAL SHAPE DROPLETS

Maximum size of the spherical shape particle, solidified during flight is determined by observing the powder particles under SEM and using the following analogy:

According to observations reported in Section 4.2.3.2, it appears that particles are solidifying from centre to surface. This mode of solidification gives enough time for droplets to spheroidize before the completion of solidification. Since the droplet is solidified and spheroidized, surface of the droplet should be free from cracks. On the other hand, the presence of any crack on the surface of the spherical shape particle indicate that the particle is partially solidified and the crack is formed due to hitting of such particles on the surface of the powder collection tray.

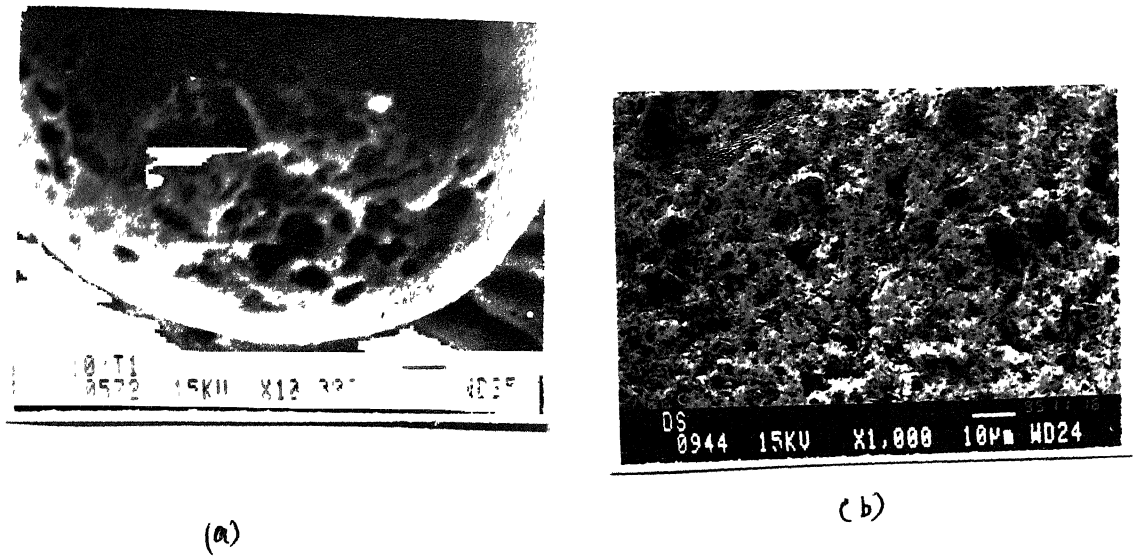

(a) (b)

Figure 4.43 : SEM photographs of a powder particle (a) lead (b) aluminium. Black spots are the porosity

(a) (b)

Figure 4.44 : SEM photographs of particle having (a) Waviness (b) Waviness and Black spots

Thus, if the powder collective is observed under SEM, then by observing the spherical particles without and with surface cracks, one can find the maximum size of a spherical particle which has been solidified under the chosen experimental conditions.

Figure 4.45 (a) is a SEM photograph of the maximum spherical shape particle (109 μm) without any crack and Figure 4.45 (b) of the particle with a surface crack as found on a tray positioned at a distance of 400 mm from the geometric point. This powder is produced at 1100 kPa using A412 atomizer. The spherical shape of this particle appears to be distorted on hitting the tray, which is an evidence of incomplete solidification. The average size of the particle is 115 μm. All the particles greater than 109 μm were found to be like Figure 4.45 (b).

Similarly, the sizes of maximum size spherical particle collected on six conical trays were determined for the powder produced at 1000 kPa, 1500 kPa and 1900 kPa using an atomizer A412 (Parameters corresponds to run No. 36, 37 and 38). The size of aforementioned particles produced at 1000 kPa and 1500 kPa plenum pressure using an atomizer A612 (parameters corresponds to run No. 68 and 69) and collected on six conical trays were also determined. All the collected data are reported in Table 4.7.

The solidification distance of spherical droplets is determined from vertical distance of each tray as follows:

Maximum size of the spherical shape droplet found on a tray represents that it has been solidified completely just upto the tray. Six trays intercepted the liquid metal droplets, moving with the gas stream, along the horizontal plane N_1Q_1, N_2Q_2, N_3Q_3, N_4Q_4, N_5Q_5 and N_6Q_6 as shown in Figure 4.46. Let us take the example of the first tray. The

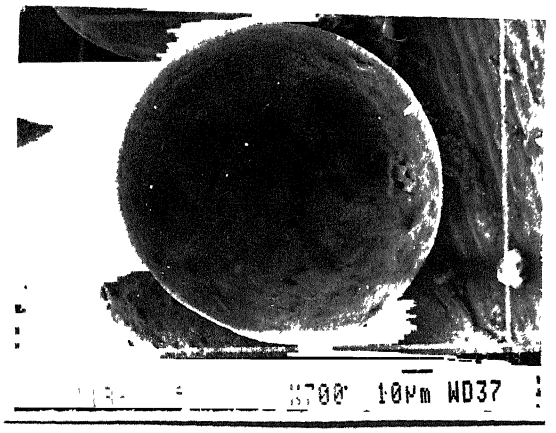

(a)

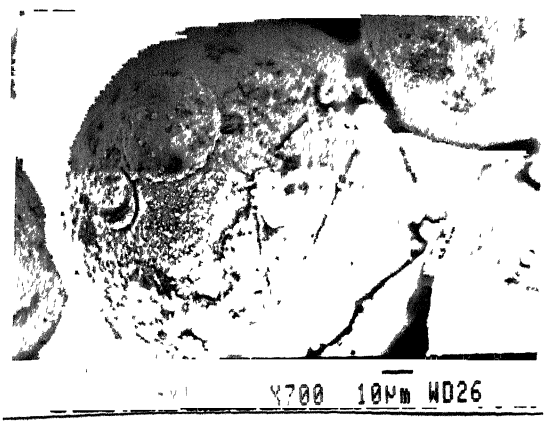

(b)

Figure 4.45 : SEM photographs of particle found on first tray

(a) Spherical particle of maximum size

(b) Particle showing crack (P = 1000 kPa, $\alpha = 40°$, $\Delta T = 150$ K)

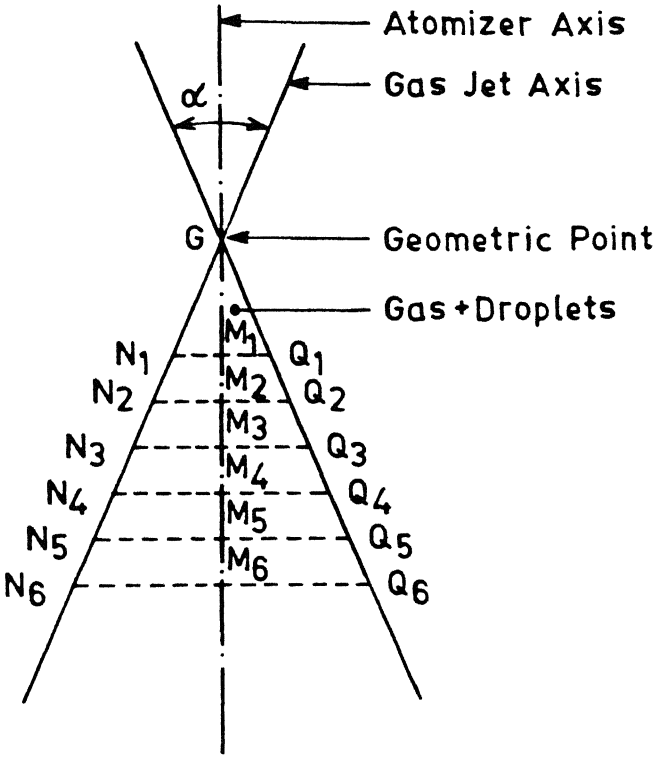

Figure 4.46 : Schematic sketch of the scheme of calculation to determine solidification distances of metal droplets moving in the gas stream

Table 4.7 : Maximum size (μm) of spherical particle without any crack observed on the trays

Run No.	α deg	P kPa	Tray No. 1	2	3	4	5	6
36	40	1000	109	150	200	226	280	309
37		1500	95	133	160	233	243	252
38		1900	75	122	140	182	226	245
68	60	1000	107	137	195	240	260	310
69	60	1500	97	126	171	200	226	250

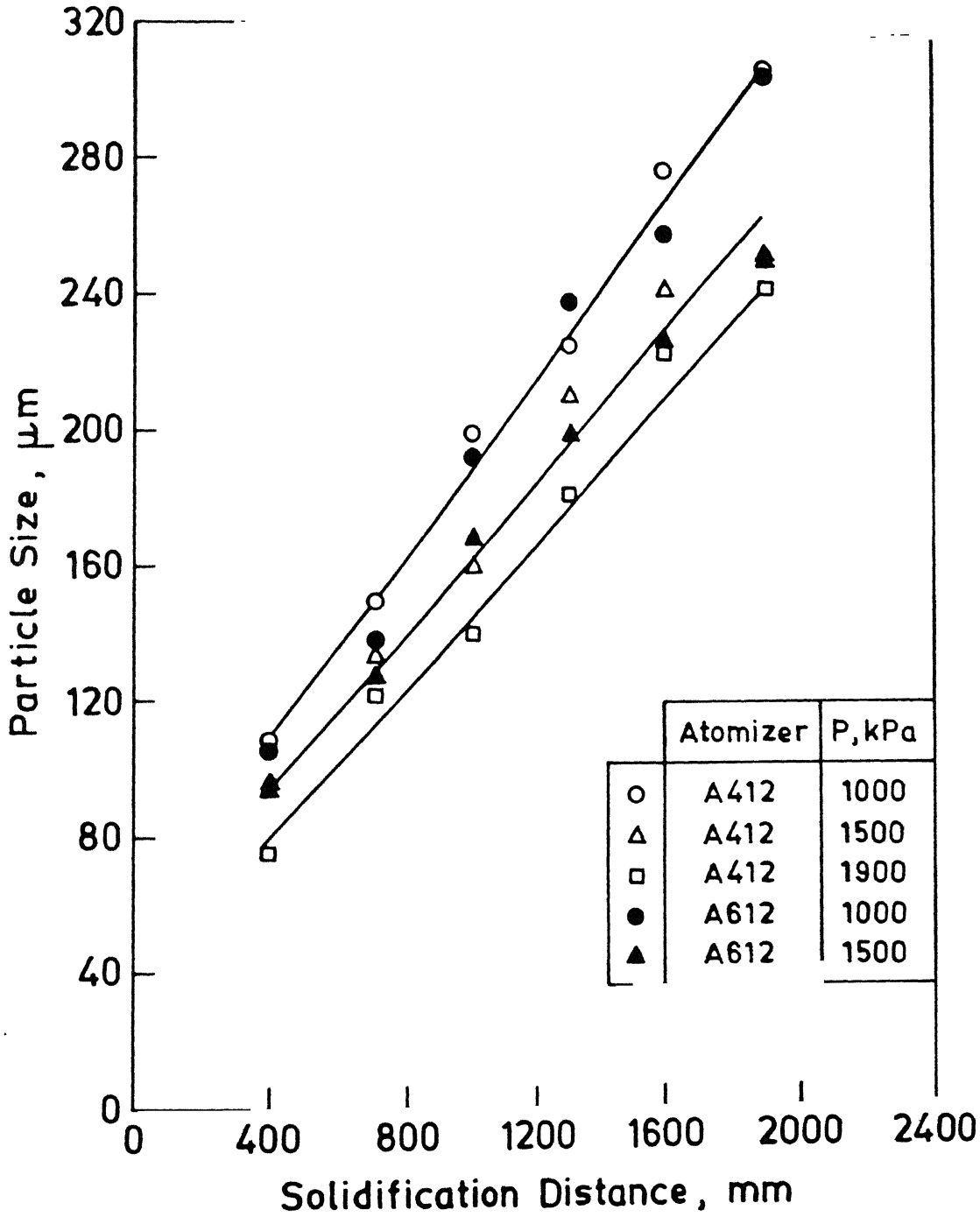

Figure 4.47 : Effect of size on solidification distance of spherical particles

solidification distance for the maximum size spherical powder obtained on the tray would be in between the minimum value of GM_1, or the maximum value of inclined distance GN_1. Since motion of particle is not known, hence a mean of GN_1 and GM_1 was taken for the solidification distance.

Figure 4.47 show the variation of the particle size versus their solidification distance for atomizer A412 and A612, operated at different plenum pressures. It can be observed that the solidification distance varies linearly with the particle size. The solidification distance is higher at higher plenum pressure for the particle of same size. For example, the solidification distances for 160 μm size particle are 80 cm and 110 cm at plenum pressure of 1000 kPa and 1900 kPa, respectively. It can be seen that the values of solidification distances are almost same for same size of particle produced by atomizers of different apex angles of 40° or 60°.

CHAPTER - 5

DISCUSSIONS

This chapter discusses the results obtained on variation of pitot pressure in terms of velocity of atomizing gas produced by the atomizer. From the results on atomization of liquid metals, velocity of gas to produce metal powder and the resulting powder characteristics are discussed. From the large data collected on the above aspects, empirical correlations are derived as a function of parameters related to atomizer and liquid metal to determine the velocity of the atomizing gas field, velocity of gas for atomization of liquid metals, mass median size of a powder collective. The shape of the particles in a powder collective and the factors influencing the shape are also discussed. From the results on the specific surface area of collectives, the atomization efficiency is also calculated and its variation is presented as a function of atomizer/liquid related parameters.

5.1 VELOCITY OF ATOMIZING GAS FIELD

The atomization gas field created by impingement of gas jets is found to possess large variation in velocities both in horizontal and vertical directions with reference to geometric point of atomizers (see figures 4.8 and 4.9 for the magnitude of variations). In the free fall atomization, the metal stream coincides with the atomizer axis and the liquid stream is accelerated and disintegrated by the energetic gas field consisting of wide

varying velocities. In order to simplify experimentation and theoretical analysis the gas velocities along the vertical axis passing through the geometric point of the atomizer is employed as representative of the gas flow behavior and accordingly correlations are developed to determine the velocities.

5.1.1 VELOCITY AT GEOMETRIC POINT

The experimental results suggest that the velocity at geometric point of atomizers of different focal lengths and number of nozzles increases with increase in plenum pressure and nozzle diameter (see Fig. 4.1). This observation can be explained by considering the formation of the gas field around the geometric point.

The nozzles of an atomizer converts certain flow rate of gas into jets which carry with them the momentum flow rates.[23-25] These jets on impingement creates a gas field of a certain force. The momentum flow rate within the jet, though increases with increase in plenum pressure, number of nozzles and with the square of the nozzle diameter but the effect of momentum flow rate on the force of the gas field depends on the impinging distance (the impinging distance is the focal length in the present study). Lower impinging distances as attained by smaller focal lengths will produce more force as compared with greater ones.[23,24] Thus, an atomizer of any given focal length will produce greater force in the gas field at either larger plenum pressure or nozzle diameter (both the parameters increases the momentum flow rate) on account of which the velocity at geometric point will increase as observed in Fig. 4.1.

On the contrary, increase in focal length of the atomizer will decrease the impinging effect of the jet of a given momentum flow rate, i.e. less force will be produced

in the gas field as a consequence of which the velocity must decrease with increase in focal length as observed in Fig. 4.3. The effect of number of nozzles is slightly different than that of plenum pressure or focal length. Though, an increase in number of nozzles at a constant plenum pressure increases the momentum flow rate but simultaneously increases the number of jets impinging to form the gas field. Increase in number of jets will entrain more surrounding air prior to impingement. Thus, on impingement, the increase in velocity caused by increase in momentum flow rate appears to be counterbalanced by the decrease in velocity caused by the entrainment of the surrounding.

From the above analysis, it follows that the velocity at the geometric point should bear the following relationship:

$$V_g = a\, D^b\, F^c\, P^d \qquad (5.1)$$

where a is a constant and b, c, and d are exponents. The value of the exponent determines the extent of influence of the respective parameter on velocity. The value of 'a' and exponents are determined by the least-square analysis.[26] the values are : a = 5.58 *10^{-4}, b = 0.48, c = -0.75 and d = 0.96. Inserting these values in Equation (5.1), gives the following:

$$V_g = \frac{5.58 \times 10^{-4} D^{0.48} P^{0.96}}{F^{0.75}} \qquad (5.2)$$

In the Equation (5.2) D and F are to be substituted in m and P in Pa in order to get V_g in m/s. The calculated values of velocity by Equation (5.2) are compared in Figure 5.1, with the measured ones by drawing a 45° line. It appears from the figure that the Equation (5.2) predicts satisfactorily the experimental values. In open technical literature no such correlation is available and therefore a direct comparison of the exponents and the

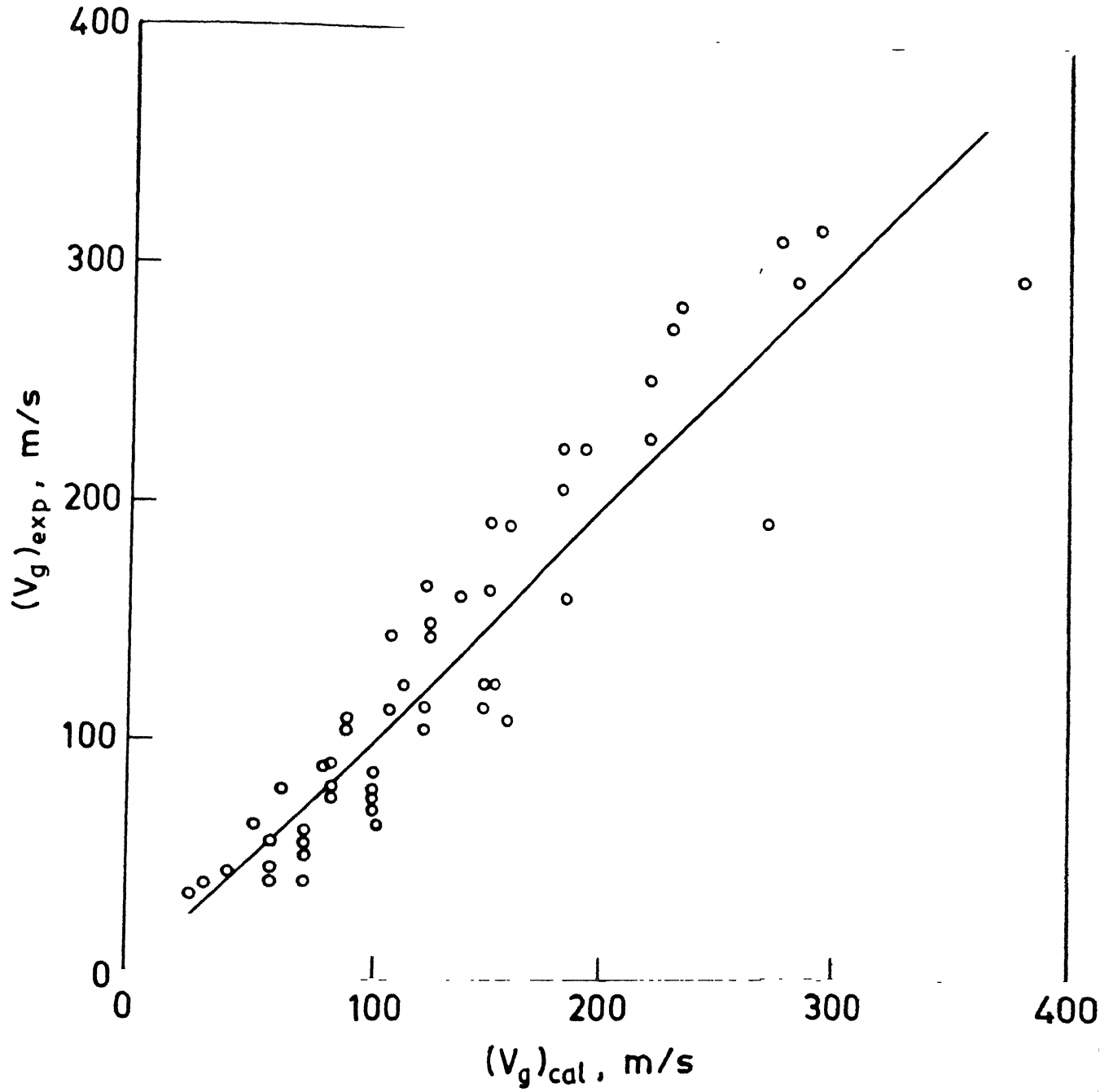

Figure 5.1 : Comparison of the air velocities at geometric point calculated by Equation (5.1) with experimental ones.

constant can not be made[4,9,10]. Moir and Jones[9] studied the velocity of gas as a function of plenum pressure at the geometric point of atomizers of different focal lengths and apex angles. They reported a linear variation of velocity with plenum pressure, but no correlation of any kind is given. The exponent of P (=0.96) of the present study predicts a slightly non-linear variation. In addition the correlation 5.2 suggest that the velocity of the atomizing gas is due to the cumulative effect of nozzle diameter, plenum pressure and focal length. It appears that for a given type of atomizer, plenum pressure, relatively, increases velocity faster than focal length of the atomizer.

5.1.2 DOWNSTREAM VELOCITY

A knowledge of downstream velocity of atomizing gas as a function of downstream distance is very much useful to study the heat transfer of droplets during their flight in the cooling chamber.

The results show that the velocity of gas downstream of the geometric point starts to decay after a certain distance (Z_c). The velocity within this distance Z_c is observed to be constant and is equal to the velocity at geometric point (see Figs. 4.8 - 4.10). The following power law is used to describe the decay of velocity as a function of downstream distance Z (for the value of $Z \geq Z_c$):

$$\frac{V_z}{V_g} = \left(\frac{Z_c}{Z}\right)^n \qquad (5.3)$$

where n is the exponent. The exponent n determines spread of the jet. Using the value of Z_c = 12 mm, the value of exponent n is determined by the least-square analysis[26]; this value is 0.5, therefore Equation (5.3) becomes:

$$\frac{V_z}{V_g} = \left(\frac{Z_c}{Z}\right)^{0.5} \tag{5.4}$$

Many investigators have studied velocity of different types of gases downstream the geometric point of atomizers used in confined[27-31] and free fall atomization[9,10] (See Table 5.1). In Table 5.1 available data are given. They have not given values of all the parameters, so a direct comparison is not possible to make between the velocities calculated by Equation (5.4) and those reported by them. However, they reported the variation of V_z as a function of Z. According to Equation (5.3), the value of the exponent n does not depend on V_g and Z_c. Accordingly, the value of n of Equation (5.3) was determined in the present study from the V_z versus Z plots reported by other workers[9,10,27-31]. All the values of n are given in Table 5.1 for different types of gases. It can be seen that the exponent value of helium gas is much greater than that of argon. It is known that a jet of lighter gas (e.g. helium) spreads faster compared with heavier gas (e.g. argon), when discharged in the same surrounding medium. This means that the exponent n must bear the relationship with the ratio of the density of gas to that of surrounding air (ρ_g/ρ_a). This relationship is shown in the Figure 5.2 by the following exponential correlation

$$n = 0.515\left(\frac{\rho_g}{\rho_a}\right)^{-0.58} \tag{5.5}$$

All the values of n of Table 5.1 are shown in the figure. The different values of n can be seen to be distributed uniformly along the curve plotted by Equation (5.5).

Substituting V_g and n from Equations (5.2) and (5.5) in Equation (5.3) and simplification results:

Table 5.1 : Exponent of equation (5.3) and discharge coefficient

Atomizer			Gas	ρ_g^*	P	n	C_D	Ref
Type	N	D		kg/m^3	kPa			
con	-	-	He	0.163	-	1.465	-	27
con	-	-	Ar	1.630	-	0.254	-	28
con	-	-	N_2	1.141	1040	0.576	-	29
con	-	-	N_2	1.141	560	0.623	-	29
con	-	-	N_2	1.141	850	0.624	-	30
con	18	0.75	N_2	1.141	690	0.558	-	31
ff	06	1.00	N_2	1.141	690-1380	0.651	0.635±0.015	9
ff	04	2.00	Air	1.182	700-1900	0.500	0.825±0.025	PS
ff	04	3.00	Air	1.182	700-1900	0.500	0.575±0.025	PS
ff	06	3.00	Air	1.182	700-1500	0.505	0.560±0.010	PS

– : Not available.

con : Confined

ff : Free fall

PS : Present Study

* : Density of gas at 25°C, 1 atm

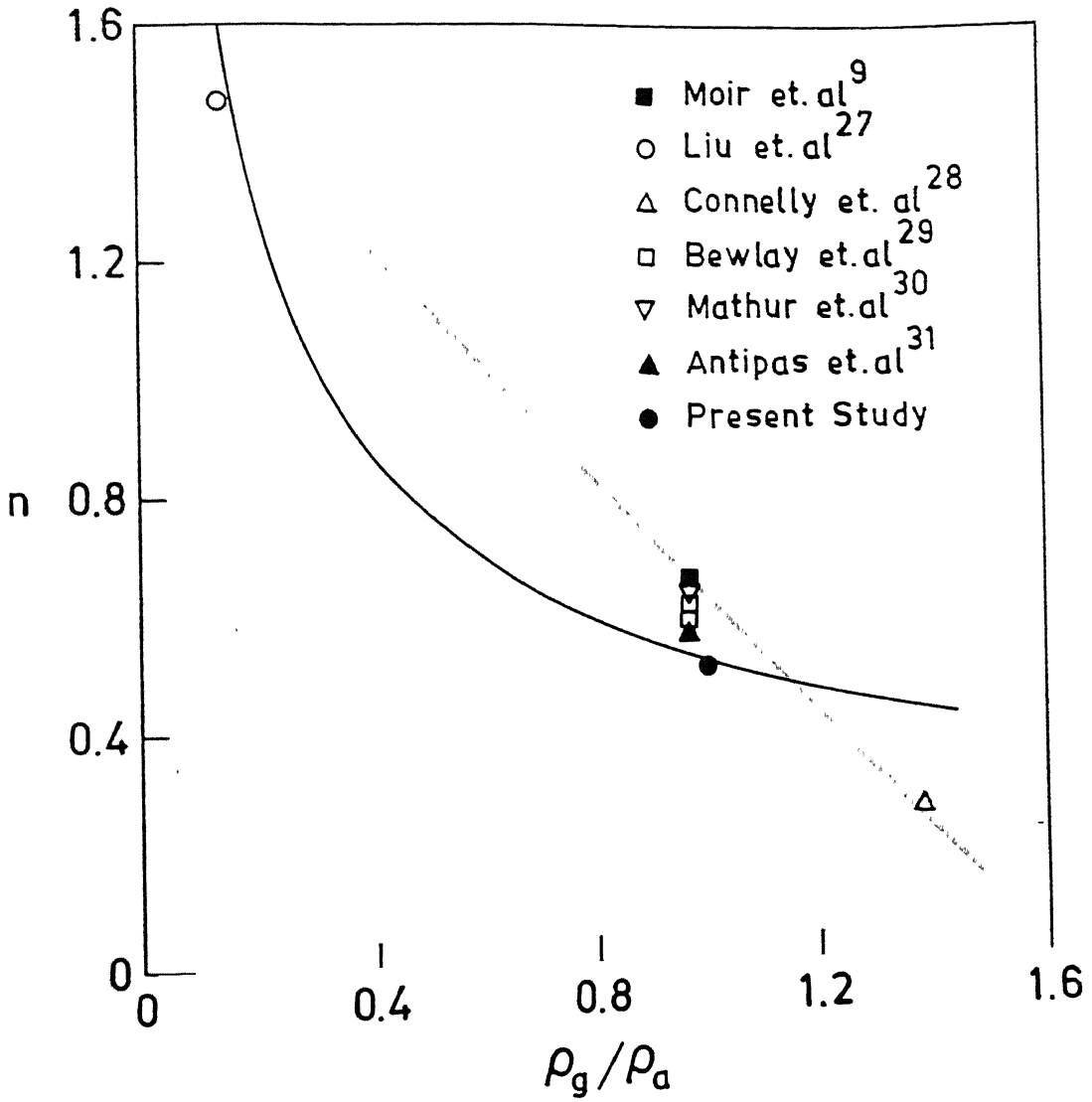

Figure 5.2 : Variation of exponent n of Equation 5.5 with the ratio of densities of gas jet and air

$$V_z = 5.58 \times 10^{-4} \frac{D^{0.48} P^{0.96}}{F^{0.75}} \left(\frac{Z_c}{Z}\right)^n \qquad (5.6)$$

The value of n for a given type of gas can be calculated by Equation (5.5). In Equation (5.6) D and F are to be substituted in m and P in Pa in order to get V_z in m/s. The Equation (5.6) relates the axial velocity decay of different types of gases downstream the geometric point with the parameters related to the atomizer design, on which no information is available in the literature. This Equation may prove to be very useful to study the dynamics of solidification of droplets in free fall gas atomization of liquid metals to produce either metal powder or preforms. The validity of the Equation (5.6) is tested by using own data. The calculated values of V_z from Equation (5.6) are compared in Figure 5.3 with that of measured ones of the present study. There are deviations on both sides of the line, but overall Equation (5.6) can be considered to predict satisfactorily the downstream velocity of the present study.

5.1.3 DISCHARGE COEFFICIENT OF ATOMIZER

Rate of flow of gas through an atomizer of a given cross sectional area is an important parameter since it not only influences droplet sizes, but also the economic viability of the atomization process.[32] The flow rate of the gas can be readily determined by considering the flow to be isentropic (i.e. reversible adiabatic). The maximum mass flow rate of gas passing through a nozzle of a given cross sectional area under isentropic flow condition is given by:[33]

$$m_N = AP\sqrt{\frac{\gamma M}{RT}}\left(\frac{2}{\gamma+1}\right)^{\frac{\gamma+1}{2(\gamma-1)}} \qquad (5.7)$$

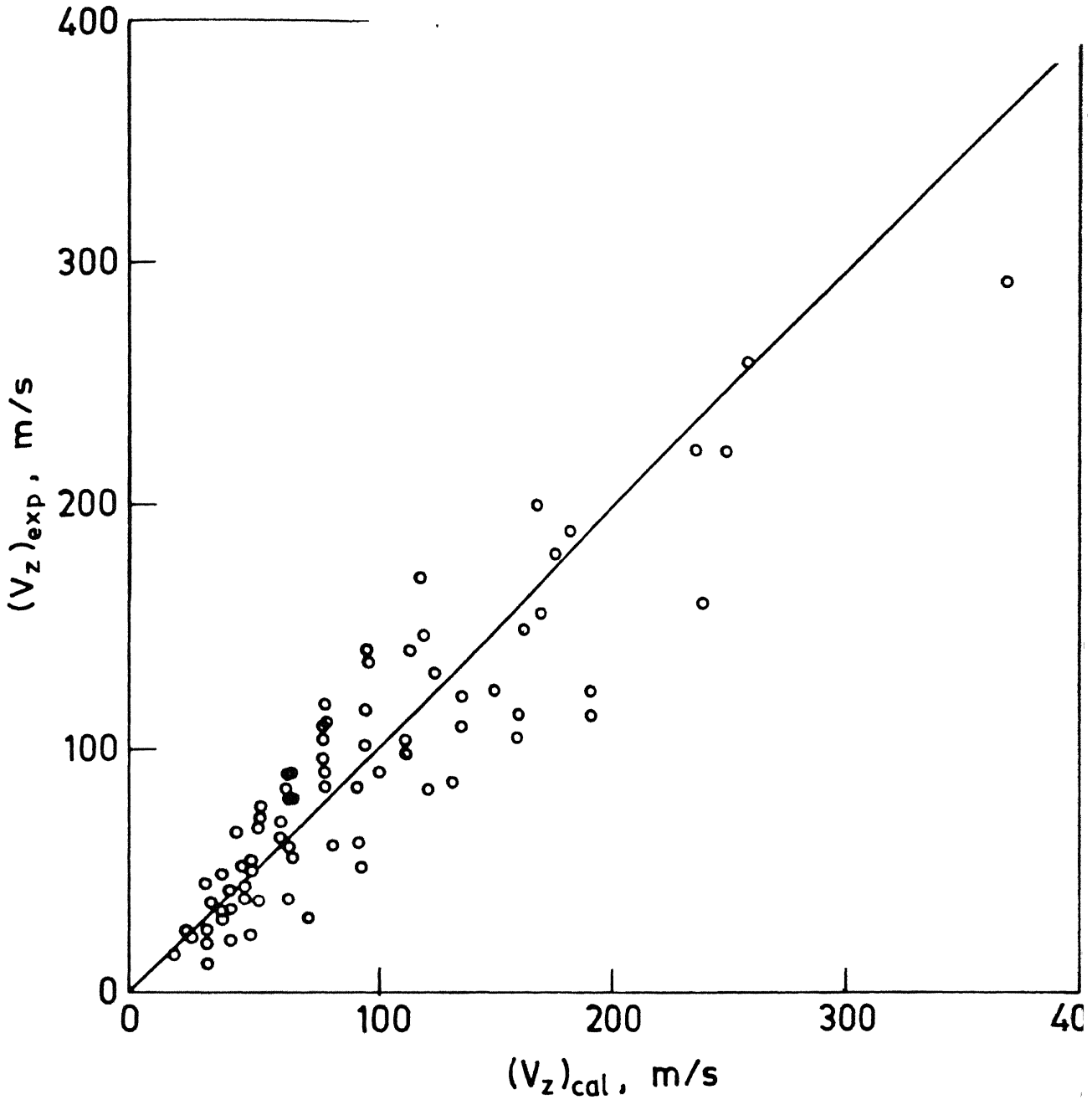

Figure 5.3 : Comparison of air velocities downstream the geometric point calcula
Equation (5.6) with experimental ones.

An atomizer consists of nozzles and accordingly Equation (5.8) is written for the flow of gas through N number of nozzles:

$$m_N = N \times A_n P \sqrt{\frac{\gamma M}{RT}} \left(\frac{2}{\gamma + 1} \right)^{\frac{\gamma+1}{2(\gamma-1)}} \qquad (5.8)$$

The flow of gas in an atomizer does not follow the isentropic flow condition. The deviation from isentropic flow condition is caused by the atomizer design such as nozzle geometry, pressurizing manifold, total area of nozzles etc. Therefore, a correction factor has to be applied is Equation (5.8) to take into account the effect of the aforementioned factors on the flow rate of gas. Discharge coefficient is one such factor and is given by[33]

$$C_D = \frac{\dot{m}}{m_A} \qquad (5.9)$$

In the Equation (5.9) $\dot{m}$ is the actual mass flow rate of gas passing through atomizer. In the experiments volume flow rate of air passing through atomizers of different cross-sectional areas is measured as a function of plenum pressure (Fig. 4.11). The volume flow rate was converted into mass flow rate by taking density of air as 1.18 kg/m^3 (at 25°C and 1 atm). The value of m_A is determined by Equation (5.8) using the values of physical constants given in Appendix - B. In the Equation (5.8), $N \times A_n$ is the total cross sectional area of the flow passage of an atomizer which is equal to $N^* \pi D^2/4$. The discharge coefficient is determined by Equation (5.9) and is given in Table 5.1.

Moir et al.[10] have measured the gas flow rate ($\dot{m}$) through the atomizers of free fall type as a function of plenum pressure. From their data m_A is calculated at various

plenum pressures by Equation (5.8) and C_D is determined by Equation (5.9). The values of C_D are given in Table 5.1. It can be seen that the discharge coefficient of the atomizers of the present study and that of Moir et al. are almost independent of plenum pressure. However, it appears that C_D tends to decrease with the increase in the total cross sectional area of the nozzles of atomizers.

Thus, flow rate of gas passing through an atomizer can be determined readily by Equations (5.8) and (5.9) by using an appropriate value of C_D.

5.2 ATOMIZATION

In a free fall atomization unit, atomizer is located at a very small distance upward from the geometric point in relation to powder collection arrangement which is placed downward from the geometric point at a distance several times that of atomizer. The atomizer converts the required gas rate into an energetic gas field, and it also directs the liquid stream for its disintegration continuously into the gas field. For the successful running of an atomizing unit to produce powder, the atomized droplets should not hinder the flow of gas or metal and at the same time be solidified completely before reaching the powder collection arrangement. The velocity of droplets is an important consideration for the above purpose and is controlled by velocity of atomizing gas.

5.2.1 VELOCITY OF GAS AND CORRELATION

Velocity of gas controls not only the fineness of the powder but also the dynamics of movements and solidification of droplets in the atomizing unit. Higher velocity of gas, though desirable to disintegrate liquid stream into fine droplets, but at the same time forces the droplets to fly with higher velocities, both in upward direction, i.e. toward the

atomizer and downward direction, i.e. toward the powder collection tray. For a given distance of location of atomizer and powder collection tray in the atomizing unit, droplets may hit the atomizer and powder collection tray and deposit there. Both conditions are not conducive for the successful operation of the atomizing unit. In the experiments large data are collected on the atomizer and liquid related parameters which avoid the deposition of droplets and in the following the results are given in the form of a correlation:

5.2.1.1 Selection of Parameters

In the present experiments, the atomizers are located at different distances from their geometric points but the powder collection tray is at a constant distance of 2.4 m from the geometric point. (This constant height is also the height of the cooling chamber). Because of the constant height of the chamber, a relationship between the height of the chamber and the total heat removal rate from the droplets of different metals to produce powder could not be developed. From the limited data, it can be said that the present height of cooling chamber can produce metal powders of Zn, Al and Sn within a very narrow range of plenum pressures (See run No. 94, 95 for Zn, 107 for Al and 121 for Sn in Table 3.3).

However, large number of data on plenum pressures which avoid droplet deposition on the atomizer surface are collected for various types of atomizers located at different distances from their respective geometric points (this distance is focal length of the atomizer) using aluminium, tin, zinc and lead. All these runs are marked with + and $ signs in column O3 of Table 3.3. In each type of atomizer, it is observed that their is a

particular value of pressure beyond which droplet deposition occurs (this value of pressure corresponds to runs marked with + sign in column O2 of Table 3.3). The particular value of pressure at which no deposition occurs is termed "critical pressure" and is marked with $ sign in column O3 of Table 3.3. The difference in the value of pressures between column 2 and 3 is around 50 to 100 kPa. It can be noted that critical pressure of gas could not be determined for atomization of tin, since this pressure is higher than the limits of pressure achieved by the compressor of the present study. By using the value of pressure, focal length and nozzle diameter of runs corresponding to $ sign of Table 3.3, velocity is calculated by Equation 5.2 (This velocity is critical velocity of the atomizing gas). This critical velocity is different for different distances of location of atomizer (distance of location of atomizer is equal to focal length of the respective atomizer) and this variation is shown in Fig. (5.4) for different type of atomizers of different apex angles and liquid metals; lead (solid lines), zinc (dashed line) and aluminum (dotted dashed line).

It can be seen that critical velocity of gas for each type of atomizer of a given apex angle increases with increase in free fall distance for all types of atomizers and metals. Remembering that the velocity of the atomized droplet's increases with the increase of the velocity of gas, therefore increase in free fall distance of liquid stream will require higher droplet velocity to reach to the atomizer surface, which in turn can be obtained by higher velocity of atomizing gas. Moreover, for any given free fall distance, the critical velocity is higher for A4 type (apex angle = 40°) atomizer as compared to that of A6 type (apex angle = 60°). As seen in Table 3.3, the critical velocity for an atomizer of apex angle 20° is more than that of 40° (see table 3.3, run no. 15 for 20° and 27 for 40° apex angle, in

which critical pressures are given. The critical pressures of these runs corresponds to the velocity of 265 m/s and 130 m/s, respectively).

The critical velocity is highest for lead and lower for aluminium at critical free fall distances.

The higher velocity of lead than aluminium is probably due to the density difference. Density of lead is around 3-4 times greater than aluminium, therefore, lead droplets will require more thrust than aluminium to lift them upto the same height of atomizer. The increase in critical velocity due to decrease in apex angle can be explained by considering the dynamics of atomization of liquid stream, since velocity of gas does not depend on the apex angle (see Figure 4.4). It appears that for a given velocity of gas, apex angle influences the solidification behaviour of droplets in such a way that smaller angle results in faster solidification as compared to greater one.

5.2.1.2 Development of Correlation

From the above analysis and remembering that the droplet velocity increases with the increase in gas velocity, and noting the role of apex angle on solidification, the critical velocity of gas for atomization may be represented by the following function:

$$V_c = a\,\rho^b\,L^c\,\alpha^e \qquad (5.10)$$

The values of constant a and exponents b, c and e are calculated by least square analysis using the data of the present study (data are given in Table 3.3). The values are: $a = 2.7\times10^3$, $b = 0.218$, $c = 0.618$ and $e = 0.93$. Substituting these values in Equation (5.10) results the following expression:

$$V_c = 2.7\times10^3\,\frac{\rho^{0.218}L^{0.618}}{\alpha^{0.93}} \qquad (5.11)$$

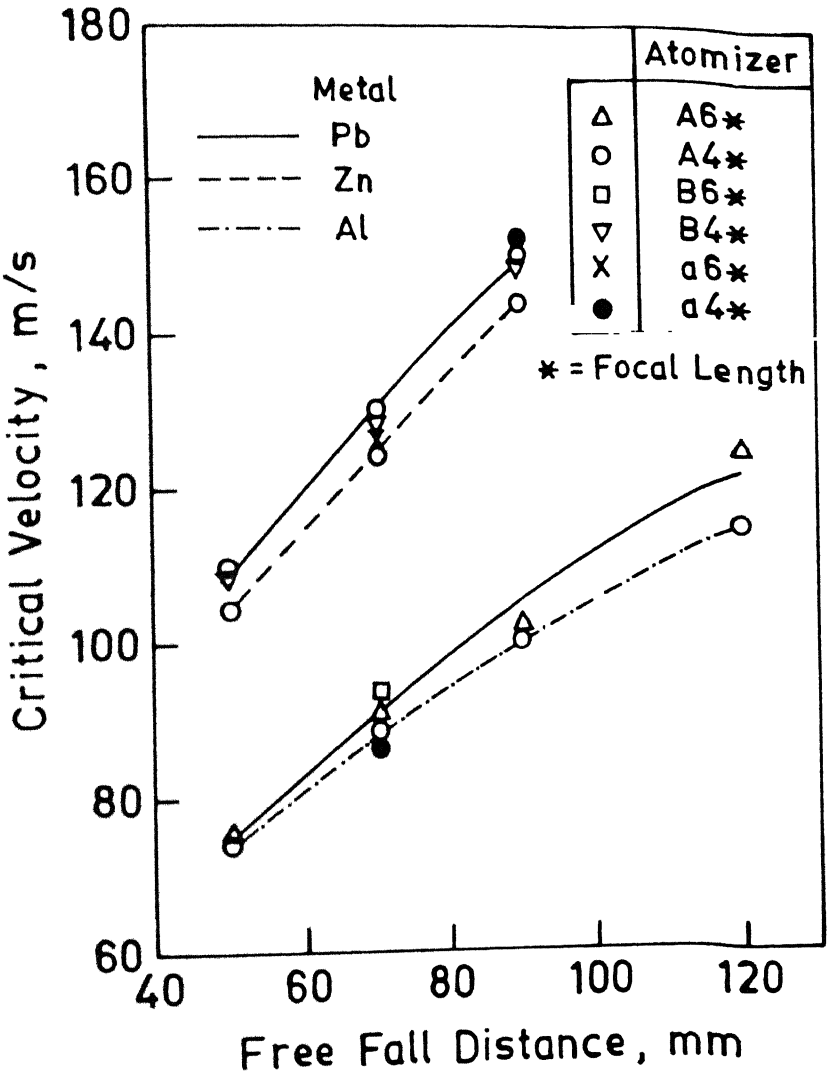

Figure 5.4 : Variation of critical velocity of atomizing gas with free fall distance

where ρ, L and α are to be substituted in kg/m^3, m and degree, respectively in order to get V_c in m/s. The values of V_c calculated from the above Equation are compared in figure (5.5) with that of experimental ones. The line separates the region of no deposition with that from deposition. An atomizer operated at velocities lying in the deposition region will no doubt produce fine powder but deposition of droplet over the atomizer surface may cause interruption of atomization process when atomization is continued for longer time. Equation (5.11) shows that the critical velocity increases faster with increase of free fall distance as compared to that of density of metal. Decrease in apex angle increases the critical velocity.

5.2.1.3 Validation

See and Johnston[4] have studied the disintegration of lead and tin stream using free fall type atomizer. They observed deposition of droplet on the gas nozzle ring of atomizer whose apex angle was 90°. However, no deposition was observed on the surface of atomizer whose apex angle was either 30° or 60°. The focal length of all atomizer was 78 mm. By considering the focal length to be equal to free fall distance (as the focal length is considered to be the minimum distance for droplet deposition), the critical velocity is calculated by Equation (5.11) in the present study for the experimental conditions of See and Johnston. The critical velocities for atomization of lead are 178 m/s for 30° apex angle, 93.6 m/s for 60° and 64.2 m/s for 90° apex angle of the atomizer. Whereas these velocities are 162 m/s, 85.3 m/s and 58.5 m/s for atomization of tin using atomization experiments at different velocities of gas; the highest velocity is 82 m/s in their experiments. The droplet deposition was found by them to occur at 82 m/s for 90°

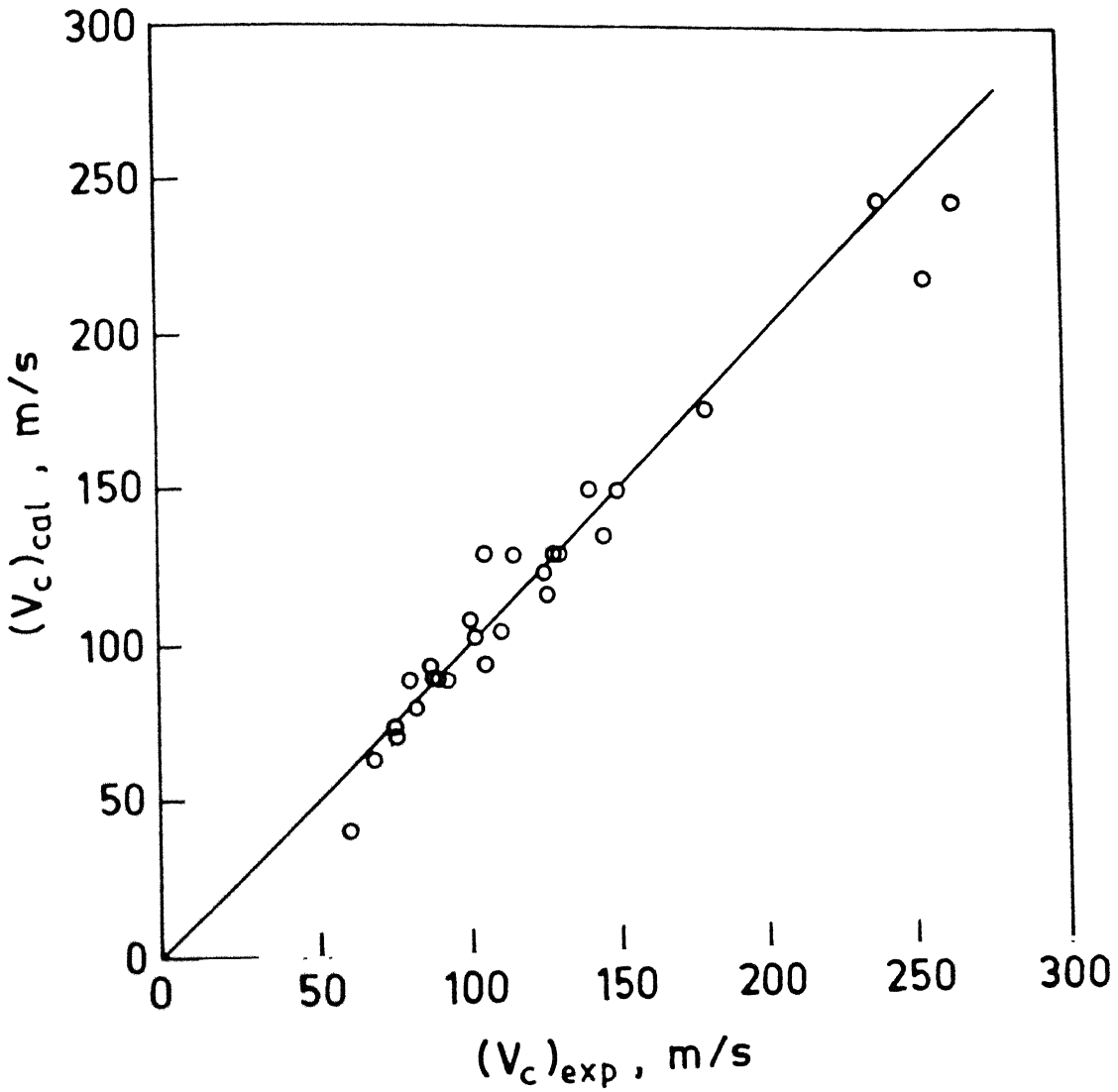

Figure 5.5 : Comparison of critical velocities calculated by Equation (5.11) with experimental ones

atomizer. Comparing the experimentally reported velocity (82 m/s) with that calculated by Equation (5.11) for 90° atomizer (the values are 64.2 m/s for lead and 58.5 for tin) it appears that droplet deposition on 90° apex angle atomizer can not be prevented, which confirms the observation of See and Johnston. Thus, it appears that the concept of critical velocity of gas for atomization, as proposed in this study, may be useful to provide guideline for the selection of atomizer related parameter. In the open technical literature one does not find much on the guidelines for the selection of atomizer related parameters. It is often necessary to select the maximum pressure (or gas rate) for atomization of a metal stream using an atomizer of a given number of nozzles and their diameters. The Equations (5.11), (5.12) and (5.8) can be used to obtain the above information as follows: Assuming metal is lead (density = 19760 kg/m^3) and apex angle of atomizer is 40°, we get by Equation (5.11).

$$V_c = 660\, L^{0.618} \tag{5.12}$$

Thus V_c is the critical velocity at geometric point of the atomizer. According to the definition of critical velocity; this velocity is the maximum velocity which will avoid droplet deposition of the atomizer surface. All velocities lower than V_c can also be used for atomization. Inserting the value of V_c from Equation (5.12) in Equation (5.2) and noting that L = F, we get after simplification

$$P_{c_r} = \frac{2.112 \times 10^6\, F^{1.425}}{D^{0.5}} \tag{5.13}$$

For nozzle diameter D = 3 mm and F = 120 mm, we get $P_{c_r} \approx 19 \times 10^5$ Pa. This critical pressure according to Equation (5.8) would require 0.071 kg/s of air when four nozzles are used.

5.2.2 MASS MEDIAN SIZE

Mass median size of the powder collective is one of the important parameter of log normal distribution and its inter-relationship with the atomizer and liquid metal related parameters is very useful in gas atomization to predict the powder size distribution. It may be mentioned that in a fixed height of 2.4 m of the cooling chamber in the present study, only lead powder collectives could be produced for a wide range of parameters related to atomizer and liquid metal. Accordingly, the discussion in the following is related to lead powder.

5.2.2.1 Selection of Parameters

Mass medium size of lead powder collective is found to decrease either with increase in pressure or with increase in nozzle diameter, but with either decrease in focal length or apex angle of the atomizer. It is found to be independent of number of nozzles, superheat of liquid metal and diameter of liquid metal delivery tube upto a value of 9.0 mm. The effect of the focal length, diameter of nozzle and plenum pressure on the mass median size can be explained by considering the velocity of the atomizing gas relative to that of liquid metal stream. The velocity of liquid stream is several times smaller than velocity of atomizing gas and hence is neglected in the following discussion.

The velocity of the atomizing gas at the geometric point increases with either increase in plenum pressure or nozzle diameter but with decrease in focal length. Therefore, increase in velocity decreases the mass median size. This explanation for decrease in mass median size with the increase in velocity is in consistent with the view expressed by several other investigators.[4,5,12,13,16,36]

See and Johnston[4] have studied atomization of lead and tin, and Shinde and Tendolkar[36] that of lead only by varying superheat within the range 70K to 220K of the liquid metal. According to them the mass median size does not change with superheat of liquid metal. These observations are consistent with the finding of present study of independence of mass median size on superheat of liquid metal.

The influence of superheat temperature on atomization is related to the dependence of the physical properties of molten metals on temperature.[1,10]. The relevant physical properties are: viscosity, surface tension, and density. Within the range of superheats of the present study and that of Shinde and Tendolkar[36] the change in density of lead is 1.8%, surface tension 3.7% and viscosity by 17.3%. The density and surface tension changes with the change in superheat are almost negligible with change in superheat. The effect of viscosity is intimately related to the flow of liquid metal. Decrease in viscosity should result in increase in metal flow rate. The effect of metal flow rate is explained below.

It is found that the mass medium size at all velocities of gas is independent of the diameter of delivery tube up to a value of 9 mm. Further increase in diameter is found to increase the mass median size. Helmersson et al. [42] have studied the effect of liquid metal delivery tube diameter on atomization of nickel-based alloys using free fall type atomizer. According to them, diameter of liquid metal delivery tube has no influence on mass median size.

Both observations suggest that for a given velocity at geometric point, size of the atomizing gas field of constant velocity bears a relationship with the liquid metal delivery

tube diameter. It has already been shown in Section 4.1.2 that there is a constant velocity zone which extends upto certain distance both in horizontal and vertical direction with reference to geometric point. Thus for a given value of V_g, as long as size of the constant velocity zone is less or equal to diameter of the liquid delivery tube, the atomization should produce powder collectives of more or less same mass median size simply because atomizing gas velocity is not changing. Thus, increase in diameter of liquid delivery tube maximum upto size of the constant velocity zone will feed more mass of liquid for atomization which results in better utilization of the gas without affecting the mass median size.

The decrease in mass median size by decreasing the apex angle at constant velocity of gas can be explained by considering the location of impingement of gas jet vertically above the geometric point. In Figure (5.6) velocity of gas is shown as a function of distance upstream of the geometric point of atomizers of 20° and 60° apex angles at various plenum pressures. At each plenum pressure the velocity at geometric point is shown on the figure at distance equal to zero.

The distance at which V becomes zero is 60 mm for 20° and 40 mm for 40° apex angle. These distances indicate stream is impinged by an atomizing gas field created by an atomizer of 20° apex angle that the boundaries of gas jets begins to impinge at 60 mm and 40 mm distance upstream of the geometric point of 20° and 40° atomizers, respectively. This suggests that a vertically falling stream will begin to interact with the atomizing gas field created by 20° atomizer sooner than 40° atomizer (Interaction distance = FFD - distance of location of atomizer gas field). Thus, it appears that the liquid metal stream

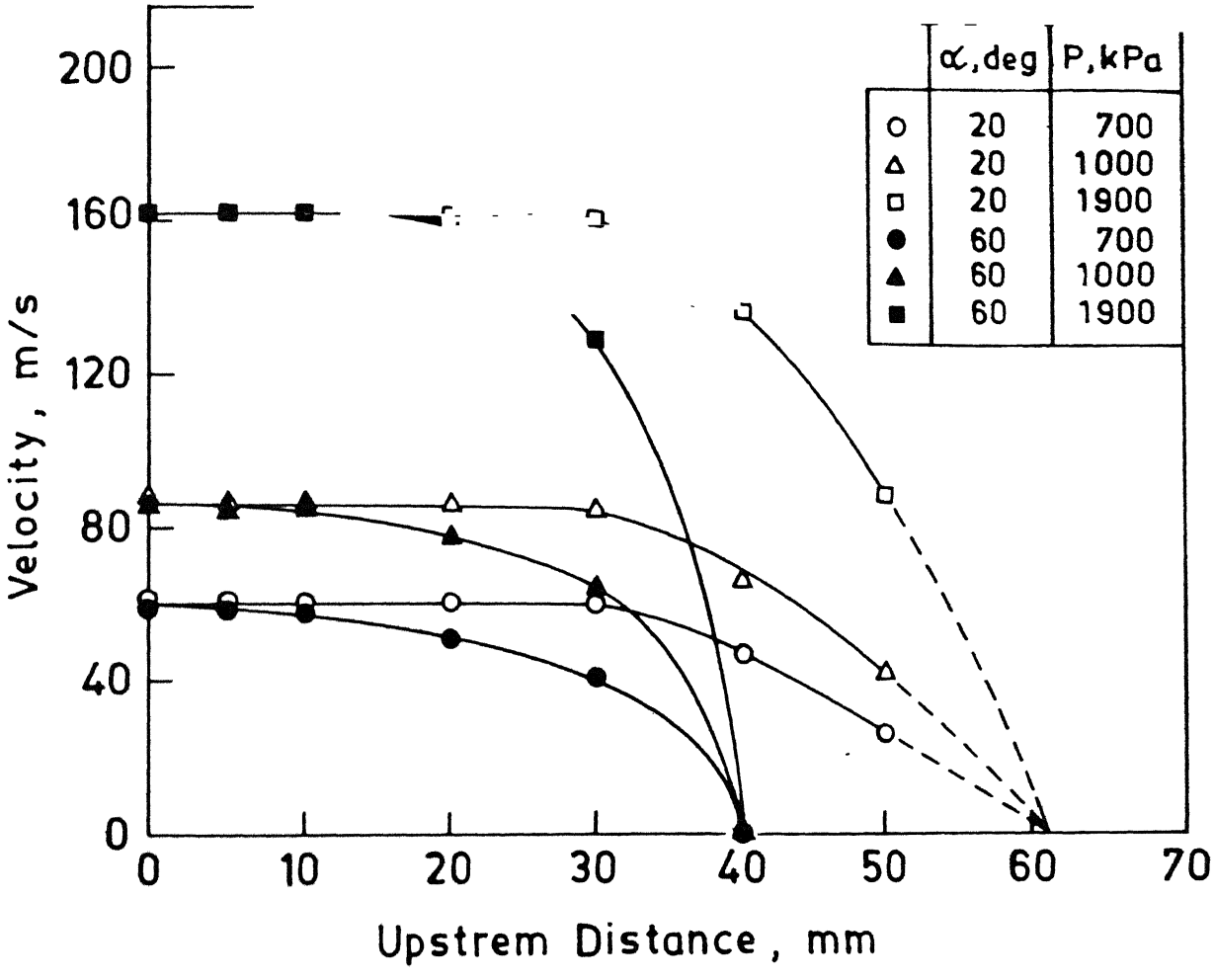

Figure 5.6 : Variation of gas velocity as a function of distance upstream of the geometric point of atomizers of different apex angles

remains in the gas field for a relatively large time for 20° atomizer as compared with 40°. According to See and Johnston, longer residence time of the liquid stream in the gas field yield finer size as compared to short residence time for identical velocity of gas at geometric point.

5.2.2.2 Development of Correlation

From the above analysis, it follow that the mass median size of the powder collective produced by an atomizer of a given apex angle is mainly influenced by the velocity of the atomizing gas. Thus, the following functional relationship is considered:

$$X_g = f(V_g) \tag{5.14}$$

Equation (5.14) should also contain the influence of mass flow rate of gas on mass median size. The effect of mass flow rate of gas on mass median size is evaluated as follows. In figure (5.7) mass median size is plotted as a function of velocity of gas for A4 type atomizers having different focal lengths. It can be seen that increase in velocity decreases mass median size at all focal lengths of atomizers. But at constant velocity of gas (say 80 m/s) increase in focal length from 70 mm to 120 mm decreases mass median size from 190 μm to 178 μm (i.e. 6.7%). Since same velocity of gas at 120 mm and 70 mm focal length of a given type atomizer can be obtained only by increasing the plenum pressure i.e., by increasing the mass flow rate of gas (the increase in mass flow rate of gas is from 0.0190 kg/s to 0.0375 kg/s i.e. 49.3%), therefore, it follows that the influence of increase in mass flow rate of gas on decrease in mass median size is much smaller than velocity itself.

Inserting the condition that at $V_g = V_c$, $X_g = X_c$ function (5.14) is modified to

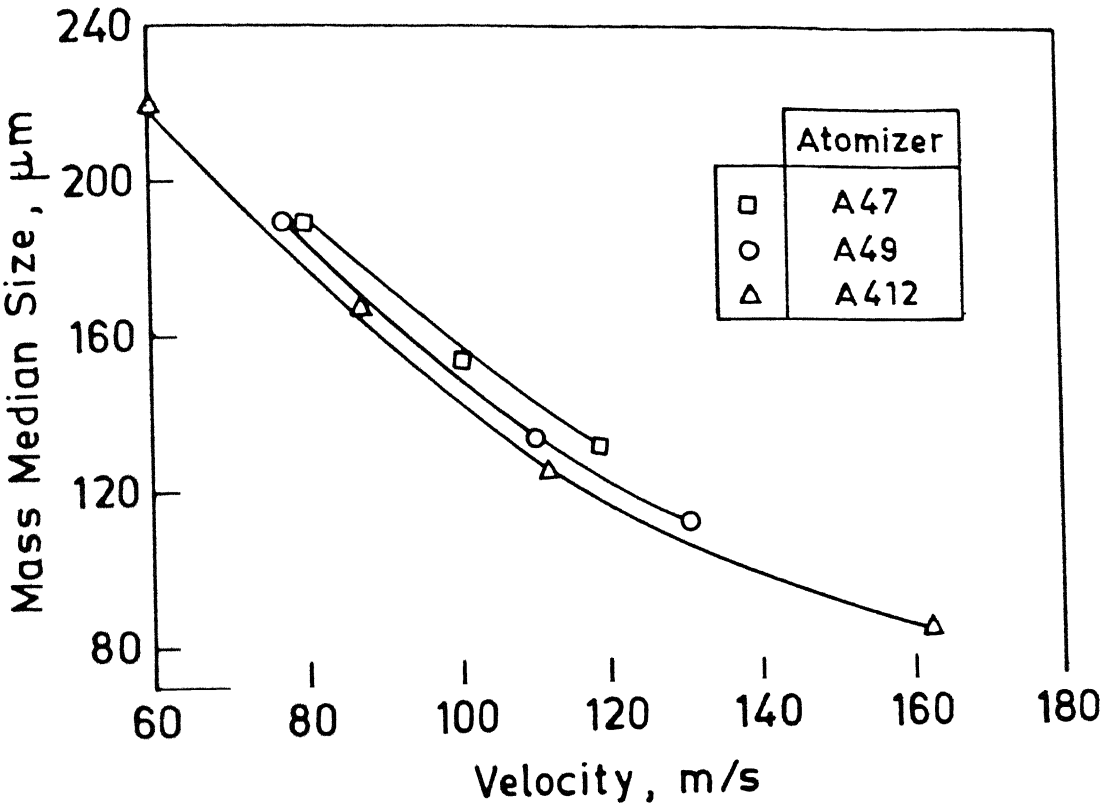

Figure 5.7 : Variation of mass median size of powder particles with velocity of air

$$\frac{X_g}{X_c} = f\left(\frac{V_g}{V_c}\right) \tag{5.15}$$

Figure (5.8) shows the plot of X_g/X_c against V_g/V_c for atomizer of difference apex angle. It can be observed the mass median size decreases by increasing the gas velocity for all α of atomizer. The effect of change of apex angle from 20° to 40° is more as compared to that of from 40° to 60°. Taking into account the condition that when X_g/X_c = 1 then V_g/V_c = 1 the following dimensionless function is taken to correlate the mass median size with gas velocity at geometric point.

$$\frac{X_g}{X_c} = \left(\frac{V_g}{V_c}\right)^b \tag{5.16}$$

where, b is an exponent which is found to depend on the apex angle of the atomizer. It is correlated by the following Equation.

$$b = -0.19\,\alpha^{0.4} \tag{5.17}$$

In Figure (5.9) the values of X_g/X_c calculated by Equations (5.16) and (5.17) are compared with the experimental derived values of X_g/X_c. It can be seen that the comparison is satisfactory.

In order to calculate mass median size X_g the relationship between X_c and V_c must be known. This relationship is shown in Figure (5.10) by the following regression Equation:

$$Xc = \frac{0.075}{V_c^{1.32}} \tag{5.18}$$

In Equation (5.18) V_c is to be inserted in m/s in order to get X_c in m.

Combining Equations (5.16) and (5.18) follows:

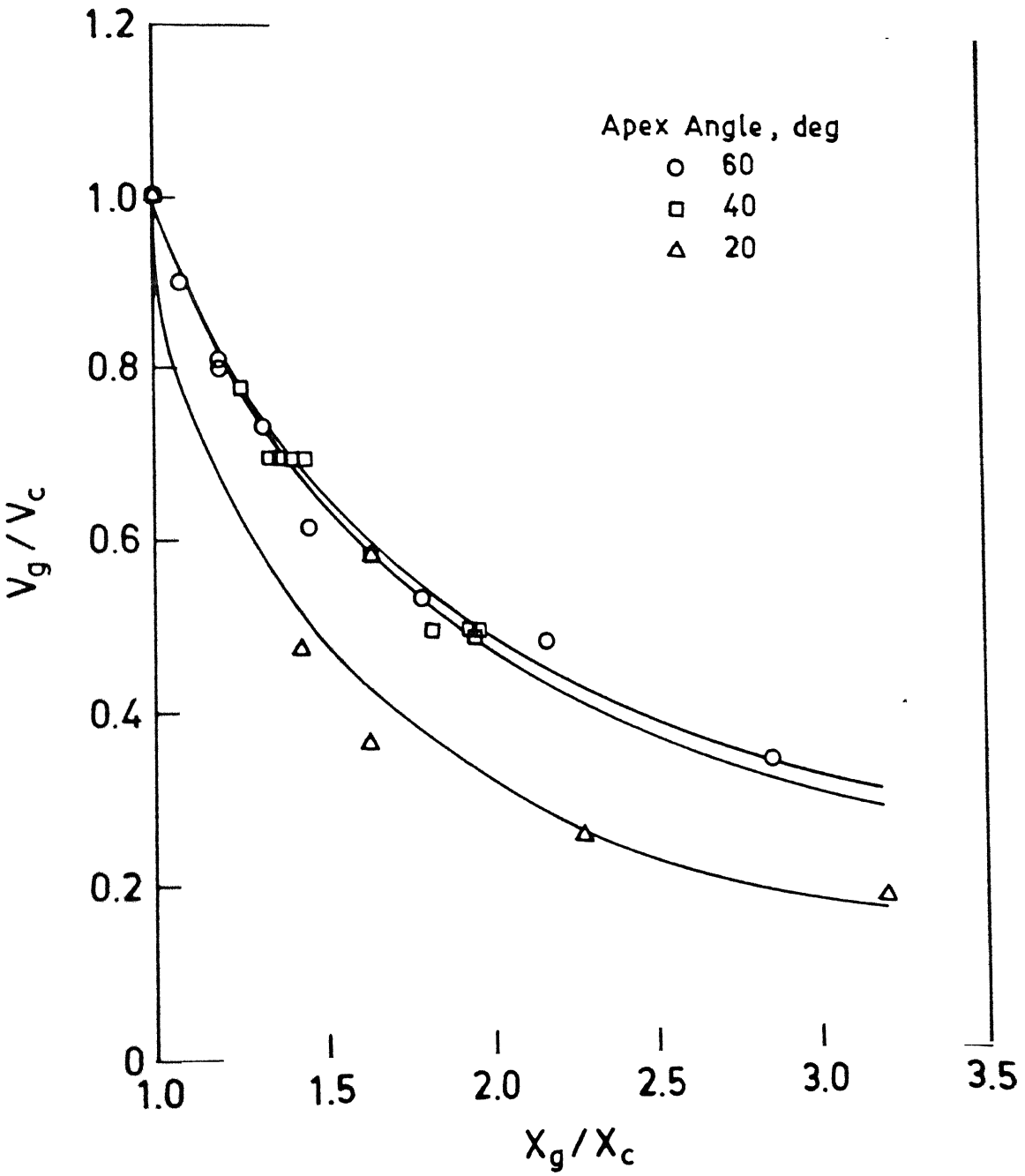

Figure 5.8 : Effect of the ratio V_g/V_c on X_g/X_c

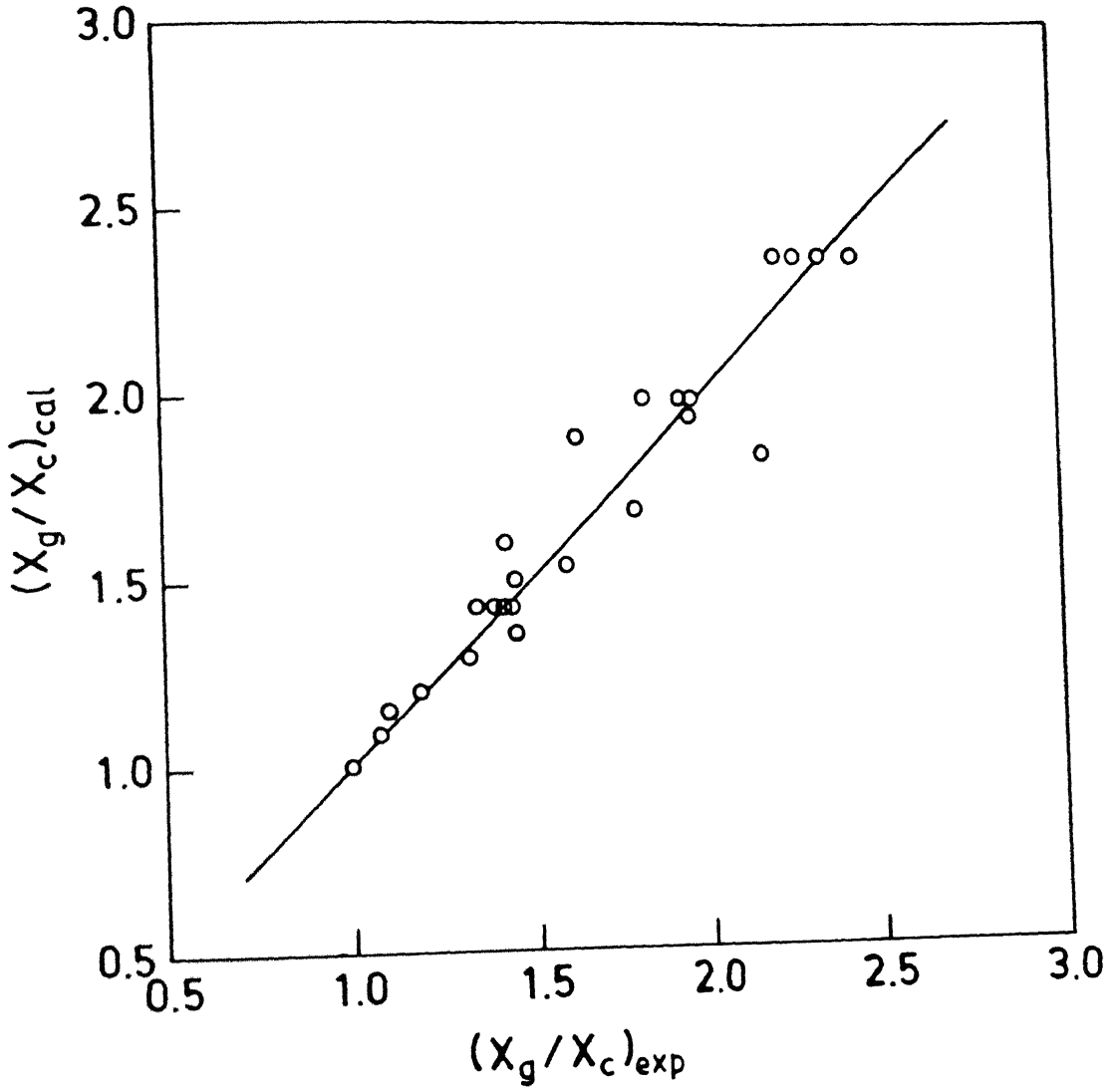

Figure 5.9 : Comparison of the values of X_g /X_c calculated by Equation (5.16) wi
experimental ones

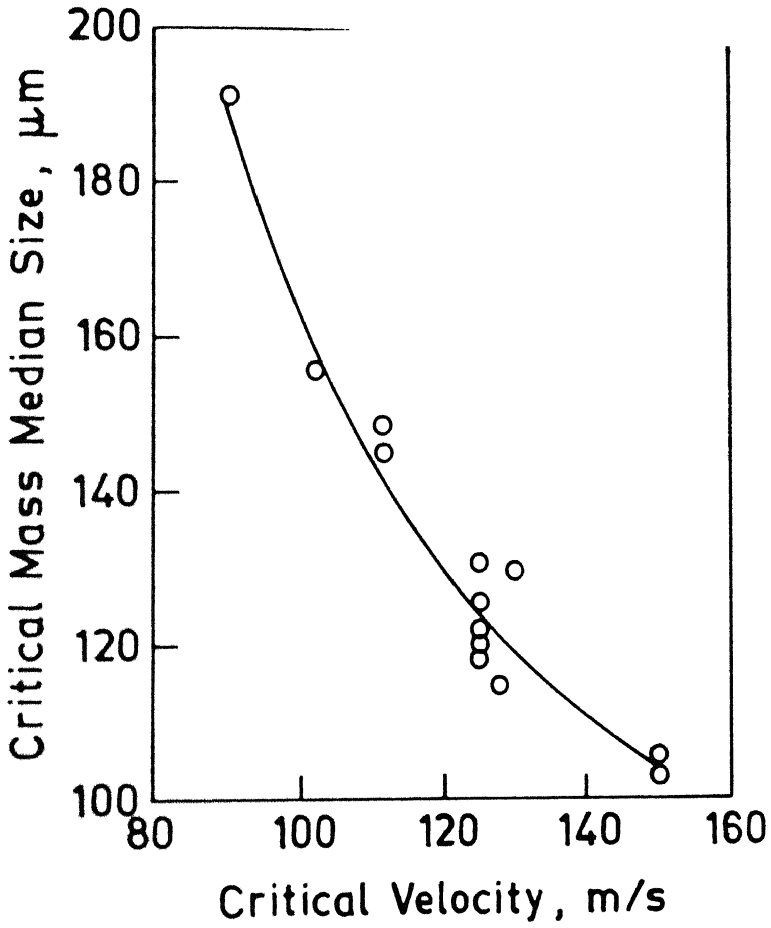

Figure 5.10 : Variation of critical mass median size of powder particles with critical velocity of air

$$X_g = \frac{0.075 V_g^b}{V_c^{b+1.32}} \tag{5.19}$$

Inserting the value of V_c from Equation (5.11) results the following expression:

$$X_g = \frac{0.075\, V_g^b \alpha^{0.93b+1.23}}{\left(2.7 \times 10^3 \rho^{0.218} L^{0.618}\right)^{b+1.32}} \tag{5.20}$$

where, b is given by Equation (5.17).

The Equation (5.20) is valid for all velocities lower than $V_g = V_{c_r}$. Further, the Equation does not contain the influence of physical properties like density, viscosity and surface tension of the liquid metal. Within the very limited data of the present study on the atomization of Al, Zn and Sn, the effect of aforementioned parameters on X_g is not incorporated in Equation (5.20). However, the value of X_g is calculated by Equation (5.20) using the data for atomization of Al, Zn and Sn of the present study (Run No. 107 for Al, 94, and 95 for Zn and 121 for Sn) and the calculated values of X_g are compared in Table 5.2 with the own experimentally derived values. It can be seen that Equation (5.20) predicts lower values of X_g as expected than experimentally observed. It is known that density and surface tension of liquid metal mainly influence X_g at constant velocity of gas[2]. With reference to lead (Equation (5.20) is for lead), the density of all metals decreases and surface tension increases in the order Sn, Zn and Al. Thus, if atomization of different metals is done by same velocity of gas as that reported in Table (5.2), the atomization of liquid Al with reference to Pb must produce coarse size fraction which is also indicated by the experimental value of X_g of Al in Table (5.3).

Table 5.2 : Comparison of mass median size calculated by equation 5.20 with that experimentally observed.

Run No.	Metal	V_g (m/s)	X_g (μm)	
			Cal.	Exper.
94	Zn	125	70	94
95	Zn	162	59	81
107	Al	162	69	106
121	Sn	162	59	61

5.2.2.3 Validation

Lubanska[13] studied the atomization behavior of molten iron using a spray ring type atomizer and proposed the following correlation to predict mass median size of powder collective.

$$X_g = K\left[\frac{\mu_m \rho_g \gamma_m d}{\mu_g \rho_m^2 V_g^2}\left(1+\frac{M}{m}\right)\right]^{1/2} \qquad (5.21)$$

The values of X_g calculated by Equations (5.20) and (5.21) using experimental parameters of present study are compared in Figure (5.11). The comparison shows that values of X_g calculated by Equation (5.20) and (5.21) are uniformly distributed along the line, except few which are much away from the line.

5.2.3 POWDER YIELD

The powder yield in different size range is given by the log-normal distribution function[11]:

$$\frac{dW}{dX} = \frac{1}{\sqrt{2\pi}\, x \ln \sigma_g} \exp\left[-\left(\frac{\ln x - \ln x_g}{\sqrt{2}\ln \sigma_g}\right)^2\right] \qquad (5.22)$$

The powder yield in different size range depends on X_g and σ_g. It has been shown (Figure 4.41) that the geometric standard deviation σ_g, though vary from one investigator to other and also within each investigator, but can be represented by a value 1.95. Putting this value in Equation (5.22) results the following:

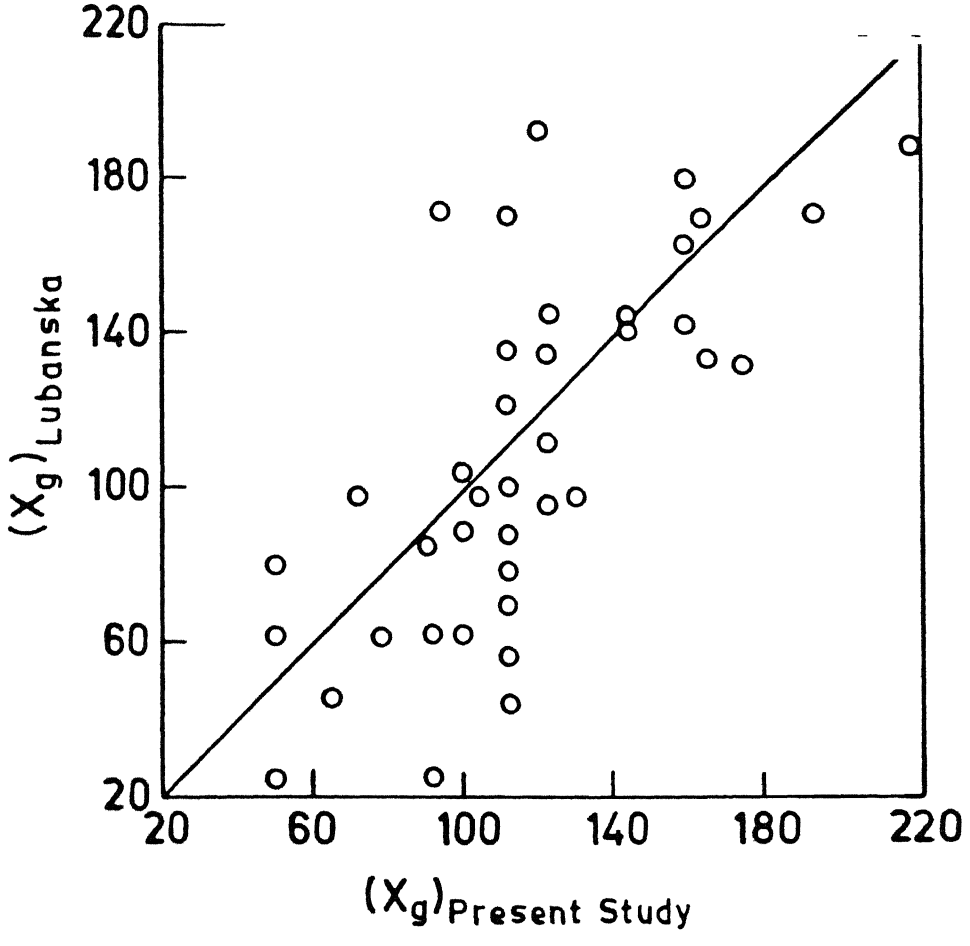

Figure 5.11 : Comparison of mass median size calculated by Equation (5.20) of the present study with that of calculated by Equation (5.21) of Lubanska

$$\frac{dW}{dX} = \frac{1}{1.67X} \exp\left[-\left(\frac{\ln\left(\frac{X}{X_g}\right)}{0.94}\right)^2\right] \qquad (5.23)$$

The Equation (5.23) can be used to determine the yield of powder within different size range for the powder collective produced by gas atomization of lead stream. The value of X_g can be calculated by Equation (5.20). For run no. 1 i.e. for atomizer a27 operated at P = 1800 kPa the value of X_g calculated from Equation (5.20) is 58.8 μm. Therefore, from Equation (5.23) the powder fraction in size range 152 - 211 μm is 0.046 whereas the experimental value is 0.043 (see Table 4.4).

5.2.4 ATOMIZATION EFFICIENCY

In free fall gas atomization, a part of the kinetic energy of gas field is transferred to the molten metal stream as a consequence of which metal stream is atomized into fine droplets and surfaces are generated. Remaining kinetic energy of the gas field, after atomizing the stream, dissipates into the environment and imparts momentum to the atomized droplets during their flight. The total new surface energy created per unit mass of powder produced, can be given by

$$E_p = \gamma(S - S_m) \qquad (5.24)$$

where, γ is the surface energy of the molten metal, S and S_m are the total surface area of the droplets and that of the bulk liquid metal per unit mass of powder produced. The surface area of bulk liquid metal is negligible as compared to that of the collection of atomized droplets of equivalent mass and therefore, it is neglected in the following.

The efficiency of atomization can be defined as the total surface energy created to the total energy supplied for atomization, and hence it is given by

$$E = \frac{\gamma S M}{\frac{1}{2} m V_g^2} \tag{5.25}$$

For any given metal the surface area of powder droplets per unit mass of powder from Equation (4.41) can be expressed by the following expression.

$$S = \frac{K_1}{X_g} \tag{5.26}$$

where K_1 is a constant depending on type of metal. Replacing X_g from above Equation by using Equation (5.16) results the following:

$$X_g = \frac{K_1}{X_c}\left(\frac{V_c}{V_g}\right)^b \tag{5.27}$$

where b is given by Equation (5.17). Substituting S and X_g from Equations (5.26) and (5.27) into Equation (5.25) gives:

$$E = \frac{2\gamma \dot{M} K}{m_c X_c V_g^2}\left(\frac{V_c}{V_g}\right)^b \tag{5.28}$$

The condition of no deposition of droplets requires $V_g = V_c$ and hence $m = m_c$. Under this condition the atomization efficiency will be critical also, i.e. $E = E_c$, E_c. Substituting these into Equation (5.28) yields

$$E = \frac{2\gamma \dot{M} K_1}{m_c X_c V_c^2} \tag{5.29}$$

From Equation (5.28) and (5.29), we get

$$\frac{E}{E_c} = \frac{m_c}{m}\left(\frac{V_c}{V_g}\right)^{2+b} \tag{5.30}$$

Figure (5.12) shows the variation of E/E_c against m/m_c calculated by Equation (5.30) for all types of atomizers using V_c and V_g corresponding to $\dot{m}$ and $\dot{m}_c$. Since the effect of pressure, nozzle diameter, number of nozzles and focal length are included in either $\dot{m}/\dot{m}_c$ or V_g/V_c and both are related to E/E_c according to Equation (5.30), therefore, the effect of individual parameters on E/E_c disappears and the, variation of E/E_c against m/m_c follows a single line as shown in Figure (5.12). It can be seen that E/E_c decreases faster with the increase in $\dot{m}/\dot{m}_c$ upto a value of 0.6 beyond this value E/E_c nearly becomes constant.

It can be seen that E/E_c decreases faster with increase in $\dot{m}/\dot{m}_c$ upto 0.6, beyond this value of $\dot{m}/\dot{m}_c$, the ratio E/E_c decreases slowly and attains a minimum value at $\dot{m}/\dot{m}_c = 1$. Remembering that increase in $\dot{m}$ for any atomizer increases V_g which is necessary to produce powder collective of fine size. The plot indicates that the E decreases with decrease in X_g and the value of E is minimum at $\dot{m}/\dot{m}_c$ i.e. $X_g = X_c$ (X_c is the critical mass median size or minimum size as described earlier).

Consider a given type of atomizer of a given focal length. For this atomizer M_c, V_c and E_c are constant. The plot suggests that the different atomization efficiency can be obtained at different value of $\dot{m}$. Increase in $\dot{m}$ is achieved by increasing plenum

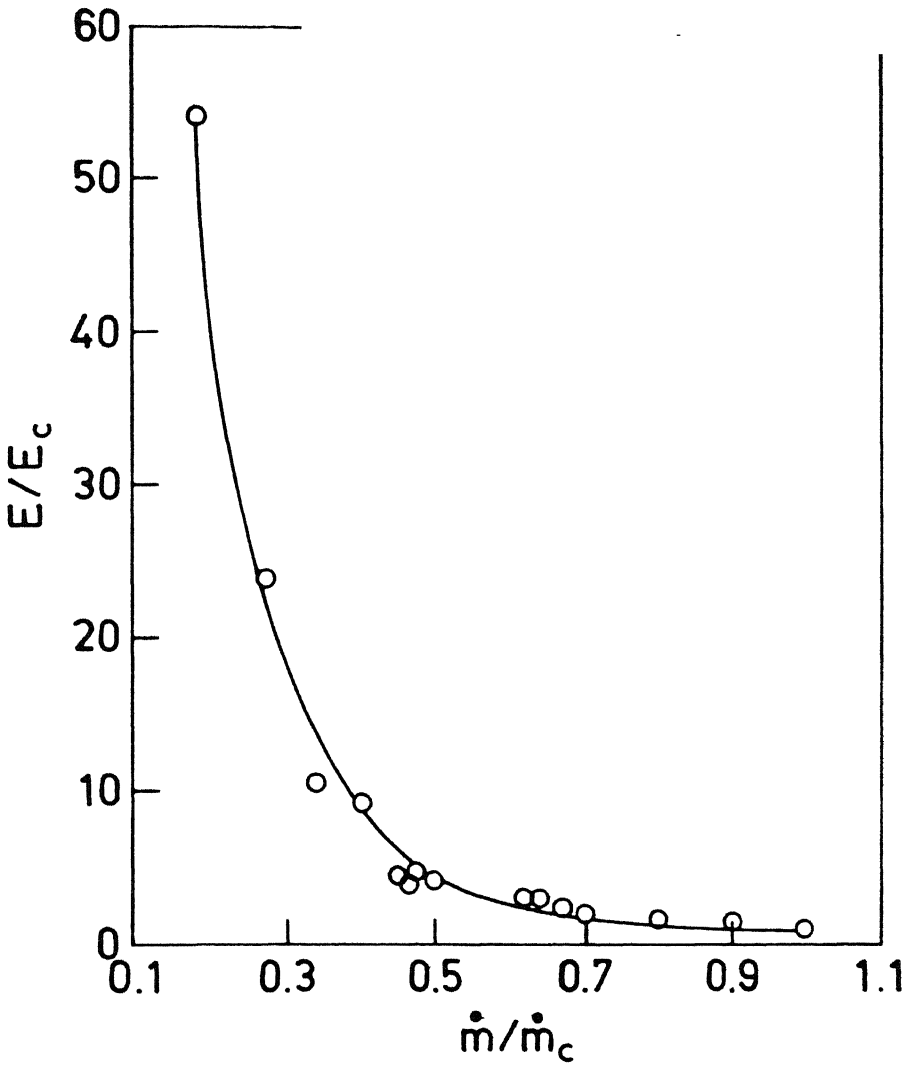

;ure 5.12 : Variation of E/E_c with m_c / m according to Equation (5.30) for various values of v_c/v_g

pressure (Equation 5.8) which results in decrease in mass median size. Thus the atomization efficiency is low when the powder collective of fine size is required to be produced. For coarse powder collectives, the efficiency is higher. As an example, consider atomization efficiency for atomizer A412 at 1000 kPa and 1900 kPa plenum pressures. The mass median sizes at respective plenum pressures are 166 μm and 80 μm. The atomization efficiencies for these pressures are 0.24% and 0.08%, respectively. Reinshagen and Neupaver[6] reported that the efficiency of gas atomization is not more than 1%.

The decrease in apex angle decreases the mass median size without affecting the m and V_g. That is why Equation (5.28) show that the decrease in apex angle decreases the efficiency of atomization for a given velocity of gas. For example, the efficiency for atomizer A212 and A412 of different apex angles of 20° and 40° are 0.26% and 0.46%, respectively at 1500 kPa plenum pressure.

5.2.5 PARTICLE SHAPE

Results of present study show that the shape of particles of a powder collective produced by a given gas velocity depends on superheat of liquid metal, apex angle of the atomizer and type of metal. Shape is found to be independent of the velocity of the atomizing gas and metal flow rate. Large proportion of lead particles are found spherical below the size of 211 μm of different powder collectives produced by atomizers of either 40° or 60° apex angle at superheat of 150 K. Other than 150 K superheat of liquid metal i.e. 70 K, 110 K and 190 K the large proportion of particles of powder collectives are found to be rounded and irregular in shape in all size ranges. Whereas large proportion of

particles of powder collectives in all size ranges produced by atomizer of 20° apex angle are observed to be rounded and irregular in all size ranges at all superheats. The observation of the spherical shape of the particle in the powder collectives produced at 150 K superheat is explained by considering the time for spherodization and solidification.

It is known that the shape of particle is controlled by the solidification and spherodization time of the droplet[4]. If spherodization time is less than that of solidification time the resulting particle will be spherical in shape. Nichiparenko and Naida have proposed the following Equation to calculate the time of spherodization of the ligament into spherical shape droplet:

$$t_{sph} = \frac{3\pi^2 \mu_m}{4V\rho_m}\left(R_p^4 - r_p^4\right) \qquad (5.31)$$

The r_p is the radius of the ligament prior to and R_p is radius after spherodization. V is the volume of the droplet which is equal to $\frac{4}{3}\pi R_p^3$. Assuming the value[3] of $r_p = 0.1$ R_p Equation (5.31) reduces to

$$t_{sph} = 0.883 \frac{\mu_m}{\sigma_m} dp \qquad (5.32)$$

where, $dp = 2\ R_p$. According to Equation (5.32) time for spherodization increases with decrease in surface tension but with increase in viscosity and droplet diameter. Thus t_{sph} for a given diameter of droplet can be determined from the physical properties of lead. The calculated values of t_{sph} are given in Table 5.3.

In the experiments maximum size of the spherical particle that is solidified in a collective produced at 150 K superheat is determined at various distances downstream of

Table 5.3 : Spheroidization and solidification time of particles produced under conditions of different runs.

Particle Size μm	Spherodization Time μs	Solidification time, ms		
		Run No. 36 V_g = 87 m/s	Run No. 37 V_g = 125 m/s	Run No. 38 V_g = 162 m/s
95	0.47	12.3	11.1	10.2
133	0.66	22.2	20.7	19.5
160	0.80	31.5	29.7	27.9
233	1.16	66.3	61.8	57.6
243	1.21	71.7	66.9	62.1
252	1.26	76.8	71.7	66.6

the geometric point. It is found that the maximum size of the spherical particle increases with the distance (see Figure 4.47). In the appendix - C the time required for the droplet to reach a given distance is calculated by analyzing Equation of motion of the droplet. Since the droplet is solidified at that distance, hence this time is the solidification time. The so determined time of solidification is also given in Table 5.2 for different droplet diameters at two different velocity of gas.

From the table it can be seen that $t_{sph} < t_{sol}$ which suggests that large proportion, if not all, of the particles should be spherical.

For aluminium, zinc and tin and all other combinations of superheats for lead i.e. 70 K, 110 K and 190 K and apex angles i.e. 20°, 40° and 60°, the shape of the powder particle is found to be irregular. This observation suggests that the molten metal ligaments formed during disintegration of liquid metal stream might have solidified due to the vigorous energy exchange that takes place between metal and gas. Other possibility could be that the surface of the molten metal ligament is instantaneously solidified while the centre may remain liquid. Once the surface solidifies, no further change in shape can occur.

Thus it appears that for a given velocity of gas, ΔT and α determines the dynamics of solidification of the ligament in order to obtain the final powder shape. Thus, both the mechanisms of solidification of the ligaments i.e. from surface to centre and centre to surface are important in order to obtain the desired powder shape. The former mechanism appears to produce irregular shaped powder since surface of the ligament is already

solidified, and the later mechanism produces spherical powder since enough time is available for spherodization.

CHAPTER - 6

CONCLUSIONS

The following conclusions are made:

1. The gas field around the geometric point is found to consist of widely varying velocities both in horizontal and vertical directions. Velocity is found to be constant for some horizontal and vertical distances, measured from geometric point.

2. The velocity at the geometric point increases with increase in plenum pressure and nozzle diameter, but with decrease in focal length. The influence of apex angle and number of nozzles on velocity is found to be negligibly small. The data on velocity are correlated empirically with a power function. It is found that the plenum pressure increases the velocity much faster (exponent value = 0.96) as compared with focal length (exponent value = -0.75) and nozzle diameter (exponent value = 0.48).

3. The axial velocity downstream the geometric point is found to decrease exponentially with the increase in downstream distance. The exponent value of the distance is found to decrease exponentially in the ratio of gas density to that of surrounding air.

4. The value of the discharge coefficient of atomizers with 2 mm and 3 mm nozzle diameters is found to be almost independent of plenum pressure and number of nozzles. However, the mean value increases from 0.57±0.3 to 0 82±0.4 with the decrease in nozzle diameter from 3 mm to 2 mm.

5 In relation to atomization of molten aluminium, lead, tin and zinc to produce powder, a fraction of the droplets is found to deposit on the surface of the atomizer and/or powder collection tray, whenever atomizer is operated beyond a certain gas velocity. The velocity of gas at which droplets do not deposit on the atomizer surface is termed critical velocity of gas. The critical velocity is found to increase with increase in free fall distance but with decrease in apex angle of the atomizer. The critical velocity is independent of liquid related parameters.

6. Within 2.4 m height of cooling chamber, it has become possible to produce lead powder for a wide range of velocities of atomizing gas. Powders of aluminium, tin and zinc could be produced only for a very limited velocity range.

7. Size distribution of all powder collectives follows log normal distribution. The mass median size decreases with increase in velocity of gas and decrease in apex angle of the atomizer. At critical velocity of gas, mass median size is found to be minimum. Geometric standard deviation is found to be independent of all parameters; its mean value is determined to be 1.95. The ratio of X_g/X_c is correlated with V_g/V_c and apex angle of the atomizer, from which the value of X_g of a powder collective can be calculated.

8. The atomization efficiency is found to be less than 1%.

9. Shape of the powder particle is observed to depend on superheat and apex angle of atomizer for all velocities of atomizing gas. AT 70 K, 110 K and 190 K superheats, and 20°, 40° and 60° apex angles, the shape of most of the particles is found to be irregular, rounded etc., whereas at 150 K superheat and 40° and 60° apex angles, a large fraction of the particles in the powder collectives is found to be spherical in shape.

CHAPTER - 7

SUGGESTION FOR FUTURE WORK

The following suggestions are felt necessary for further development of free fall atomization of liquid metals :

1. The correlation given for the prediction of gas velocity at the geometric point determines air velocity satisfactorily. This correlation may be verified for other gases and if required the modification of the equation can be made.
2. The study of the deposition of particles at the atomizer surface above a critical pressure was carried out of air as atomizing gas, and lead, aluminum and zinc as the metals to be atomized. This study can be extended for the different combinations of metals and gases. Accordingly, equation derived for calculating critical velocity may be modified.
3. Other metals except lead, i.e. aluminium, zinc and tin could not completely solidify within the height of 2.4 m of cooling chamber. Therefore, study on powder characteristics could not be possible in the present study for these metals. It is felt necessary that the study should be extended to these metals by increasing the height of cooling chamber of powder particles.
4. The reasons to describe the variation in shape of particle of the same collective should be verified experimentally.

5. Further work should be carried out to increase the efficiency of atomization without increasing the mass median size of powder.

REFERENCES

1. A. Lawley, 'Atomization, the production of metal powders, Monographs in P/M series, MPIF, Princeton, New Jersey, 1992, p.8.

2. E.J. Lavernia and Y. Wu, 'Spray Atomization and Deposition', John Wiley and Sons, Chichester, 1996, p. 124.

3. Atomization, in 'Metals Handbook', Vol. 7 (Powder Metallurgy), Coordinator E. Klar, 1984, p.25.

4. J.B. See and G.H. Johnston, 'Interaction between Nitrogen Jets and Liquid Lead and Tin Streams', Powder Tech., vol. 21, 1978, p. 119.

5. J. Bruce See, C. Runkle and T. B. King, 'The Disintegration of Liquid Lead Streams by Nitrogen Jets', Met. Trans., vol. 4(11), 1973, p. 2669.

6. J.H. Reinshagen and A.J. Neupaver, 'Principles of Atomization', in 'Physical Chemistry of Powder Metals Production and Processing', ed. W. Murray Small, The Minerals Metals and Materials Society, 1989, p.3.

7. C. Tornberg, 'Particle size Prediction in an Atomization System', in Advances in Powder Metallurgy and Particulate Materials, vol. 1, Metal Powder Industries Federation, Princeton, NJ, 1992, p. 137.

8. R.I.L. Howells, G.R. Dunstan, and C. Moore, 'Production of Gas Atomized Metal Powders and their Major Industrial Uses', Powder Met., vol. 31 (4), 1988, p. 259.

9. S.A. Moir and H. Jones, 'The Gas Velocity Profile of a Free Fall Atomizer and its Relation to Solidification Microstructure of Collected Spray Droplets of 2014 aluminum Alloy', Mat. Sci. Eng., A173, 1993, p. 161.

10. S.A. Moir, H. Jones and S. B. M. Beck, 'Gas Velocities from Free Fall Gas Atomizer', Powder Met., vol. 39(4), 1996, p. 271.

11. R. K. Dube, S. C. Koria and R. Subramanian, 'Atomisation of Aluminum by Multiple Discrete Nitrogen Jets', Powder Met. Int., vol. 20(6), 1988, p. 4.

12. G. Helmersson, A. Hede, T. Johannesson, B. Bergman and H. Hallen, 'On the Control of Powder-size Distribution in Full - Scale Gas Atomization of Nickel-based Alloys', Scandianavian Journal Met., 26, 1997, P. 93.

13. H. Lubanska, 'Correlation of Spray Ring Data for Gas Atomization of Liquid Metals', J. Metals, Feb. 1970, p. 45.

14. A.R.E. Singer, 'The Principles of Spray Rolling of Metals', Metals and Materials, Vol. 4(6), June 1970, p.246.

15. C. Tornberg, 'Gas Efficiency in Different Atomization Systems', Advances in Powder Metallurgy and Particulate Materials, vol. 1, Metal Powder Industries Federation, Princeton, NJ, 1992, p. 127.

16. G. Helmersson and K. Burgdorf, 'Effect of Process Parameters on Microstructure of Gas Atomized Powder', Scandinavian Journal Met., 25, 1996, p. 51.

17. Y.I. Naida, A.B. Medvedovskil, L.M. Diyuk and E.G. Mitrov, 'Analysis of Conditions of Cooling of Atomized Metal Powders and Calculation of the Dimensions of the Atomizing Chamber, 7(139), 1974, p. 527.

18. Schmitt, 'Mathematical - Physical Considerations Regarding the Production of Metal Powders for Powder Metallurgy (Part II), Powder Met. Int., vol. 11(2), 1979, p. 68.

19. M. Lieblich, G. Caruana, M. Torralba and H. Jones', Characteristics of Al-Cr-Zr Alloy Powders made by Confined Nozzle Atomisation', Mat. Sci., Tech., vol. 12(1), 1996, p. 25.

20. S. Ozbilen, A. Unal and T. Sheppard, 'Influence of Liquid Metal Properties on Particle Size of Inert Gas Atomised Powders', Powder Met., vol. 39(1), 1996, p. 44.

21. C. Subramanian, P. Mishra and A. K. Suri', Preparation of fine metal powders using a confined low pressure nozzle, Int. J. Powder Met., vol. 31(2), 1995, p. 137.

22. A.R.E. Singer, J.S. Coombs, A.G. Leatham , 'Modern Developments in Powder Metallurgy', Ed. H. H. Hausner and W.E. Smith, Princeton, Metal Powder Industry Federation, 8, 1974, p. 263.

23. S. C. Koria, Nozzle design in impinging jet steelmaking process, Steel Res., 59, 1988, p. 104.

24. S. C. Koria, Dynamic variation of lance distance in impinging jet steelmaking practice, Steel Res., 59, 1988, p. 257.

25. S. C. Koria, Thermodynamic consideration in designing gas injection lances submerged in melt, Ironmaking Steelmaking, 16, 1989, p. 21.

26. G.S.G. Beveridgr and R. S. Schechter, 'Optimization : Theory and Practice', NY, McGraw Hill., 1970, p. 67.

27. J. Liu, L. Arnberg, N. Backstrom, H. Klang and S. Savage, 'Mass and Heat Transfer During Ultrasonic Gas Atomization', Powder Met. Int., vol. 20(2), 1988, p. 17.

28. S. Connelly, J.S. Coombs and J.O. Medwell, 'Flow Characteristics of Metal Particles in Atomised Sprays', Metal Powder Report, 40, 1986, p. 653.

29. B.P. Bewlay and B. Cantor, Modeling of spray deposition : Measurements of particle size, gas velocity, particle velocity and spray temperature in gas atomized sprays, Met. Trans. B., 21, 1990, p. 899.

30. P. Mathur, D. Apelian and A. Lawley, 'Analysis of the spray Deposition Process', Acta Metall., vol. 37(2), 1989, p. 429.

31. G. Antipas, C. Lekakou and P.Tsakiropoulos, 'Proceedings of the Second International Conference on Spray Forming, edited by John Wood, Woodhead Publishing Ltd., Swansea, Sep. 1993, p. 15.

32. E. J. Lavernia and Y. Wu, 'Spray Atomization and Deposition', John Wiley and Sons, Chichester, 1996, p. 57.

33. M.H. Aksel and O. C. Enralp, 'Gas Dynamics', Prentice Hall., London, 1994, pp. 79-124, pp. 197-198.

34. J. Szekely and N.J. Themelis, 'Rate Phenomena in Process Metallurgy', Wiley - Interscience, A division of John Wiley and Sons, Inc., N.Y., 1971, p. 119.

35. N. P. Cheremisinoff, 'Encyclopedia of Fluid Mechanics Vol. 1, Flow Phenomena and Measurement', Gulf Publishing Company, Houston, 1986, p. 296.

36. S. L. Shinde and G. S. Tendalkar, 'Analysis of Atomization - A review', Powder Met. Int., vol. 9(4), 1977, p. 180.

APPENDIX - A

DETERMINATION OF METAL FLOW RATE

$$\text{The average mass flow rate of metal} = \frac{\text{Mass of Metal}}{\text{Total Drainage Time}} \qquad \text{(A-1)}$$

where, total drainage time of metal was calculated from the following equation[34].

$$t = \left(\frac{D_t}{d}\right)^2 \sqrt{\frac{2}{g}\left(\sqrt{h_o + 1} - \sqrt{1}\right)\sqrt{1 + \frac{4fl}{d}}} \qquad \text{(A-2)}$$

where, the friction factor, f is calculated from the following expression:[35]

$$f = 0.0791\ Re^{-1/4} \qquad \text{(A-3)}$$

The velocity of liquid metal for the determination of Reynold's number is calculated from the following equation:[34]

$$V_m = \sqrt{\frac{2g(h_o + 1)}{1 + \frac{4fl}{d}}} \qquad \text{(A-4)}$$

Example

Using

D_t	=	0.07m	l	=	0.15 m
d	=	0.055 m	μ_m	=	0.0023 $P_{a\text{-}s}$
g	=	9.8 m/s^2	ρ_m	=	10670 kg/m^3
h_o	=	0.012m			

The friction factor 'f' from equations (A-3) and (A-4) is 5.77×10^{-3}.

Using this value in equation (A-2), t = 2.04 s

Therefore, average mass flow rate = $\frac{500}{2.04} \approx 250$ gm / s.

APPENDIX - B

METHOD OF CALCULATION OF VELOCITY

The relationship between Pitot pressure and Mach number of the jet is given by:[33]

$$\frac{P_t}{P_s} = \left(1 + \frac{\gamma - 1}{2} M^2\right)^{\frac{\gamma}{\gamma-1}} \qquad \text{(B-1)}$$

The Mach number is given by:

$$M^2 = \frac{V^2 w}{\gamma R T} \qquad \text{(B-2)}$$

where

$$T = T_o / \left(1 + \frac{\gamma - 1}{2} M^2\right) \qquad \text{(B-3)}$$

Combining equation (B-2) and (B-3) follows:

$$V = \sqrt{\frac{\gamma R T_o}{w\left(\frac{1}{M^2} + \frac{\gamma - 1}{2}\right)}} \qquad \text{(B-4)}$$

By equations (B-1) and (B-4) velocity is calculated The following values of physical constants are used: P = 101.3 kPa, γ = 1.4, T_o = 298 K, R = 8.314 kj/kg moles K and w = 29 kg/kg mole.

APPENDIX - C

METHOD USED TO CALCULATE FLIGHT TIME FROM FLIGHT DISTANCE OF PARTICLE MOVING WITH GAS STREAM

The flight time of particle was calculated from its flight distance using following force balance formulation:

The assumptions made in the force balance formulation are as follows :

(i) Particle is spherical.

(ii) There is no particle - particle interaction i.e. volume fraction of particles in the gas is negligible. (No coalescence of particles).

(iii) There is no disintegration of particle.

(iv) There is no mass transfer between particle and gas.

(v) There is no radial displacement of particle.

(vi) Within the limit of calculation temperature does not have significant effect on physical properties of liquid metals.

(viii) Density difference between particle and gas is large.

The force balance equation on a particle of size 'd' along the central vertical axis of atomizer is given by -

F = force exerted on the particle by atomizing gas + gravitational force acting on the particle - buoyancy force acting on the particle + force depending on previous history of particle.

or

$$\frac{1}{6}\pi d_p^3 \rho_m \frac{dv_p}{dt} = \frac{C_d}{2}\rho_g \frac{\pi d_p^2}{4}\left(v_g - v_p\right)\left|v_g - v_p\right| + \frac{1}{6}\pi d_p^3 g\left(\rho_m - \rho_g\right) \quad \text{(C-1)}$$

Force depending on previous history of particles is assumed to be negligible.

or

$$\frac{dv_p}{dt} = \frac{3}{4}\frac{C_d \rho_g}{d_p \rho_m}(v_g - v_p)|v_g - v_p| + \left(1 - \frac{\rho_g}{\rho_m}\right)g \qquad \text{(C-2)}$$

Therefore, axial position of the particle along the said axis of the atomizer is given by -

$$\frac{d^2 z_p}{dt^2} = \frac{3}{4}\frac{C_d \rho_g}{d_p \rho_m}\left(v_g - \frac{dz_p}{dt}\right)\left|v_g - \frac{dz_p}{dt}\right| + \left(1 - \frac{\rho_g}{\rho_m}\right) g \qquad \text{(C-3)}$$

The value of C_d is calculated by ( )

$$C_d = 0.28 + \frac{6}{Re^{1/2}} + \frac{21}{Re} \qquad 0.1 < Re < 4000 \qquad \text{(C-4)}$$

where

$$Re = \frac{\rho_g \, d\,|v_g - v_p|}{\mu_g} \qquad \text{(C-5)}$$

Equation (C-3) was used numerically to find the value of z_p with time t. The following values of physical constants were used ρ_g = 1.18 kg/m^3, ρ_m = 10670 kg/m^3 and g = 9.8 m/s^2.

A 131080

Date Slip

This book is to be returned on the date last stamped.